คอมพอสิทที่เติมสารเติมปริมาณสูงจากนาโนซิลิกาและเบนซอกซาซีน-อิพอกซีโคพอลิเมอร์

นางสาวอิสลาห์ ดือราแม

วิทยานิพนธ์นี้เป็นส่วนหนึ่งของการศึกษาตามหลักสูตรปริญญาวิศวกรรมศาสตรดุษฎีบัณฑิต
สาขาวิชาวิศวกรรมเคมี ภาควิชาวิศวกรรมเคมี
คณะวิศวกรรมศาสตร์ จุฬาลงกรณ์มหาวิทยาลัย
ปีการศึกษา 2555

HIGHLY FILLED COMPOSITES FROM NANO-SILICA AND BENZOXAZINE-EPOXY COPOLYMER

Miss Isala Dueramae

A Dissertation Submitted in Partial Fulfillment of the Requirements
for the Degree of Doctor of Engineering Program in Chemical Engineering
Department of Chemical Engineering
Faculty of Engineering
Chulalongkorn University
Academic Year 2012

Thesis Title	HIGHLY FILLED COMPOSITES FROM NANO-SILICA AND BENZOXAZINE-EPOXY COPOLYMER
By	Ms. Isala Dueramae
Field of Study	Chemical Engineering
Thesis Advisor	Associate Professor Sarawut Rimdusit, Ph.D
Thesis Co-advisor	Professor Tsutomu Takeichi, Ph.D.

Accepted by the Faculty of Engineering, Chulalongkorn University in Partial Fulfillment of the Requirements for the Doctoral Degree

……..……..Dean of the Faculty of Engineering
(Associate Professor Boonsom Lerdhirunwong, Dr.Ing.)

THESIS COMMITTEE

……Chairman
(Associate Professor Tharathon Mongkhonsi, Ph.D.)

…….Thesis advisor
(Associate Professor Sarawut Rimdusit, Ph.D.)

…….Thesis Co-advisor
(Professor Tsutomu Takeichi, Ph.D.)

..……...Examiner
(Associate Professor Seeroong Prichanont, Ph.D.)

..……Examiner
(Associate Professor Siriporn Damrongsakkul, Ph.D.)

……..External Examiner
(Phiriyatorn Suwanmala, Ph.D.)

……..External Examiner
(Chanchira Jubsilp, D.Eng.)

อิสลาห์ ดือราแม : คอมพอสิทที่เติมสารเติมปริมาณสูงจากนาโนซิลิกาและเบนซอกซาซีน-อิพอกซีโคพอลิเมอร์ (HIGHLY FILLED COMPOSITES FROM NANO-SILICA AND BENZOXAZINE-EPOXY COPOLYMER) อ. ที่ปรึกษาวิทยานิพนธ์หลัก: รศ. ดร. ศราวุธ ริมดุสิต, อ. ที่ปรึกษาวิทยานิพนธ์ร่วม: Prof. Tsutomu Takeichi, Ph.D., 138 หน้า.

อิพอกซีทำหน้าที่เป็นตัวทำเจือจากให้กับเบนซอกซาซีนเรซิน ซึ่งแสดงงานร่วมของอุณหภูมิในการเปลี่ยนสถานะคล้ายแก้วสูงสุดที่อัตราการผสมของเบนซอกซาซีนกับอิพอกซี 80:20 โดยมวล แต่อย่างไรก็ตามเบนซอกซาซีนแสดงการยึดเกาะที่ดีต่อนาโนซิลิกามากกว่าการใช้โคพอลิเมอร์เมตริกซ์ ดังนั้น จุดประสงค์ในงานวิจัยนี้เพื่อมุ่งเน้นการพัฒนาระบบคอมพอสิทที่เติมสารปริมาณสูงจากนาโนซิลิกาและเบนซอกซาซีน โดยศึกษาถูกคุณสมบัติเชิงกลและทางความร้อน นาโนคอมพอสิทถูกเตรียมด้วยการผสมแบบแรงเฉือนสูงตามด้วยการใช้แรงอัด เบนซอกซาซีนมอนอเมอร์ซึ่งมีความหนืดต่ำทำให้ความสามารถในการอาบนาโนซิลิกาดีเยี่ยม ซึ่งสามารถเติมนาโนซิลิกาได้สูงถึง 30 เปอร์เซ็นต์โดยน้ำหนัก (หรือ 18.8 เป็นเซ็นต์โดยปริมาตร) โดยไม่เกิดรุพรุนในชิ้นงาน มากกว่านั้น การวิเคราะห์ทางความร้อนของกระบวนการบ่มสำหรับสารประกอบคอมพอสิทจากเบนซอกซาซีนและนาโนซิลิกาพบว่าเป็นกระบวนการแบบ autocatalytic ให้ค่าพลังงานก่อกัมมันต์สำหรับการบ่ม 79–92 kJ mol^{-1} ภาพจากกล้องจุลทรรศน์ไมโครสโครบแบบส่องกราดพบว่านาโนซิลิกาสามารถกระจายตัวในพอลิเบนซอกซาซีนอย่างเป็นอย่างดี ไม่มีการเกาะกลุ่มกัน มากกว่านั้นมอดูลัสสะสมของระบบนาโนซิลิกาคอมพอสิทที่ใช้เบนซอกซาซีนเป็นเมตริกซ์สูงกว่าระบบอิพอกซี มากกว่านั้น ค่าความแข็งที่ได้สูงถึง 600 MPa ค่าอุณหภูมิการเปลี่ยนสถานะคล้ายแก้ว เพิ่มสูงขึ้น 16^{o}C สำหรับการเติมนาโนซิลิกา 30 เปอร์เซ็นต์โดยน้ำหนักเมื่อเทียบกับเมตริกซ์พอลิเบนซอกซาซีน สำหรับผลของปริมาณนาโนซิลิกาต่อจลพลศาสตร์การสลายตัวทางความร้อนถูกศึกษาเนื่องจากเชื่อว่าปฏิกริยาระหว่างหมู่ฟังก์ชันของนาโนซิลิกากับพอลิเบนซอกซาซีนสามารถเพิ่มเสถียรภาพทางความร้อนได้ โดยใช้การวิเคราะห์หารสลายตัวทางความร้อนแบบอุณหภูมิไม่คงที่ จากกราฟ DTG พบว่าเบนซอกซาซีนแสดงกระบวนการสลายตัวเป็น 3 ช่วงที่มีการซ้อนทับกัน ขณะที่ช่วงแรกที่อุณหภูมิต่ำของนาโนคอมพอสิทหายไป และยังพบอีกว่าช่วงที่มีการสลายตัวสูงสุดของสารสูงขึ้นตามปริมาณนาโนซิลิกา มากกว่านั้น อัตราการสลายตัวในทุกช่วงลดลงลงตามปริมาณนาโนซิลิกา จากการวิเคราะทางด้านจลพลศาสตร์ ค่าพลังงานก่อกัมมันต์ในการสลายตัวทางความร้อนขึ้นสัดส่วนการสูญเสียมวล ซึ่งบ่งบอกว่า เป็นปฏิกริยาที่ซับซ้อนอย่างน้อยมีการสลายตัวสองกลไก จากการวิเคราะห์ด้วยวิธี Coat-Redfern และ Integral master plot พลังงานก่อกัมมันต์ (E_a) และค่า pre-exponential factor (A) ของนาโนคอมพอสิทให้ค่าที่สูงกว่าพอลิเบนซอกซาซีน แสดงให้เห็นว่านาโนซิลิกาสามารถหน่วงการสลายตัวความร้อนของพอลิเบนซอกซาซีนได้ โดยการสลายตัวทางความร้อนในช่วงสูงสุด แสดงค่า E_a and lnA ของเบนซอกซาซีนเป็น 116 kJ/mol and 13.6 ตามลำดับ ขณะที่เบนซอกซาซีนที่เติมนาโนซิลิกา 10 เปอร์เซ็นต์โดยน้ำหนัก เป็น 157 kJ/mol and 19.1 โดยกลไกการสลายตัวของเบนซอกซาซีนเป็นแบบ F1 ขณะที่นาโนคอมพอสิทเป็นแบบ D3

ภาควิชา.....วิศวกรรมเคมี.....ลายมือชื่อนิสิต.....

สาขาวิชา...วิศวกรรมเคมี.....ลายมือชื่อ อ.ที่ปรึกษาวิทยานิพนธ์หลัก.....

ปีการศึกษา.....2555.....ลายมือชื่อ อ.ที่ปรึกษาวิทยานิพนธ์ร่วม.....

5271869321 : MAJOR CHEMICAL ENGINEERING
KEYWORDS: POLYBENZOXAZINE/NANOSILICA/THERMOMECHANICAL ANALYSIS/YHERMAL DEGRADATION KINETICS

ISALA DUERAMAE: HIGHLY FILLED COMPOSITES FROM NANO-SILICA AND BENZOXAZINE-EPOXY COPOLYMER. ADVISOR: ASSOC. PROF. SARAWUT RIMDUSIT, Ph.D., CO-ADVISOR: PROF. TSUTOMU TAKEICHI, Ph.D., 138 pp.

Epoxy act as diluent for benzoxazine resin. A synergistic behavior with the maximum glass transition temperature value was found at the benzoxazine-epoxy composition of 80:20 mass ratio. However, the nano-SiO_2 showed better interfacial adhesion with benzoxzaine than copolymer matrix. Therefore, highly filled polybenzoxazine nanocomposites filled with nano-SiO_2 particles were investigated for their mechanical and thermal properties as a function of filler loading. The nanocomposites were prepared by high shear mixing followed by compression molding. A very low A-stage viscosity of benzoxazine monomer gives it excellent processability having maximum nano-SiO_2 loading as high as 30wt% (18.8vol%) with negligible void content. Moreover, thermal analysis of the curing process of the compound of the PBA-a/nano-SiO_2 composites was found to be autocatalytic in nature with average activation energy of 79–92 kJ mol^{-1}. Microscopic analysis (SEM) performed on the PBA-a/nano-SiO_2 composite fracture surface indicated a nearly homogeneous distribution of the nano-scaled silica in the polybenzoxazine matrix. In addition, the enhancement in storage modulus of the nano-SiO_2 filled polybenzoxazine composites was found to be significantly higher than that of the recently reported nano-SiO_2 filled epoxy composites. The dependence of the nanocomposites' modulus on the nano-SiO_2 particles content is well fitted by the generalized Kerner equation. Furthermore, the relatively high micro-hardness of the PBA-a/nano-SiO_2 composites up to about 600 MPa was achieved. Finally, the substantial enhancement in the glass transition temperature (T_g) of the PBA-a/nano-SiO_2 composites was also observed with the $\triangle$Tg up to 16^oC at the nano-SiO_2 loading of 30wt%. The effects of the nano-filler on their thermal degradation kinetics were investigated using non-isothermal thermogravimetric analysis (TGA). The DTG curves revealed three stages of decomposition process in the neat PBA-a while the first peak at low temperature was absent in its nanocomposites. As a consequence, the maximum degradation temperature of the nanocomposites shifted significantly to higher temperature as a function of the nano-SiO2 contents. Moreover, the degradation rate for every degradation stage was found to decrease with increasing amount of the nano-SiO2. From the kinetics analysis, dependence of activation energy (E_a) of the nanocomposites on conversion (α) indicates a complex reaction with the participation of at least two different mechanisms. From Coat-Redfern and integral master plot methods, the average E_a and pre-exponential factor (A) of the nanocomposites showed systematically higher value than that of the PBA-a, likely from the shielding effect of the nanoparticles. For example, at the main degradation stage, the neat PBA-a has E_a and lnA of 116 kJ/mol and 13.6 while the 10wt% nano-SiO2 filled PBA-a has E_a and lnA of 157 kJ/mol and 19.1. The main degradation mechanism of the PBA-a was determined to be a random nucleation type with one nucleus on the individual particle (F1 model) while that of the PBA-a nanocomposite was best described by diffusion- controlled reaction (D3 model).

Department: Chemical Engineering ….Student's Signature……...
Field of Study: Chemical Engineering ..Advisor's Signature.....
Academic Year :.....2012.....Co-advisor's Signature.....

ACKNOWLEDGEMENTS

I am sincerely grateful to my advisor, Assoc. Prof. Dr. Sarawut Rimdusit, for his invaluable guidance and valuable suggestions including constant encourage throughout this study. Furthermore, I deeply appreciate all things, I have learnt from him and for the opportunity to work in his group. I am also grateful to my co-advisor, Professor Dr. Tsutomu Takeichi from Department of Environmental and Life Sciences, Toyohashi University of Technology, Toyohashi, Aichi, JAPAN. He guided me through every difficulty in this thesis and taught me how to face the problems in my life intellectually.

I am also grateful to my committee members, who provided constructive and scientific advices for the completion of this thesis. This includes, Assoc Prof. Dr. Tharathon Mongkhonsi, Chairman, Assoc Prof. Dr. Muenduen Phisalaphong, Assoc. Prof. Dr. Siriporn Damrongsakkul from the Department of Chemical Engineering, Faculty of Engineering, Chulalongkorn University, Dr. Phiriyatorn Suwanmala from Thailand Institute of Nuclear Technology, and Dr. Chanchira Jubsilp from the Department of Chemical Engineering, Faculty of Engineering, Srinakharinwirot University.

I am very thankful for every inspiration that they have made throughout my difficult years. They are more than my best friends. Thank are also extended to every polymer engineering research laboratory member for every constructive discussion they contributed and all their help.

Finally, my deepest regard to my beloved family and parents, who have always been the source of my support and encouragement. There is never a single day without them standing by me. It is why I can journey this far. I am lifetime beholden.

CONTENTS

PAGE

ABSTRACT IN THAI..…….. iv

ABSTRACT IN ENGLISH..... v

ACKNOWLEDGEMENTS..... vi

CONTENTS..... vii

LIST OF TABLES……..……..…….. x

LIST OF FIGURES……..……..……. xi

CHAPTER I INTRODUCTION……..……..……. 1

1.1 Introduction…….…… 1

1.2 Objectives…….…….. 4

1.3 Scopes of Research……. 5

1.4 Chemical and Equipments……..... 5

CHAPTER II THEORY……. 7

2.1 Nanocomposite Materials …….…….…… 7

2.2 Fundamentals of Particle Packing Characteristics.…… 18

2.3 Theory/Calculation of Thermal Degradation Mechanism……. 24

CHAPTER III LITERATURE REVIEWS…….……. 28

CHAPTER IV EXPERIMENTAL……..…….. 48

4.1 Materials…….…….…… 48

4.2 Sample Preparations…… 48

4.3 Sample Characterizations…….... 49

4.3.1. Chemorheology of benzoxazine resins and their mixtures with epoxy……..... 49

4.3.1 Density measurement……. 49

4.3.2 Fourier transform infrared spectroscopy (FT-IR)…….. 49

PAGE

4.3.3 Differential scanning calorimetry measurements…….. 50
4.3.4 Hardness measurements…… 50
4.3.5 Dynamic mechanical analysis…… 50
4.3.6 Morphology of PBA-a /nano-SiO_2 composites…….. 50
4.3.7 Thermogravimetric analysis…….. 51

CHAPTER V RESULTS AND DISCUSSION……. 52
5.1 Selecting Resin Matrix for Nanocomposite Fabrication…… 52
5.1.1 Chemorheological properties…… 52
5.1.2 Differential scanning calorimetry (DSC) for curing process investigation……. 55
5.1.3 Characterization of BY/nano-SiO_2 composites…… 56
5.2 High Thermal and Mechanical Properties Enhancement Obtained in Highly Filled Polybenzoxazine Nanocomposites with Nano-SiO2……. 58
5.2.1 Maximum packing density of highly filled PBA-a/nano-SiO_2 composites……. 58
5.2.2 Spectroscopic properties of the polybenzoxazine nanocomposites… 59
5.2.3. Curing characteristics of BA-a/nano-SiO_2 molding compounds….. 60
5.2.4. Microhardness of PBA-a /SiO_2 nanocomposites……... 62
5.2.5. Dynamic mechanical properties of the polybenzoxazine nanocomposites……..... 63
5.2.5.1 Modeling studies of modulus of highly filled polybenzoxazine/nano-SiO_2 composites…… 65
5.2.5.2 Comparison between experimental results and model prediction…… 67
5.2.6. Glass transition temperature (T_g) of highly filled PBA-a/nano-SiO_2 composites…….. 68
5.2.7. Microstructure of nano-SiO_2 filled PBA-a……..... 69
5.2.8. Thermal stability of nano-SiO_2 filled PBA-a…… 70

PAGE

5.3. Thermal Degradation Mechanism of Highly Flled Nano-SiO_2-Polybenzoxazine Nanocomposites…….. 70

5.3.1.Thermogravimetric analysis (TGA) of nano-SiO_2 filled polybenzoxazine……. 71

5.3.2. Thermal degradation kinetics parameters of nano-SiO_2 filled PBA-a system…… 72

5.3.3. Isoconversional analysis of nano-SiO_2 filled PBA-a system……. 73

5.3.4 Determination of the kinetic model by means of generalized master plots of nano-SiO_2 filled polybenzoxazine system……. 74

CHAPTER VI CONCLUSIONS..... 121

REFERANCES……..……... 123

APPENDICES…….……. 136

Appendix A List of publications…… 137

VITAE…….……...…….……. 138

LIST OF TABLES

TABLE		PAGE
2.1	Properties of nano-SiO_2……..	9
2.2	Comparative properties of various high performance polymers……	13
2.3	Curing agents for epoxy resins……..	17
2.4	Typical properties of EPOTEC YD 126……	18
2.5	Effect of particle size distribution on packing density showing relation between particle size ratio and maximum packing density……	24
2.6	Algebraic expressions of f(α) and g(α) for the reaction models……	27
3.1	Activation energy (E*) and activation volume (V*) for nanocopmposites and the control resin……..	33
3.2	Activation energies for catalyzed 12- and 40-nm nano-SiO2/BECy from differential scanning calorimeter……..	41
5.1	The kinetic parameter of Arrhenius equation at the gel points of benzoxazine resins mixed with epoxy resin at various epoxy content…...	117
5.2	Mechanical property comparison of polymer matrix/nano-SiO_2 composite with particle size of 5-50 nm……	117
5.3	Material parameters used in composite CTE and moduls predictions…...	118
5.4	Thermo-mechanical parameters of PBA-a and its nanocomposites……...	118
5.5	Activation energies obtained by using Kissinger method and Flynn-Wall-Ozawa method for polybenzoxazine and theirs nanocomposites….	118
5.6	Values of E_a and A by using Coats-Redfern method for maximum stage process at a heating rate of 10^oC/min for PBA-a and theirs nanocomposites……..	119
5.7	Degradation mechanism by using Coat-Redfern method of all degradation stages……..	120
5.8	Degradation parameter by using Coat-Redfern method Integral Master curves of all degradation stages…….	120

LIST OF FIGURES

FIGURE		PAGE
2.1	Synthesis method of nano-SiO_2……..	8
2.2	SEM images of (a) nano-SiO_2 aggregates and (b) agglomerates…….....	8
2.3	Schematic illustrations of three types of surface silanol…….	10
2.4	Schematic of aggregate formation between adjacent nano-SiO_2 particles through hydrogen bonding among the silanol Groups…….....	10
2.5	Synthesis of bifunctional benzoxazine monomer…….....	12
2.6	General structure of an epoxy resin…….	14
2.7	Major types of commercial epoxy resins…….....	15
2.8	Sources of epoxy properties…….....	16
2.9	The structure of EPOTEC YD 126……..	18
2.10	Fractional density for monosized powders versus roughness as expressed by a typical particle profile……..	19
2.11	A change in packing density with the length to diameter ratio (L/D) for fibers. (i.e. best packing occurs with equiaxed particles)…….....	20
2.12	Plot of fractional packing density versus composition for bimodal mixtures of large and small spheres…….	22
2.13	Effect of particle size ratio on the packing density for mixtures consisting of 70% large particles and 30% small particles……...	23
3.1	^{1}H-NMR of the benzoxazine monomer……..	29
3.2	Processing window of BA-a (B)/Ph-a (P) resin mixtures at various Ph-a resin using a heating rate 2^{o}C/min: (●) BA-a resin, (■) BP91, (♦) BP82, (▲) BP73, (▼) BP64, (◣) BP55, (◢) Ph-a resin……	30
3.3	Reaction of benzoxazine with epoxy……..	31
3.4	Processing window of BA-35x mixed with epoxy resin at various compositions: (●) 60:40, (■) 70:30, (♦) 80:20, (▲) 90:10, and (▼) neat BA-35x…….....	32
3.5	Effect of organoclay on the T g of the hybrids……	35

FIGURE **PAGE**

3.6 Effect of OMMT content on the glass transition temperature of PBZ-PBO/OMMT nanocomposites……. 36

3.7 Effect of the modified-mica content on the cure of benzoxazine…… 37

3.8 The effect of the nano-SiO_2 contents on the T_g of the SiO_2/ polybenzoxazine nanocomposites……... 38

3.9 Ring-opening polymerization of benzoxazine monomer and modified nano-SiO_2……..... 38

3.10 Loss modulus of woodflour-filled polybenzoxazine composites as function of temperature at different filler contents: (■) neat resin, (♦) 34.6 vol %, (▲) 44.3 vol %, (●) 54.4 vol %, (▭) 65.0 vol %, (◊)70.5 vol %……..... 40

3.11 SEM image of a nanocomposite based on silica and epoxy resin (25 wt% silica). Surface prepared by cryoscopic fracture…….. 42

3.12 TGA thermogram and its derivative from the degradation of BA–a polybenzoxazine in nitrogen…… 44

3.13 The degradation product of BA–a polybenzoxazine…….... 45

5.1 Processing window of BA-a/YD126 resin at various compositions: (●) BA-a/YD126 100/0, (■) BA-a/ YD126 90/10, (▲) BA-a/ YD126 80/20, (◣) BA-a/ YD126 70/30 and (◆) BA-a/YD126 60/40…… 78

5.2 Effect of gel temperature on the gel time of BA-a: (●) 1.6Hz, (■) 2.8Hz, (♦) 5.0Hz, (▲) 9.0Hz, and (◣) 15.9Hz…… 79

5.3 Gelation behavior of BA-a mixed with epoxy resin at various composition as a function of gel temperature(●) BA-a/YD126 100/0, (■) BA-a/ YD126 90/10, (▲) BA-a/ YD126 80/20, (◣) BA-a/ YD126 70/30 and (◆) BA-a/YD126 60/40……... 80

FIGURE **PAGE**

5.4 The Arrhenius plot of the gelation behavior of BA-a mixed with epoxy resin at various composition:(●) BA-a/YD126 100/0, (■) BA-a/ YD126 90/10, (▲) BA-a/ YD126 80/20, (◣) BA-a/ YD126 70/30 and (◆) BA-a/YD126 60/40……. 81

5.5 DSC thermograms of BA-a/YD126 resin at various compositions: (●) BA-a/YD126 100/0, (■) BA-a/ YD126 90/10, (▲) BA-a/ YD126 80/20, (◣) BA-a/ YD126 70/30 and (◆) BA-a/YD126 60/40…… 82

5.6 DSC thermograms showing glass-transition temperature of BA-a/ YD126 alloys at various compositions : (●) BA-a/YD126 100/0, (■) BA-a/ YD126 90/10, (◆) BA-a/ YD126 80/20, (▲) BA-a/ YD126 70/30 and (▼) BA-a/ YD126 60/40…….. 83

5.7 Dependence of storage modulus and mechanical damping factor of PBA-a with temperature for samples with different filler contents: (●) 0wt%, (■) 10wt% nano-silica, (♦) 20wt% nano-silica, (▲) 30wt% nano-silica……. 84

5.8 Dependence of storage modulus and mechanical damping factor of PBA-a/ YD126 80/20 with temperature for samples with different filler contents: (●) 0wt%, (■) 10wt% nano-silica, (♦) 20wt% nano-silica, (▲) 30wt% nano-silica…….. 85

5.9 Dependence of storage modulus and mechanical damping factor of PBA-a/ YD126 60/40 with temperature for samples with different filler contents: (●) 0wt%, (■) 10wt% nano-silica, (♦) 20wt% nano-silica…….. 86

5.10 Maximum packing density of nano-SiO2-filled polybenzoxazine: (-) theoretical density, (●) experimental density……. 87

5.11 FT-IR spectra of (a) nano-silica, (b) PBA-a, and (c) 30wt% nano-SiO_2-filled PBA-a……. 88

5.12 DSC thermograms of benzoxazine molding compound at different nano-SiO 2 contents: (●) BA-a, (■) 10wt%, (♦) 15wt%, (▼) 20wt%, (▲) 25wt% and (◣) 30wt% nano-SiO 2 -filled BA-a……..... 89

FIGURE **PAGE**

5.13 DSC thermograms of BA-a at different heating rate: (●) 1 $Kmin^{-1}$, (■) 2 $Kmin^{-1}$, (♦) 5 $Kmin^{-1}$, and (▲) 10 $Kmin^{-1}$…….. 90

5.14 DSC thermograms of 30wt% nano-SiO_2-filled BA-a at different heating rate: (●) 1 $Kmin^{-1}$, (■) 2 $Kmin^{-1}$, (♦) 5 $Kmin^{-1}$, and (▲) 10 $Kmin^{-1}$…… 91

5.15 Kissinger plot with multi-heating rate of (●) BA-a, (◣) 30wt% nano-SiO_2-filled BA-a…….. 92

5.16 Friedman plot with multi-heating rate of (●) BA-a, (◣) 30wt% nano-SiO_2-filled BA-a…….. 93

5.17 Effect of filler volume fraction on the microhardness of PBA-a/SiO_2 nanocompositess…….. 94

5.18 Dependence of storage modulus with temperature for samples with different filler contents: (●) PBA-a, (■) 10wt% nano-silica, (♦) 15t% nano-silica, (▲) 20wt% nano-silica, (▼) 25% nano-silica, (◣) 30wt% nano-silica. Inset: storage modulus at glassy state…….. 95

5.19 Storage modulus at 30^oC versus volume content of PBA-a/nano-SiO_2 composite……. 96

5.20 Mechanical damping factor of neat PBA-a and different amount of SiO_2-filled PBA-a……..... 97

5.21 Fracture surface of (a) PBA-a (b) 10wt% nano-silica filled PBA-a…….. 98

5.22 Thermal degradation temperature at 5% weight loss and (●) solid residual at 850^oC of PBA-a/SiO_2 nanocomposites…….. 99

5.23 Thermogravimetric curves of polybenzoxazine and its nanocomposites at various nano-SiO2 contents: (●) PBA-a, (■) 10 wt%, (◆) 20 wt%, (▲) 30 wt% of nano-SiO_2 filled PBA-a composites…….. 100

5.24 DTG curve and individual contributions of PBA-a, R^2 = 0.9962 (●) experimental data, (○) simulated curve at 10^oC/min, (—) deconvolution of each stage…… 101

5.25 DTG curve and individual contributions of 10wt% nano-SiO_2-filled PBA-a nanocomposites, R^2 = 0.9982 (●) experimental data, (○) simulated curve at 10^oC/min, (—) deconvolution of each stage……. 102

FIGURE **PAGE**

5.26 DTG curve and individual contributions of 20wt% nano-SiO_2-filled PBA-a nanocomposites, $R^2 = 0.9993$ (●) experimental data, (○) simulated curve at 10^oC/min, (—) deconvolution of each stage…….... 103

5.27 DTG curve and individual contributions of 30wt% nano-SiO_2-filled PBA-a nanocomposites, $R^2 = 0.9978$ (●) experimental data, (○) simulated curve at 10^oC/min, (—) deconvolution of each stage…….. 104

5.28 Plots of ln β/T^2_p versus $1000/T_p$ at different heating rates according to Kissinger method for the PBA-a……. 105

5.29 Plots of ln β/T^2_p versus $1000/T_p$ at different heating rates according to Kissinger method for the 10wt% nano-SiO_2-filled PBA-a nanocomposites……... 106

5.30 Plots of ln β/T^2_p versus $1000/T_p$ at different heating rates according to Kissinger method for the 20wt% nano-SiO_2-filled PBA-a nanocomposites…… 107

5.31 Plots of ln β/T^2_p versus $1000/T_p$ at different heating rates according to Kissinger method for the 30wt% nano-SiO2-filled PBA-a nanocomposites…… 108

5.32 Dependence of activation energy (E_a) on degree of the conversion (α) of the weight loss for the main degradation process as determined by Flynn–Wall–Ozawa's method of PBA-a……..... 109

5.33 Dependence of activation energy (E_a) on degree of the conversion (α) of the weight loss for the main degradation process as determined by Flynn–Wall–Ozawa's method of 10wt% nano-SiO_2-filled PBA-a nanocomposites…… 110

5.34 Dependence of activation energy (E_a) on degree of the conversion (α) of the weight loss for the main degradation process as determined by Flynn–Wall–Ozawa's method of 20wt% nano-SiO_2-filled PBA-a nanocomposites…… 111

FIGURE **PAGE**

5.35 Dependence of activation energy (E_a) on degree of the conversion (α) of the weight loss for the main degradation process as determined by Flynn–Wall–Ozawa's method of 30wt% nano-SiO_2-filled PBA-a nanocomposites…… 112

5.36 Integral master plot as a function of α at different mechanism models of the main degradation stage of PBA-a: (—) theoretical model and (●) experimental data. Inset: Integral master plot as a function of α = 0-0.7… 113

5.37 Integral master plot as a function of α at different mechanism models of main degradation stage of 10wt% nano-SiO_2-filled PBA-a nanocomposites:(—) theoretical model and (●) experimental data. Inset: Integral master plot as a function of α =0-0.7……. 114

5.38 Integral master plot as a function of α at different mechanism models of the main degradation stage of 20wt% nano-SiO_2-filled PBA-a nanocomposites: (—) theoretical model and (●) experimental data. Inset: Integral master plot as a function of α =0-0.7……. 115

5.39 Integral master plot as a function of α at different mechanism models of the main degradation stage of 30wt% nano-SiO_2-filled PBA-a nanocomposites: (—) theoretical model and (●) experimental data. Inset: Integral master plot as a function of α =0-0.7……. 116

CHAPTER I

INTRODUCTION

Polymer nanocomposites have been a subject of extensive study owing to their superior performance as compared to conventional filled polymer [1-3]. Firstly, the much higher specific surface area of these materials can promote stress transfer from matrix to nanoparticles. Various studies indicated that nanoparticles can improve Young's modulus of polymers more dramatically than micro-fillers [1-2]. Secondly, the required loadings of nanoparticles in polymer matrices are usually much lower than those of micro-fillers (typically 10–40vol% for the latter) [4]. Therefore, many intrinsic merits of neat polymers, such as low weight, ductility, good processability, as well as transparency will be retained after the addition of nanoparticles. In recent years, nano-SiO_2 [1, 4-6], Clay [7], carbon nanotube [8], carbon black [9], and other nanofillers [2, 10] have been largely used as additive to achieve a significantly improved polymer performance.

Nano-SiO_2 is a very useful reinforcement of thermoplastic [9, 11-12] and thermosetting polymers [1, 4-8] and finds usage as component material for dental filling, electronic packaging, thickeners of paints and coatings, reinforcement of rubbers etc. For industrial applications, nano-SiO_2 particles are often used to reduce the price, and also to improve mechanical and thermal properties of the product. Additionally, nano-SiO_2 particles can be used for reinforcement of polymer matrices to lower shrinkage upon curing, decreasing coefficient of thermal expansion [13], increasing fracture toughness, impact strength, and modulus [1], and improving adhesion property [6]. Concerning their mechanical properties, nano-SiO_2 particles have very high Young's modulus (71.7 GPa), compressive strength >1.1 GPa, and tensile strength 48.3 MPa while it is a relatively light ceramic material because its density is only 2.203 g/cm^3 [14]. To obtain nanocomposite with good mechanical and thermal properties, large amount of silica is usually required, normally 5-30% by weight of total composite composition thus a choice of the matrix resin that can accommodate such high nanofiller loading is crucial to the success of the nanocomposite fabrication [1, 4-6].

A number of papers reported on the improving composite performance by introduction of nano-SiO_2 nanoparticles into thermoplastic [9, 11-12] and thermosetting matrices [1, 4-8]. Thermosetting polymers such as epoxies [1, 4, 6], cyanate esters [5, 7, 13] and phenolic resins [15] have been often used for highly filled composite systems because of their lower viscosity compared to those thermoplastics. Goertzen and Kessler [5] investigated the effect of the distribution of nano-SiO_2 nanoparticles on thermo-mechanical properties of cyanate ester resin. The results revealed that the storage modulus enhancement of the cyanate ester was about 75% at 20.7vol% of the nano-SiO_2. Furthermore, the substantial reduction of the CTE with the nano-SiO_2 content was also observed [13]. However, this system showed only small changes in glass transition temperature (Tg; $\pm$<4^{o}C) for all volume fractions of the filler used. Moreover, the Tg was also adversely affected by a change in humidity. For example, the Tg in 1vol% samples decreased about 2-3^{o}C for a change between 19% and 49% relative humidity [5]. In one of their report, the Tg of nanocomposites was also observed to decrease from 131 to 128^{o}C by an incorporation of the nano-SiO_2 content up to 25 wt% into epoxy matrix [16].

Polybenzoxazines are a relatively novel class of thermosetting phenolic resin that is recently attracting much attention industrially and academically as they possess various advantageous characteristics that overcome the limitations of conventional phenolic and epoxy resins [17-24]. A unique property of benzoxazine monomer is its very low A-stage viscosity. The low viscosity of this monomer gives it excellent processibility for fabrication of highly-filled composite system. In addition, the curing of benzoxazine resins can occur without any acid catalysts or producing any by-products thus minimizing void formation in the cured polymer [20]. Polybenzoxazines have been reported to exhibit a high thermal stability, high glass transition temperature, high modulus, low water absorption, low dielectric constant, and near-zero shrinkage upon curing [17-24]. Moreover, the polymers show a good adhesion with various type of filler such as boron nitride [21] and wood-flour [22], resulting in a substantial restriction of the molecular mobility of the polymer and, thereby, the substantial enhancement in the T_g of the obtained composite materials.

The successful use of polybenzoxazine as a matrix for highly filled composite has also been reported [21-22]. Ishida and Rimdusit [21] investigated the

effect of particle size and its distribution on the thermal conductivity of boron nitride-filled polybenzoxazine. The authors used large aggregates of flake-like boron nitride crystals and were able to make a composite with a maximum filler content up to 78.5vol % (88wt %). The extraordinary high thermal conductivity value of 32.5 W/mK was achieved at the maximum boron nitride content. The ternary systems of benzoxazine, epoxy and phenolic resins were also reported by Jubsilp et al. to be able to accommodate woodflour filler up to 70wt % resulting in a substantial enhancement in flexural modulus and strength as well as glass transition temperature of the wood composites [22].

Though typical bifunctional benzoxazine resins are solid at room temperature, they provide relatively low values of their molten stage or A-stage viscosity. As mentioned previously, a lower viscosity of a resin can enhance an ability of the resin to accommodate greater amount of filler and increase filler wetability of the resin during the preparation of the molding compound. Some previous studies have been done to utilize reactive diluents to lower liquefying temperature as well as to further reduce melt viscosity of the benzoxazine resins. Recently, Jubsilp et al. reported that a monofunctional phenol-aniline type benzoxazine resin (Ph-a) as a reactive diluent for bifunctional benzoxazine resin showed possible effect on curing behaviors of the monomer mixtures. Although a significant reduction in viscosity, liquefying point and curing temperature than that of the neat benzoxazine resin was obtained, the resulting alloy mixtures was reported to render decreasing in thermal stability. In the contrast, a synergistic behavior of glass transition temperature was observed in the alloy of arylamine-based benzoxazine resins and liquid epoxy. Moreover, processing windows of arylamine-based benzoxazine resins was found to be widened with the amount of the epoxy resin which provides sufficient processing window, particularly for the compounding or composite fabrication process to achieve easier handling and increase filler loading [25].

From those interesting characteristic of polybenzoxazine and the epoxy based diluent, they are chosen as a matrix for highly filled nanocomposite of nano-SiO_2. Therefore, the aim of this work is to study the effect of nano-SiO_2 content at a high loading level on major composite properties of the highly processable polybenzoxazine, comparing with the benzoxazine-epoxy copolymers matrix. The

obtained mechanical and thermal performance of their nano-SiO_2 composites will be evaluated.

Ring-opening of the benzoxazine ring at elevated temperatures produces phenolic structures and also create tertiary amine structure in the backbone of the phenolic resin. These tertiary amine groups can catalyze homopolymerization of epoxy groups as reported in several work [26-28]. Rimdusite et al [28] reported that the phenolic hydroxyl groups can react with epoxy resins at elevated temperatures. In the present work, we believed that the ability of the nano-SiO_2 to form Si-O-C bonds with polybenzoxazine or epoxy can significantly alter properties of the matrix in a positive manner, e.g. thermal degradation mechanism.

In general, thermal stability of the polymer composites plays a crucial role in determining their processing and application, because it affects the final properties of the polymer composites such as the upper-limit use temperature and dimensional stability [29]. The knowledge of the kinetic model driving a process provides a valuable insight regarding the reaction mechanism and it is useful for controlling a process, determining optimum processing temperature or for aging [30]. Consequently, the understanding of the thermal stability and thermal decomposition kinetics of materials makes it possible to develop and extend their applications as various industrial fields.

The aim of this study, therefore, is to evaluate the effect of high nano-SiO_2 nanoparticles loading on the thermal decomposition kinetic parameters of the suitable matrix, e.g., activation energy (E_a), pre-exponential factor (A), and the conversion function $f(\alpha)$ by using three well-known methods, i.e. Kissinger method, Flynn-Wall-Ozawa method, Coats-Redfern method and master plots based on the integral form of the kinetic data method. The strong interfacial bonding above should also be more pronounced and clearly seen in the highly filled system of the nano-SiO_2 in the polymer matrix.

1.2 Objectives

1.2.1. To investigate effects of high loading of silica on polybenzoxazines-epoxy matrix.

1.2.2. To examine chemorheological, mechanical, thermal properties of the resulting silica filled polybenzoxazines-epoxy matrix.

1.2.3. To evaluate effects of benzoxazine-epoxy copolymer compositions and on their composites with nano-silica filler.

1.2.4. To study the kinetics of curing and thermal degradation behaviors of the suitable obtained composites.

1.3 Scopes of Research

1.3.1. Synthesis of benzoxazine by a solventless method.

1.3.2. Preparation of copolymer between benzoxazine resins epoxy at various weight ratios.

1.3.3. Preparation of silica filled in benzoxazine resins at various percent by various weight ratios.

1.3.4. Preparation of silica filled in copolymer at various percent by various weight ratios.

1.3.5. Study of functional groups by Fourier Transform Infrared Spectroscope (FTIR).

1.3.6. Evaluation of curing condition and curing behavior by Differential Scanning Calorimeter (DSC).

1.3.7. Study of chemorheological properties by Rheometer.

1.3.8. Measurement of density of nanocomposites by water displacement method.

1.3.9. Investigation of thermal and mechanical properties.

- Dynamic Mechanical Analyzer (DMA).
- Thermal Gravimetric Analyzer (TGA).

1.3.10 Investigation of fracture surface by Scanning Electron Microscope

1.3.11. Analysis of the data and drawing of conclusions.

1.3.12. Preparation of the final report.

1.4 Chemicals and Equipment

1.4.1. Chemicals

- Bisphenol A
- Epoxy Resins based on bisphenol A (EPOTEC YD 126)
- Formaldehyde

- Aniline
- Nano-SiO_2

1.4.2. Equipment

- Hot plate
- Air-circulated oven
- Compression
- Fourier Transform Infrared Spectroscope (FTIR)
- Differential Scanning Calorimeter (DSC)
- Dynamic Mechanical Analyzer (DMA)
- Thermal Gravimetric Analyzer (TGA)
- Thermal Mechanical Analyzer (TMA)

CHAPTER II

THEORY

Many composite materials are composed of just two phases; one is termed the matrix, which is continuous and surrounds the other phase, often called the dispersed phase. The properties of composites are a function of the properties of the constituent phases, their relative amounts, and the geometry of the dispersed phase. "Dispersed phase geometry" in this context means the shape of the particles and the particle size, distribution, and orientation; and structural composites; also, at least two subdivisions exist for each. The dispersed phase for particle-reinforced composites is equated (i.e., particle dimensions are approximately the same in all directions); for fiber-reinforced composites, the dispersed phase has the geometry of a fiber (i.e., a large length-to-diameter ratio). Structural composites are combinations of composites and homogeneous materials [31].

They combine the advantages of the inorganic material (e.g., rigidity, thermal stability) and the organic polymer (e.g., flexibility, dielectric, ductility, and processability). Moreover, they usually also contain special properties of nanofillers leading to materials with improved properties. A defining feature of polymer nanocomposites is that the small size of the fillers leads to a dramatic increase in interfacial area as compared with traditional composites. This interfacial area creates a significant volume fraction of interfacial polymer with properties different from the bulk polymer even at low loadings [32]. In fact, among the numerous inorganic/organic nanocomposites, polymer/silica composites are the most commonly reported in the literature. They have received much attention in recent years and have been employed in a variety of applications. The preparation, characterization, properties, and applications of polymer/silica nanocomposites have become a quickly expanding field of research

2.1 Nanocomposite Materials

2.1.1 Nanoparticle

Nano-SiO_2 was first developed in 1941 by Dr. Harry Klopfer, as he was trying to develop a white reinforcing filler comparable to channel blacks in rubber properties. Nano-SiO_2 is widely used in industry as an active filler for reinforcement of elastomers, as a rheological additive in fluids and as a free flow agent in powders. Typical BET specific surface areas of nano-SiO_2 range from 50 to 400 m^2/ g. Some specific properties of nano-SiO_2 are shown in Table 2.4 [33-34]. Nano-SiO2 is a systhetic amorphous silicon dioxide produced by hydrothermal hydrolysis of chlorosilanes in an oxygen-hydrogen flame (as shown in Figure 2.1)

The first step, SiO_2 molecules are formed which collide and react to nano-size proto particle, which by further collision in a second step form primary particles of around 10 nm in size. The flame process itself leads to the formation of smooth particle surfaces, which provides nano-SiO_2 with a high potential for surface interactions [35-36] as present in Figure 2.2. At the high temperatures of the flame primary particles are not stable but are fused together to form space-filling aggregates. Leaving the flame, at lower temperatures, the silica agglomerates stick together by physic-chemical forces building up large micron-sized agglomerates and finally fluffy flocks [37-38].

$$2H_2 + O_2 \longrightarrow 2H_2O$$

$$SiCl_4 + 2H_2O \longrightarrow SiO_2 + 4HCl$$

$$2H_2 + O_2 + SiCl_4 \xrightarrow{> 1000°C} SiO_2 + 4HCl$$

Figure 2.1 Synthesis method of nano-SiO2 [33].

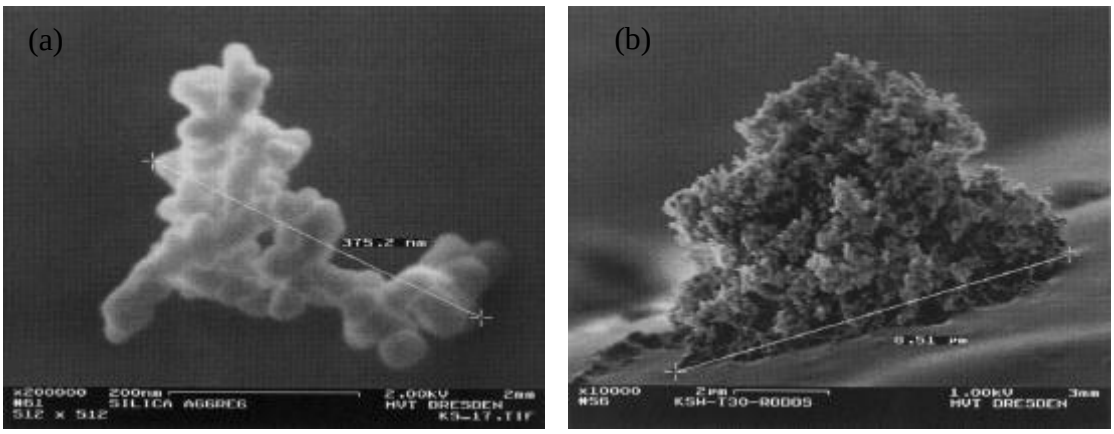

Figure 2.2 SEM images of (a) nano-SiO_2 aggregates and (b) agglomerates [39]

Nano-SiO_2 has been attracting attention as a reinforcing material for polymer because it exhibits a high transparency to light, outstanding electrical properties, and chemical resistance. Nano-SiO_2 has been used as a thixotropy or thickening agent in plastic, adhesives and paints. On these importance properties, nano-SiO_2 is widely used in many industries. The physical properties of nano-SiO_2 are shown in Table 2.1

Table 2.1 Properties of nano-SiO_2 [33].

Property	**Value**
Chemical formula	SiO_2
Density	2-2.2 g/cm^3
Decomposition temperature	> 2000 °C
Moisture content	
-hydrophilic	0.5-2.5 %
-hydrophobic	0.5%
Particle size primary	5-40 nm
Specific surface area	50-400 m^2/g
Refractive index	1.46

At present, nano-SiO_2 is evaluated as a reinforcement to improve materials properties including increase in mechanical strength, modulus, ductility and flame retardant. The structure of nanosilica shows a three-dimensional network. Silanol and siloxane groups are created on the silica surface, leading to hydrophilic nature of the particles. The surfaces of the silica are typically terminated with three silanol types: free or isolated silanols, hydrogen-bonded or vicinal silanols and geminal silanols (Figure 2.3) [39]. The silanol groups residing on adjacent particles, in turn, form hydrogen bonds and lead to formation of aggregates, as shown in Figure 2.4. These bonds hold individual nano-SiO_2 particles together and the aggregates remain intact even under the best mixing conditions if stronger filler-polymer interaction is not present [40].

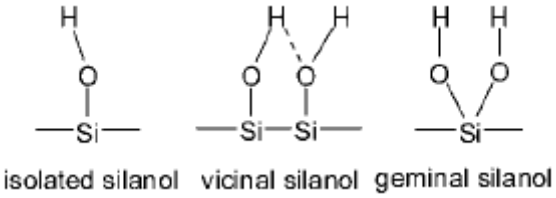

Figure 2.3 Schematic illustrations of three types of surface silanol [39].

Figure 2.4 Schematic of aggregate formation between adjacent nano-SiO_2 particles through hydrogen bonding among the silanol Groups [40]

The dispersion of nanometer-sized particles in the polymer matrix has a significant impact on the properties of nanocomposites. A good dispersion may be achieved by surface chemical modification of the nanoparticles or physical methods such as a high-energy ball-milling process and ultrasonic treatment. The great differences in the properties of polymer and silica materials can often cause phase separation. Therefore, the interfacial interaction between two phases of nanocomposites is the most decisive factor affecting the properties of the resulting materials. A variety of methods have been used to enhance the compatibility between the polymer (hydrophobic) and nanosilica. The most frequently used method is to modify the surface of silica nanoparticles (especially for the blending and in situ method), which can also improve the dispersion of nanosilica in the polymer matrix at the same time. In general, surface modification of nanosilica can be carried out by either chemical or physical methods [10].

2.1.2 Matrix

Polybenzoxazine is a newly developed class of thermosetting resin with interesting properties that are based on the ring opening polymerization of benzoxazine precursors. As a novel class of phenolic resin, it has been developed and studied to overcome several short comings of conventional novolac and resole-type phenolic resin. Polybenzoxazine resins are expected to replace traditional phenolic, polyesters, vinyl esters, epoxies, BMI, cyanate esters and polyimides in many respects [41]. The mechanical and physical properties can be tailored to various needs. The material can be synthesized using the patented solventless technology to yield a relatively clean precursor without the need of solvent elimination or monomer purification [24].

Polybenzoxazine can be synthesized from inexpensive raw materials and can be cured without the use of strong acid or base catalyst. The crosslinking reaction of the resin is through thermally activated ring-opening reaction; therefore, it does not release by-products during the polymerization. The material has excellent properties commonly found in traditional phenolic resins such as high thermal stability, flame retardance, dimensional stability, low viscosity, near-zero shrinkage upon polymerization, low water absorption, excellent electrical properties, high mechanical integrity, glass transition temperatures much higher than cure temperature, fast mechanical property build-up as a function of degree of polymerization, high modulus and high char-yield. Furthermore, the ability of benzoxazine resin to be alloyed with other polymers renders the resin with even broader range of applications [19, 20, 42].

Benzoxazine resin based on bisphenol-A and aniline is synthesized according to the following reaction scheme as shown in Figure 2.5 [43].

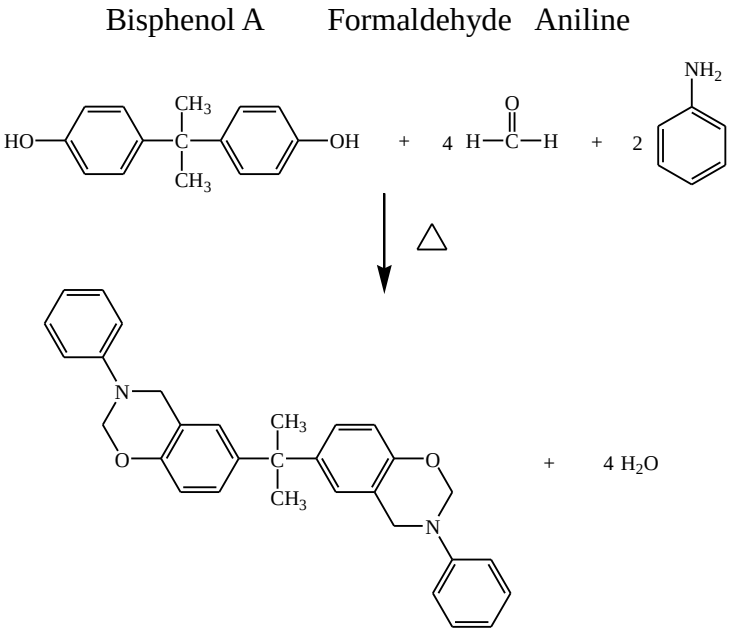

Figure 2.5 Synthesis of bifunctional benzoxazine monomer

The properties of polybenzoxazines compared with those of the state of art matrices were depicted in Table 2.2. Polybenzoxazines present the highest tensile properties. Their results from dynamic mechanical analysis reveal that these candidate resins for composite applications possess high moduli and glass transition temperatures, at low cross-link densities. Long-term immersion studies indicate that these materials have a low rate of water absorption and low saturation content. Impact, tensile, and flexural properties are also good [42].

Table 2.2 Comparative properties of various high performance polymers [42].

Property	Epoxy	Phenolics	Toughened BMI	Bisoxphen (40:60)	Cyanate ester	P-T resin	Polybenzoxazine
Density (g/cc)	1.2-1.25	1.24-1.32	1.2-1.3	1.3	1.1-1.35	1.25	1.19
Max use temperature (°C)	180	~200	200	250	150-200	300-350	130-280
Tensile strength (MPa)	90-120	24-25	50-90	91	70-130	42	100-125
Elongation (%)	3-4.3	0.3	3	1.8	0.2-0.4	2	2.3-2.9
Dielectric constant (1MHz)	3.8-4.5	0.4-10	3.4-3.7	-	2.7-3.0	3.1	3-3.5
Cure temperature (°C)	RT-180	150-190	220-300	175-225	180-250	177-316	160-220
Cure shrinkage (%)	>3	0.002	0.007	<1	~3	~3	~0
TGA onset (°C)	260-340	300-360	360-400	370-390	400-420	410-450	380-400
Tg (°C)	150-220	170	230-380	160-295	250-270	300-400	170-340
G_{IC} (J/m^2)	54-100	-	160-250	157-223	-	-	168
K_{IC} (MPa $m^{1/2}$)	0.6	-	0.85	-	-	-	0/94

Bismaleimide (BMI), Bisoxazoline-phenolics (Bisox-phen), Phenolic-triazine resin (P-T resin), Thermogrvimetric analysis (TGA), Fracture energy (G_{IC}), Fracture toughness plain-strain stress intensity factor

2.1.3 Reactive diluent

The generalized structure for an epoxy resin is given in Figure 2.6. The epoxy, epoxide or oxirane group is a three-membered ring consisting of two carbon atoms and one oxygen atom. Figure 2.7 also summarizes the major types of commercial epoxy resin.

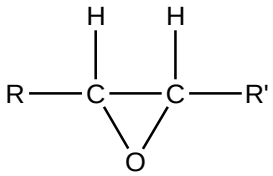

Figure 2.6 General structure of an epoxy resin [44].

Three major types of epoxy resins include

1. Cycloaliphatic epoxy resins (R and R′ are part of a six-membered ring).

2. Epoxidized oils (R and R′ are fragments of an unsaturated fatty acid, such as oleic acid in soybean oil).

3. Glycidated resins (R is hydrogen and R′ can be a polyhydroxyphenol, polybasic acid, or polyamine). There are the epoxides used in most commercial application.

Figure 2.7 gives the structures of cycloaliphatic epoxy resin, epoxidized soybean oil, glycidated polybasic acid, aromatic polyamine (methylene dianiline), and bisphenol A, bisphenol-A based epoxy resin.

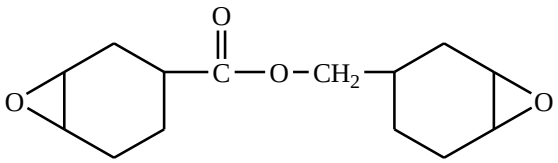

Cycloaliphatic Resin

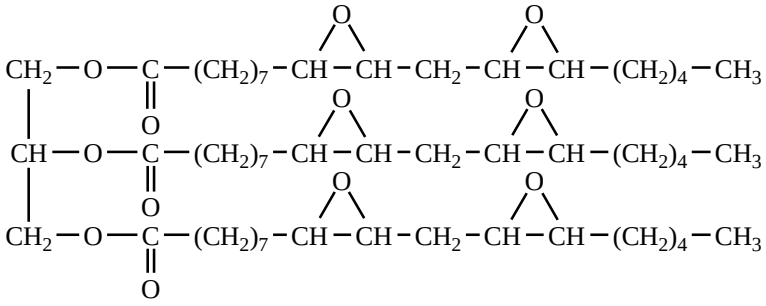

Epoxidized Soybean Oil [45]

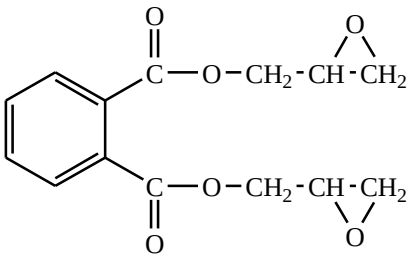

Glycidated Polybasic Acid

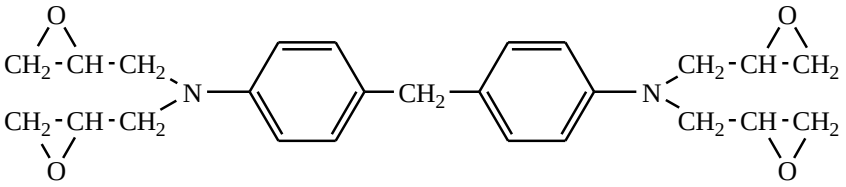

Glycidated Polyamine

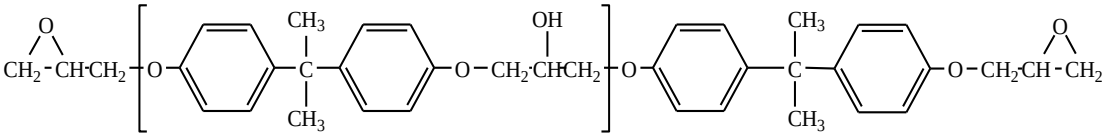

Glycidated Bisphenol A

Figure 2.7 Major types of commercial epoxy resins.

Generically epoxy resins can be characterized as a group of oligomeric materials which contain one or more epoxy (oxirane) groups per molecule. The value of epoxy resins is that they can be processed into a variety of useful products such as protective coating, adhesives, and structural components of almost any size and shape by reacting the epoxy groups with an appropriate curing agent. The products obtained from epoxy resins containing more than one epoxy group per molecule are called thermosetting polymers. Figure 2.8 exhibits contribution of chemical moieties in epoxy molecule on its properties.

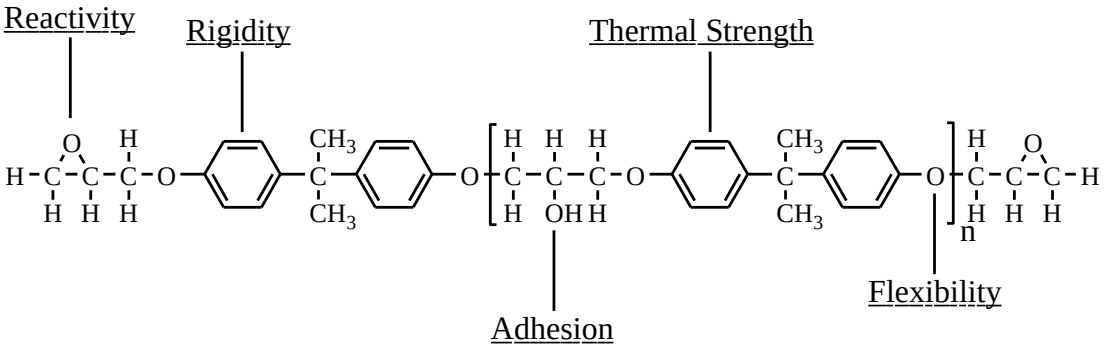

Figure 2.8 Sources of epoxy properties [46].

Basic characteristics of epoxy resins are: [44]

1. Excellent adhesion to a variety of substrates and reinforcements.
2. Low shrinkage on cure.
3. No cure volatiles.
4. Outstanding mechanical and electrical properties.
5. Good chemical resistance and solvent resistance.
6. Thermal stability.
7. Good moisture resistance.
8. Good dimension stability and fatigue resistance.
9. Versatility i.e. many modes of cure, many resin types available and wide range of modifications possible.

The choice of resin and curing agent depends on the application and on handling characteristic (viscosity, pot life, gel time); curing temperature and time; use

properties (mechanical, chemical, thermal and electrical); toxicological and environmental limits; as well as cost. A description of major epoxy curing agents is given in Table 2.3.

Table 2.3 Curing agents for epoxy resins [47].

Type	**Advantages**	**Disadvantages**	**Applications**
Aliphatic amines	low viscosity; ambient cure temperature; little color	short pot life; rapid heat evolution;critical mix ratio; moderately toxic; high moisture absorption	adhesives; small castings;electrical encapsulation; civil engineering
Aromatic amines	good elevated temperature performance; good chemical resistance; long pot life; low moisture absorption	incompatibility with epoxy resins; long cure cycles at high temperature; toxicity	high performance composites and coatings; adhesives; filament winding; electrical encapsulation
Polyamidoamines	low viscosity; ambient cure temperature; good mix ratios, mechanical properties, and pot life	poor performance at high temperature	construction adhesives; sealants; floorings; concrete bonding
Polyamides	good mix ratios, pot life,flexibility, toughness, and corrosion resistance; ambient cure temperature; low toxicity	low temperature performance; high viscosity; poor color	maintenance coatings; castings;trade sale paints; adhesives; marine coatings

In this investigation, liquid epoxy resin, grade EPOTEC YD 126, is selected as a base resin to be alloyed with benzoxazine resins. EPOTEC YD 126 is an unmodified liquid epoxy resin reaction product of Bisphenol A and epichlorohydrin. When cross- linked or hardened with appropriate curing agents, very good mechanical, adhesive, dielectric and chemical resistance properties can be obtained. The structure and the typical properties of EPOTEC YD 126 are shown in Figure 2.9 and summarized in Table 2.4 respectively.

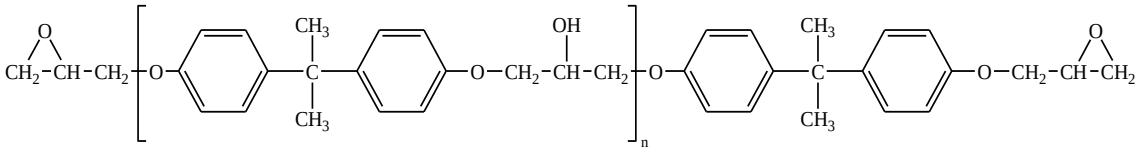

Figure 2.9 The structure of EPOTEC YD 126 [48].

Table 2.4 Typical properties of EPOTEC YD 126 [49].

Property	Test method	Unit	Specification
Epoxy equivalent weight	DIN 16945/4.15B (89) TEC-AS-C-002	g/eq	178-186
Viscosity @ 25 ^{0}C	ASTM D-1545 (89)	cps	7,500-10,000
Color	ASTM D-1544 (89) TEC-AS-P-006	Gardner	Max. 0.5
Softening point	JIS K 7234 (86) ASTM E 28-67 (82)	^{o}C	65 - 75

2.2 Fundamentals of Particle Packing Characteristics [50]

In order to achieve maximum filler packing in the composites, characteristics of the particulate filler are known to play a crucial role in this purpose. This section summarizes major features of the particulate filler to provide maximum packing density value in composite materials. The detail discussion on particle packing characteristics can be further studied in an excellent monograph by German [50].

For monosized spheres, the fractional packing density is between 0.60 and 0.64 [50]. In the case of the actual density, the value depends on the filler characteristics, namely the size and shape, and factors including the adsorbed moisture. The packing density

ranges from 30 to 65% of theoretical value; the lower value is representative of irregular and sponge filler.

Figure 2.10 gives the fractional packing density for various monosized irregular particle shapes. The figure reveals that interparticle friction depends on particle surface irregularities. The greater the surface roughness or the more irregular the particle shape, the lower the packing density as the shape departs from equiaxed (spherical). As the particle shapes become more rounded (spherical) the packing density increases.

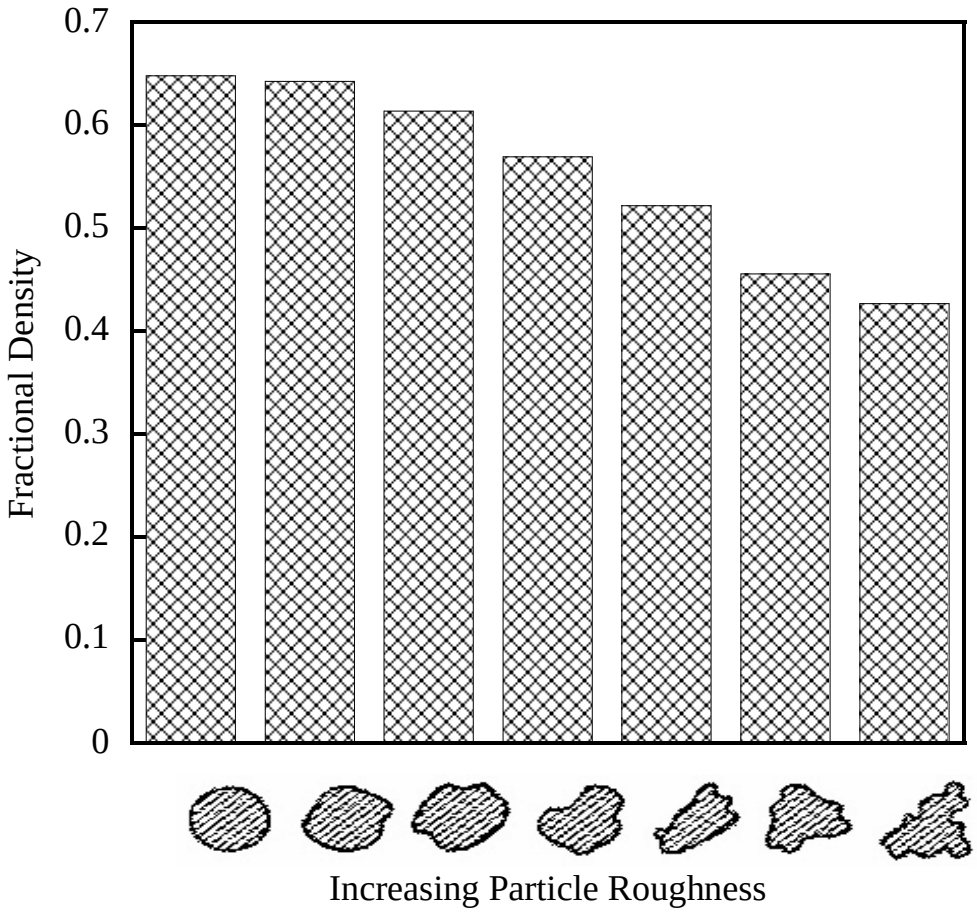

Figure 2.10 Fractional density for monosized powders versus roughness as expressed by a typical particle profile.

Furthermore, the packing of fibers provides an illustration of a decreasing packing density as the particles have a larger length to diameter or the aspect ratio (L/D). Figure 2.11 plots the fractional packing density versus the length to diameter ratio for

fibers. Obviously, fractional packing density improves as the particles approach a smooth, equiaxed shape.

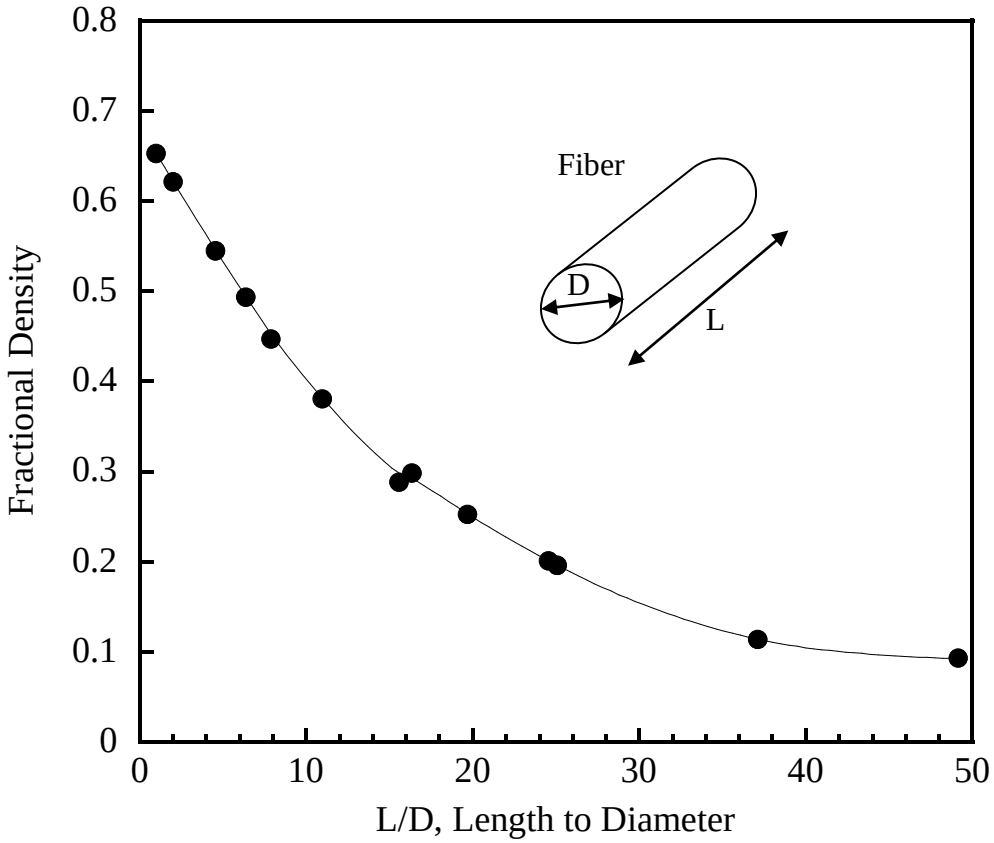

Figure 2.11 A change in packing density with the length to diameter ratio (L/D) for fibers. (i.e. best packing occurs with equiaxed particles).

To overcome the packing limits of particulate filler, we can tailor the particle size distribution for greater packing density. Bimodal particle size mixtures can pack to higher densities than monosized particles. The key to improved packing then rests with the particle size ratio. In principle, small particles are selected to fit the interstices between large particles without forcing the large particles apart. In addition, even smaller particles can be chosen to fit into the remaining pores, giving a corresponding enhancement in the particle packing density or the reduction of the void volume between the particles. The basis of the phenomenon is illustrated in Figure 2.12. In the figure, the fractional density is shown as a function of composition

for a mixture of large and small particulate spheres. At the maximum packing composition, there is a greater volume of large particles than small particles. The relative improvement in packing density depends primarily on the particle size ratio of the large and small particles. Within a limited range, the greater the size ratio shows the higher the maximum packing density [50].

Starting with the large particles, the packing density initially increases as small particles are incorporated to fill the voids between the large particles. That corresponds to the right hand side of Figure 2.12. Eventually, the quantity of small particles fills all of the spaces between the large particles. On the other hand, beginning with the small particles, clusters of small particles and their associated voids can be eliminated and replaced with a full density region everywhere when a large particle is added. The packing benefit of replacing small particles with the large particle continues until a concentration where the large particles contact one another. Figure 2.12 shows this process on the left hand side of the curve. The point of maximum packing density corresponds to the intersection of those two curves. At this point, the large particles are in point contact with one another and all of the interstitial voids are filled with the small particles. The optimal composition in terms of the weight fraction of large particle X^* depends on the amount of void spaces between large particles, which equals $(1\text{-}f_L)$, where f_L is the fractional packing density of the large particles [50],

$$X^* = f_L / f^* \tag{2.1}$$

With the packing density at the optimal composition f* given as,

$$f^* = f_L + f_S(1 - f_L) \tag{2.2}$$

And the fraction packing density for the small particle is f_S.

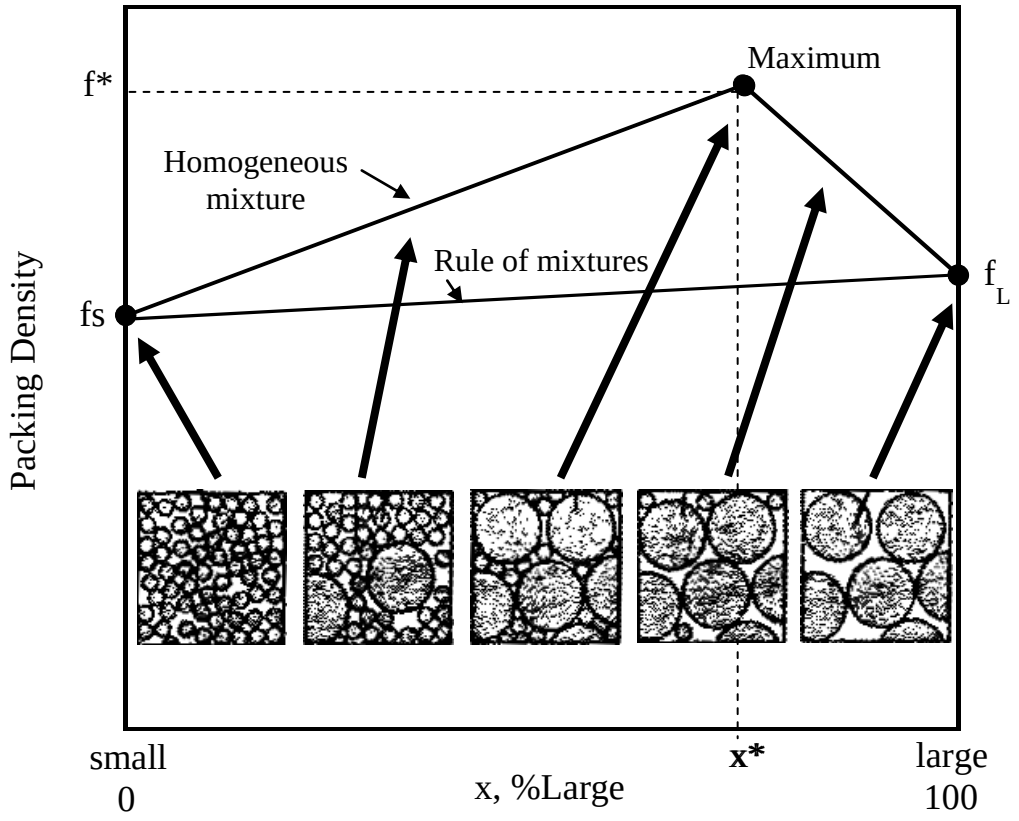

Figure 2.12 Plot of fractional packing density versus composition for bimodal mixtures of large and small spheres.

The ideal fractional density of each of spherical particle, i.e., large and small particle sizes, can pack to obtain the maximum packing density is 0.637. To require the maximum packing density value higher than 0.637, if the corresponding mass fraction of large particle for maximum packing is 0.734, while the mass fraction of the small particle sizes is of 0.266,the expected fractional packing density would be 0.86 [50].

Figure 2.13 illustrates how the packing density increases with the particle size ratio (large diameter divided by small diameter). Note the dramatic change in behavior at the particle size ratio corresponding to one particle filling the triangular pores between the large particles at roughly a 7:1 size ratio. In principle, increasing the packing density will increase with the homogeneity of the mixture. In practice,

randomly mixed systems will have property range between unmixed and fully mixed, and typically exhibit some inhomogeneities that deviate actual packing from the ideal. Analogous to the behavior of spheres, a density increase is associated with blending different particle sizes of similar shapes. However, a major difference between spherical and nonspherical particles is that the initial packing is generally higher for spheres. The greater the surface roughness, shape irregularity, or particle aspect ratio will lead to the lower the inherent packing density

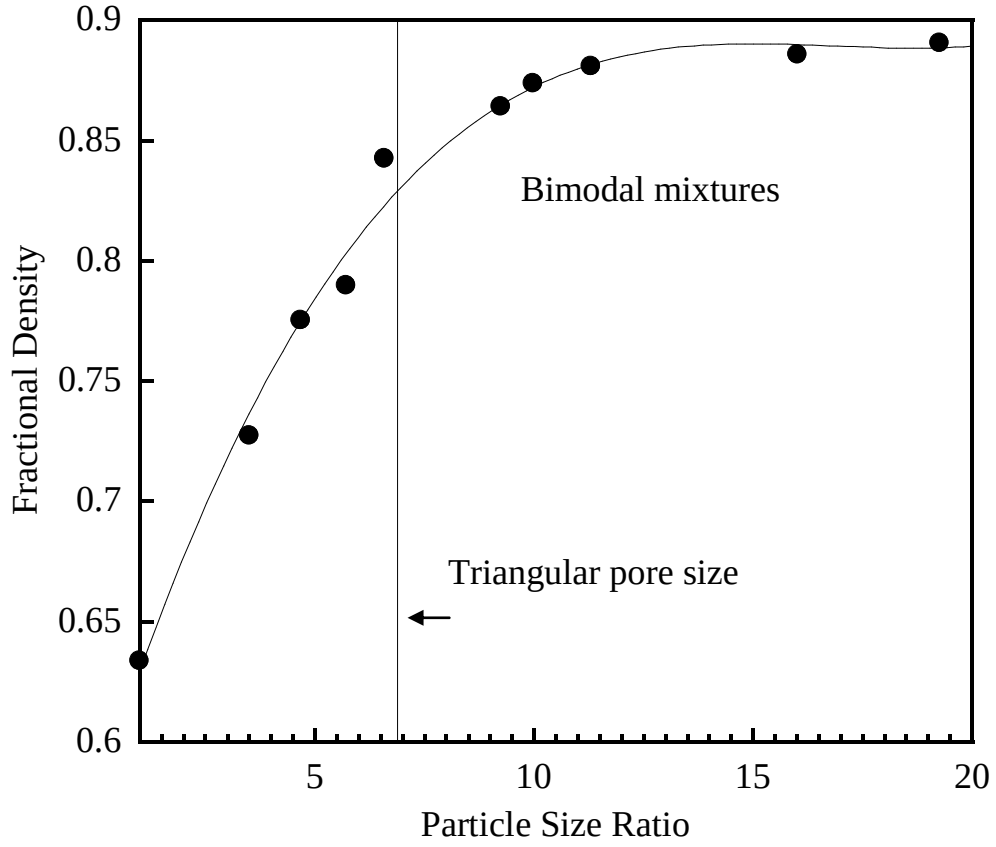

Figure 2.13 Effect of particle size ratio on the packing density for mixtures consisting of 70% large particles and 30% small particles.

Though the relative density gain is similar for spherical and nonspherical particles, the starting density for these types of particles is lower. Accordingly, at all compositions, the nonspherical mixture will be lower in density. The ideas developed for bimodal mixtures can be extended to multimodal systems, as seen in Table 2.5.

Table 2.5 Effect of particle size distribution on packing density showing relation between particle size ratio and maximum packing density

Number of component	Size ratio	Weight percent	Packing fraction
1	-	100	0.64
2	7 : 1	73 : 27	0.86
3	49 : 7 : 1	75 : 14 : 11	0.95
4	343 : 49 : 7 : 1	73 : 14 : 10 : 3	0.98

2.3 **Theory/calculation of thermal degradation mechanism [51-53]**

The kinetic analysis of a thermal degradation process shall begin by expressing the reaction rate by a general Eq. (2.3) such that:

$$\frac{d\alpha}{dt} = k(T)f(\alpha) \tag{2.3}$$

For non-isotheral thermogravimetric analysis, the fraction of decomposition (α) is defined as the ratio of weight loss of time t to total weight loss at complete decomposition temperature as show in Eq. (2.4)

$$\alpha = \frac{(M_0 - M_t)}{(M_0 - M_f)} \tag{2.4}$$

Where M_0 is the initial weight of the sample, M_t is the weight of sample at time t, M_f is the final weight of completely decomposed sample

The function k(T) is always described by the Arrhenius expression:

$$k(T) = A\exp(-E_a/RT) \tag{2.5}$$

Substituting k(T) from Eq. (2.5) into Eq. (2.3) one obtains:

$$\frac{d\alpha}{dt} = A\exp(-E_a/RT)f(\alpha) \tag{2.6}$$

According to non-isothermal kinetic theory, thermal degradation at a constant heating rate, ($\beta = dT/dt$) can be expressed by Eq. (2.7)

$$\frac{d\alpha}{dT} = \frac{A}{\beta}\exp(-E_a/RT)f(\alpha) \tag{2.7}$$

Where f (α) is the differential expression of a kinetic model function, α is the conversion, β is the heating rate (K min^{-1}), E_a and A are the so-called activation

energy (kJ/mol) and pre-exponential factor (min^{-1}) for the decomposition reaction, respectively. R is the gas constant (8.314 $Jmol^{-1}K^{-1}$). Generally, E_a can be calculated by using three well-known methods for dynamic heating experiment, i.e. Kissinger method, Flynn-Wall-Ozawa method, and Coats-Redfern method.

2.3.1 Kissinger method (Differential method) [54-55]

Kissinger method uses Eq. (2.7) to determine the E_a of solid state reactions.

$$\ln\left(\frac{\beta}{T^2}\right) = \ln\frac{AR}{E_a} + \ln\left[n\left(1-\alpha_p\right)^{n-1}\right] - \frac{E_a}{RT_p} \qquad (2.8)$$

Where T_p and α_p are the absolute temperature and weight loss at maximum weight loss rate $(\alpha_p/dt)_p$, respectively, and n is the reaction order. From the slope of the straight line $\ln(\alpha_p/T^2)$ versus $1/T_p$, the E_a can be obtained. The advantage of the Kissinger model is that the E_a can be obtained without the knowledge of any thermal degradation reaction mechanism in advance.

2.3.2 Flynn-Wall-Ozawa method (Integration method) [54, 56]

Flynn-Wall-Ozawa method can be employed to quantify E_a without any knowledge of the reaction mechanisms. The main advantage of this method is that it is not based on any assumption concerning the temperature integral, giving, thus, a higher degree of precision to the results. From Eq (2.7), it can be integrated using the Doyle approximation [55]. The result of the integration after taking logarithms is

$$\log\beta = \log\frac{AE_a}{g(\alpha)} - 2.315 - \frac{0.457E_a}{RT} \qquad (2.9)$$

The E_a of the thermal degradation process of the blending system was determined from the slope of the straight line log α versus 1/T.

For degradation behaviour, the data were fitted with different model as shown in Table 2.6 [51-53]. The degradation model is selected by Coats-Redfern method and master plot based on the integral form of kinetic data method.

2.3.3. Coats-Redfern method [54, 57]

Besides the above two methods, Coats-Redfern method is often used in kinetic analysis of solid state processes. Coats-Redfern method is presented in Eq. (2.10).

$$\ln\frac{g(\alpha)}{T^2}=\ln\left(\frac{AR}{\beta E_a}\right)-\frac{E_a}{RT} \tag{2.10}$$

From the slope of the straight line $\ln[g(\alpha)/T^2]$ versus 1/T, E_a can be calculated and A can be obtained from the intercept, i.e. from $\ln(AR/\beta E_a)$

2.3.4 Master plot based on the integral form of kinetic data [58]

The kinetic rate equation at infinite temperature is obtained by introducing the generalized time, θ , which is defined as ref [58]:

$$\theta=\int_0^t \exp\left(-\frac{E_a}{RT}\right)dt \tag{2.11}$$

Where θ denotes the reaction time considered to attain a particular at infinite temperature. Differentiation of Eq. (2.11) leads to the following relation:

$$\frac{d\theta}{dt}=\exp\left(-\frac{E_a}{RT}\right) \tag{2.12}$$

Combining Eq. (2.6) and (2.12), the following expression is obtained

$$\frac{d\alpha}{d\theta}=Af(\alpha) \tag{2.13}$$

$$\frac{d\alpha}{d\theta}=\frac{d\alpha}{dt}\exp\left(\frac{E_a}{RT}\right) \tag{2.14}$$

Where $d\alpha/d\theta$ correspond to the generalized reaction rate, obtained by extrapolating of the reaction rate in real time, $d\alpha/dt$, to infinite temperature. The integrated form of the kinetic rate equation could also be given from Eq. (2.15) as follows:

$$g(\alpha)=\int_0^\alpha \frac{d\alpha}{f(\alpha)}=A\int_0^\theta d\theta=A\theta \tag{2.15}$$

From the integral kinetic equation at infinite temperature in integral form, Eq. (2.15), we can obtain the following equation using a reference point at $\alpha = 0.5$

$$\frac{g(\alpha)}{g(0.5)}=\frac{\theta(\alpha)}{\theta(0.5)} \tag{2.16}$$

Where $\theta = 0.5$ is the generalized time at $\alpha = 0.5$

Table 2.6 Algebraic expressions of f(α) and g(α) for the reaction models [51-53].

Symbol	Reaction model	f(α)	g(α)
P3	Power law	$3\alpha^{2/3}$	$\alpha^{1/3}$
P4	Power law	$4\alpha^{3/4}$	$\alpha^{1/4}$
F1	Random nucleation with one nucleus on the individual particle	$1-\alpha$	$-\ln(1-\alpha)$
F2	Random nucleation with two nucleus on the individual particle	$(1-\alpha)^2$	$(1-\alpha)^{-1}-1$
F3	Random nucleation with three nucleus on the individual particle	$(1-\alpha)^3$	$\frac{1}{2}\left((1-\alpha)^{-2}-1\right)$
A2	Nucleation and growth (Avrami equation(n=2))	$2(1-\alpha)[-\ln(1-\alpha)]^{1/2}$	$[-\ln(1-\alpha)]^{1/2}$
A3	Nucleation and growth (Avrami equation(n=3))	$3(1-\alpha)[-\ln(1-\alpha)]^{2/3}$	$[-\ln(1-\alpha)]^{1/3}$
A4	Nucleation and growth (Avrami equation(n=4))	$4(1-\alpha)[-\ln(1-\alpha)]^{3/4}$	$[-\ln(1-\alpha)]^{1/4}$
D2	Two-dimensional diffusion (Valensi equation)	$[-\ln(1-\alpha)]^{-1}$	$(1-\alpha)\ln(1-\alpha)+\alpha$
D3	Three-dimensional diffusion(Jander equation)	$(3/2)[1-(1-\alpha)^{1/3}]^{-1}(1-\alpha)^{2/3}$	$[1-(1-\alpha)^{1/3}]^2$
R2	Phase boundary controlled reaction (contracting area)	$2(1-\alpha)^{1/2}$	$[1-(1-\alpha)^{1/2}]$
R3	Phase boundary controlled reaction (contracting volume)	$3(1-\alpha)^{2/3}$	$[1-(1-\alpha)^{1/3}]$

CHAPTER III

LITERATURE REVIEWS

Highly filled composites were achieved in many filler types by using benzoxazine as the matrix because the high processability characteristics of benzoxazine resins. One outstanding characteristic of benzoxazine resins in term of their procesability is their ease of monomer synthesis from an invention of the solventless technology by Ishida [24]. In addition, the as-synthesized monomers from the solventless synthesis have been shown to yield monomers of relatively high purity with low content of oligomers or other high molecular weight species. Consequently, even the as-synthesized monomers can provide a highly desirable low A-stage viscosity value. Solid-state ^{1}H-NMR spectroscopy is very useful for the study of the benzoxazine chemical structure and the purity of benzoxazine monomer simultaneously. For example, the structure of as-synthesized bisphenol a – aniline type benzoxazine monomer (BA-a) was investigated by Kasemsiri et al. using ^{1}H-NMR spectrum as shown in Figure 3.1 [59]. The methyl proton of bisphenol-A showed the signal at 1.58 ppm (a). The characteristic peaks assignable to methylene (Ar–CH_2–N) of oxazine ring and methylene (O–CH_2–N) were observed at 4.53 (b) and 5.24 ppm (c), respectively. The group of signals at 6.87-7.83 ppm (d) exhibits aromatic proton. Moreover, the disappearance of signal at 3.6 ppm suggested that the obtained monomers exhibited negligible quantity of methylene proton of either opening ring dimers or oligomers [23, 60]. Therefore, the spectra suggested that the as-synthesized benzoxazine resin is highly pure.

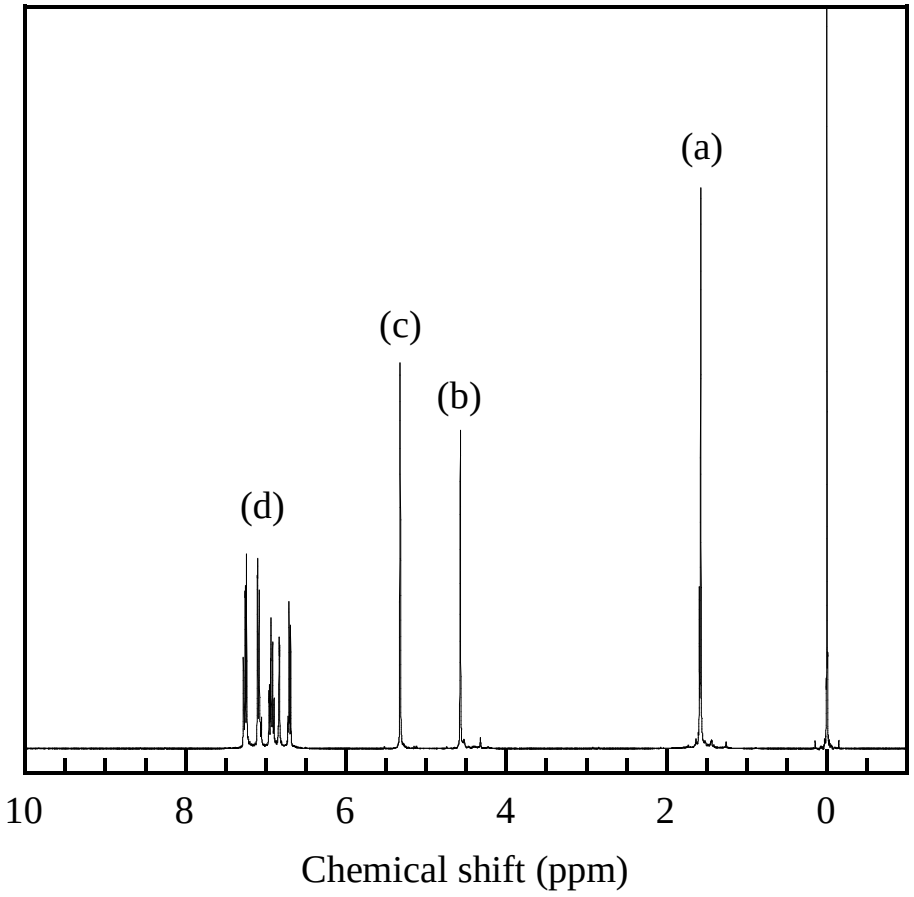

Figure 3.1 ^{1}H-NMR of the benzoxazine monomer.

Figure 3.2 exhibits the processing window of the BA-a based benzoxazine which is solid at room temperature. The viscosity of the resin initially decreases due to heating past its liquefying or softening point to reach its minimum value. At the point of minimum viscosity, the resin can conveniently be processed or transferred into the mold. In the highly filled composite manufacturing process, the low melt viscosity resins are required in typical formulations to achieve easier handling, and to increase filler loading. The softening temperature of the BA-a monomers was determined to be 76^{o}C at the viscosity of 500 Pa.s. The incorporation of the liquid Ph-a in the solid BA-a resin yielded a softer solid at room temperature, ranging from BP91 to BP64 as presented in Figure 3.2. Lowering the resin liquefying temperature enables the use of lower processing temperatures for a compounding process, which is

also highly desirable in most composite applications [25].

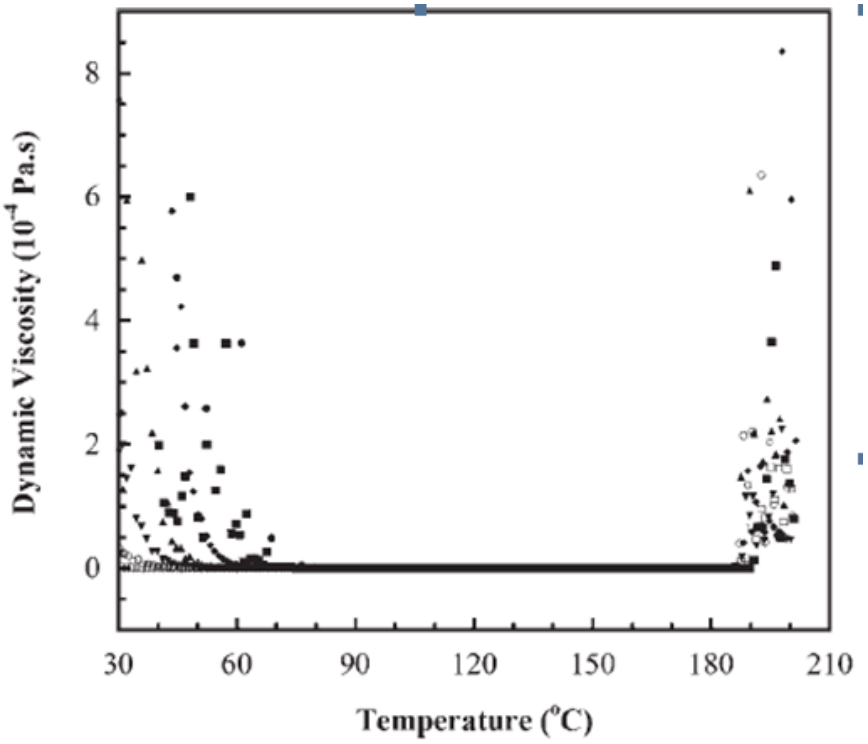

Figure 3.2 Processing window of BA-a (B)/Ph-a (P) resin mixtures at various Ph-a resin using a heating rate 2^{o}C/min: (●) BA-a resin, (■) BP91, (♦) BP82, (▲) BP73, (▼) BP64, (◣) BP55, (◢) Ph-a resin.

Epoxy resins are used as co-matrix to carry out the inclusion of high loading. Because it is liquid at room temperature. Moreover, copolymerization of the polybenzoxazine precursor with an epoxy may allow the network structure to achieve a higher crosslink density. Because the ring-opening polymerization of benzoxazine produces phenolic groups, which can react with epoxy resins at elevated temperatures, additional crosslink points are introduced into the matrix [61]. In addition, the ring-opening also produces tertiary amine structure in the backbone of the phenolic resin. These tertiary amine groups can catalyze homopolymerization of epoxy groups as shown in Figure 3.3.

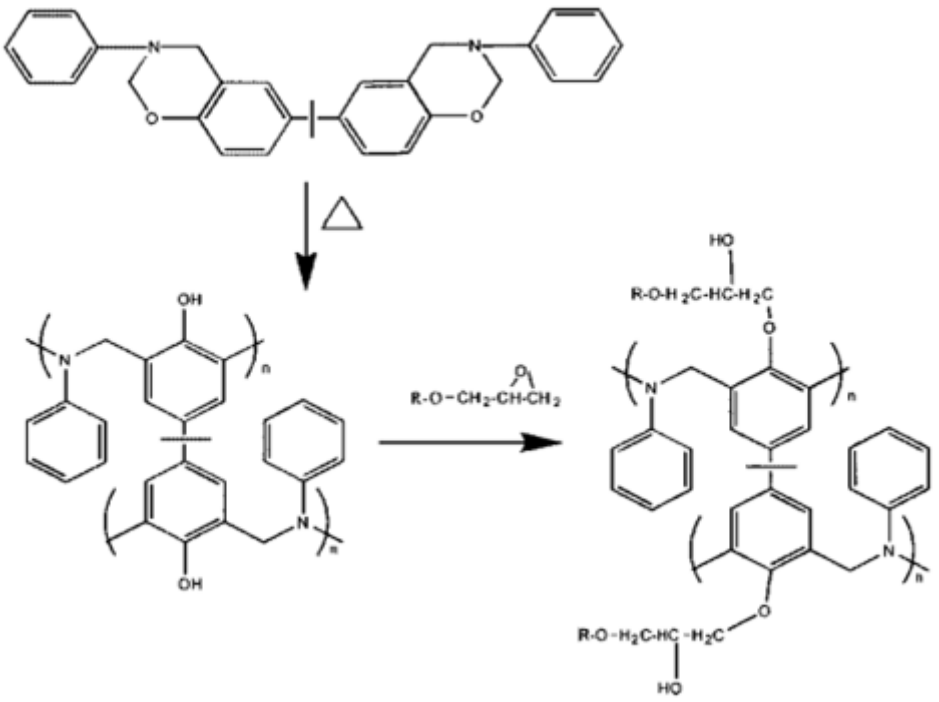

Figure 3.3 Reaction of benzoxazine with epoxy.

Benzoxazines were first copolymerized with an epoxy resin in order to modify their performance by Ishida et al. [27]. The addition of epoxy to the polybenzoxazine network greatly increases the crosslink density of the thermosetting matrix and strongly influences its mechanical properties. Copolymerization led to significant increase in the glass transition temperature, flexural stress, and flexural strain at break above those of the polybenzoxazine homopolymer, with only a minimal loss of stiffness. Copolymers from polybenzoxazines and epoxy resins were also designed keeping in mind that the ring opening reactions of benzoxazines produces phenolic hydroxyl groups, which can react with epoxy resins and provide additional cross-linking points into the matrix offer a network structure. Moreover, the viscosity of the arylamine-based benzoxazine monomer mixture can be significantly lowered comparing at the same temperature by using an epoxy as a diluent as shown in Figure 3.4 in case of the BA-35x-based benzoxazine monomer mixture. Based on the same convention, the liquefying temperature or transition of solid to liquid of the resin mixtures was decreased with an increasing amount of the epoxy resin from 0 to 40 wt% in the resin mixture. The gel temperatures of mixtures systematically shifted

to higher temperatures with the amount of the epoxy. Therefore, the processing window of the mixtures was widened by the amount of the epoxy resin. In other words, the processing window of each benzoxazine resin can be partly controlled by adding appropriate amount of epoxy. All resins are low-viscosity liquid within the temperature range of 100 to 175^{o}C which provides sufficient processing window, particularly for the compounding or composite fabrication process [62].

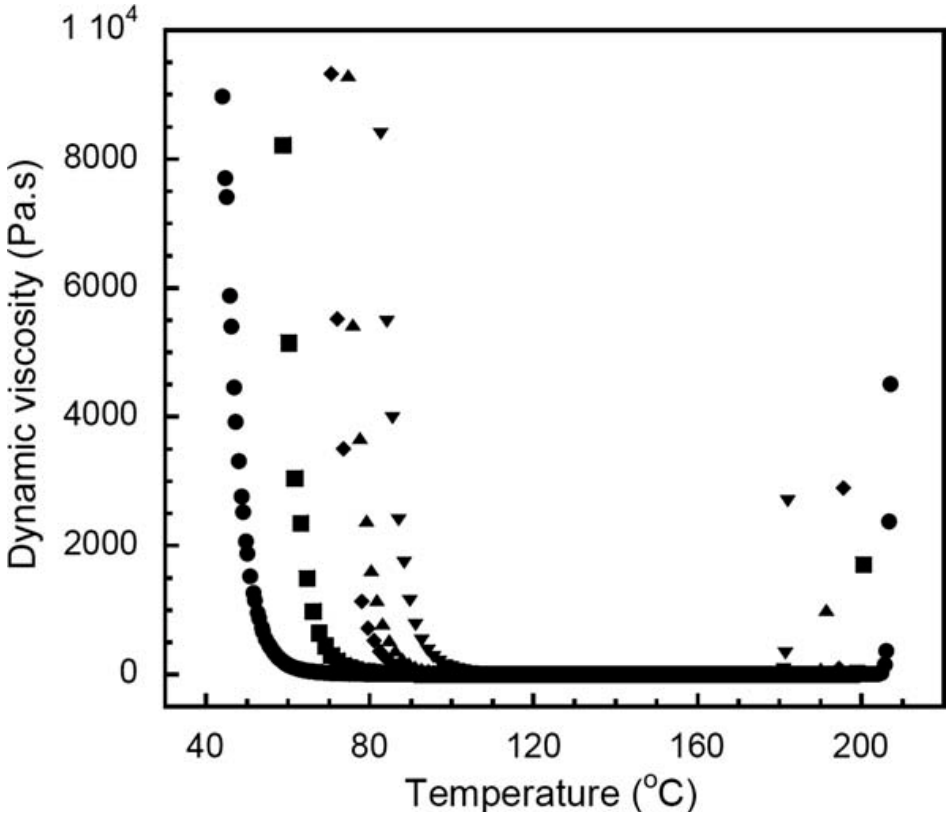

Figure 3.4 Processing window of BA-35x mixed with epoxy resin at various compositions: (●) 60:40, (■) 70:30, (♦) 80:20, (▲) 90:10, and (▼) neat BA-35x.

Generally, epoxy resin shows good mechanical strength and chemical resistance, but the properties depend on the type or quantity of hardeners or curing conditions. H. Kimura et al [61] investigated the curing reaction of epoxy resin using bisphenol A-based benzoxazine as a hardener and the properties of the cured epoxy resin. As a result, the molding compound showed good thermal stability under 150^{o}C. Above 150^{o}C, the curing reaction proceeded without curing accelerators. The epoxy resin cured by bisphenol A-based benzoxazine had superior heat resistance water resistance, and electrical insulation to those of the epoxy resin cured by bisphenol A

type novolac. Consequently, bisphenol A-based benzoxazine will be useful as a latent hardener of epoxy resin for injection molding.

Chanchira Jubsilp et al [63] used the Friedman method to determine a kinetic curing process of benzoxazine by non-isothermal differential scanning calorimetry (DSC) at different heating rates. The autocatalytic nature of the reaction kinetics of this resin with the average activation energy of 81–85 kJ mol^{-1}, was found by the authors. According to other works reported, the phenomena of this resin can be explained by the generation of free phenol groups while the benzoxazine ring starts to open. These groups can actually accelerate further ring opening [64-65].

G. Ragosta et al. [66] investigated the curing behavior of epoxy-silica nanocomposites. The reported are in Table 3.1, activation energy of composite increase with nano-SiO2 content. This behavior can be explained from considerations of the length scale of the segmental motions of the epoxy network involved in the yielding process. According to the Eyring's theory, yielding is manifest in the form of stress-activated jumps of 'flow units', which correspond to movements of network segments of the macromolecular chains. Accordingly, the reduction in activation volume for the nanocomposite implies that a lower number of chains segments are involved in the yield process as the silica content increases. This has to result from the increased constraints on the structural segments involved in the yielding process, which are brought about by the significant interfacial interactions between the silica particles and the epoxy network. At the same time these restrictions on chain. While an opposite trend is observed in previous literature [67]

Table 3.1 Activation energy (E*) and activation volume (V*) for nanocopmposites and the control resin

Sample	Activation energy (kJ/mol)	Activation volume (nm^3)
Pure epoxy resin	201	2.3
Nanocomposite with 5.0 wt% silica	301	1.2
Nanocomposite with 10.0 wt% silica	357	1.6

It is well known that many transformations may occur when a solid sample is heated. A thermal degradation heat transfer model has been developed for predicting the temperature response of composite materials when exposed to fire. The model is capable of predicting temperatures during short-term fire exposures and longer-term fire exposures which are of interest in fire resistance problems.

Inorganic materials usually have high thermal stability, good electrical properties, and high strength, but they have high density and are very brittle. On the other hand, polymeric materials have elastic properties with low density but lack the thermal stability. It is generally difficult to have high strength, toughness, low density, and high thermal stability in the same material. Thus hybridization of inorganics with organic polymer has attracted the interest of the researchers because the hybrids could combine the best attributes of the two components. For traditional composites, the adhesion between inorganics and the polymer is often poor because they are combined in a macroscopic scale. Therefore they do not offer the desired reinforcement effect to the hybrid materials. Recently, there has been an intense interest to design polymer composites containing inorganics with sizes in the order of nanometer [68-69].

Benzoxazine resin, a new class of phenolic resins, possesses various characteristics that make it suitable for use as a matrix of high performance composites, Various nanoscale fillers, including montmorillonite [41, 70-74], Mica [73], Clay [74-75], POSS [76-79], and nano-SiO_2 [80-81] have been reported to enhance mechanical and thermal properties of polybenzoxazine [68-81]. Some researcher reported in highly filled microcomposites [21-22].

Agag Tarek and Tsutomu Takeichi [71] found that the presence of allyl-functional onto MMT surface was effective to enhance the adhesion between polybenzoxazine and layer silicates through bonding. And the glass transition temperature increase with increasing of modified-MMT (ADS-MMT/PDS-MMT) but lower than neat resin because PB-ala matrix cross link with loose network structure than neat resin as show in Figure 3.5.

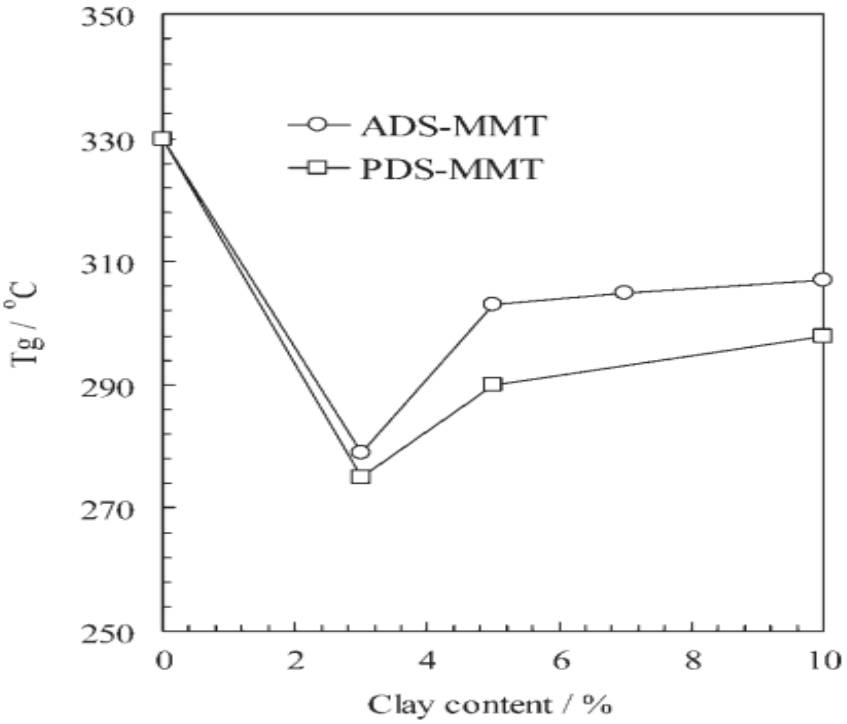

Figure 3.5 Effect of organoclay on the T g of the hybrids.

On the other hand, Chen Q et al [72] investigated the increasing of glass transition temperature with increasing of modified-OMMT and more than neat resin because of the increase in the adhesion between the polymer and OMMT surfaces, increase the restricted segmental motion of the polymer near the organic–inorganic interface as show in Figure 3.6.

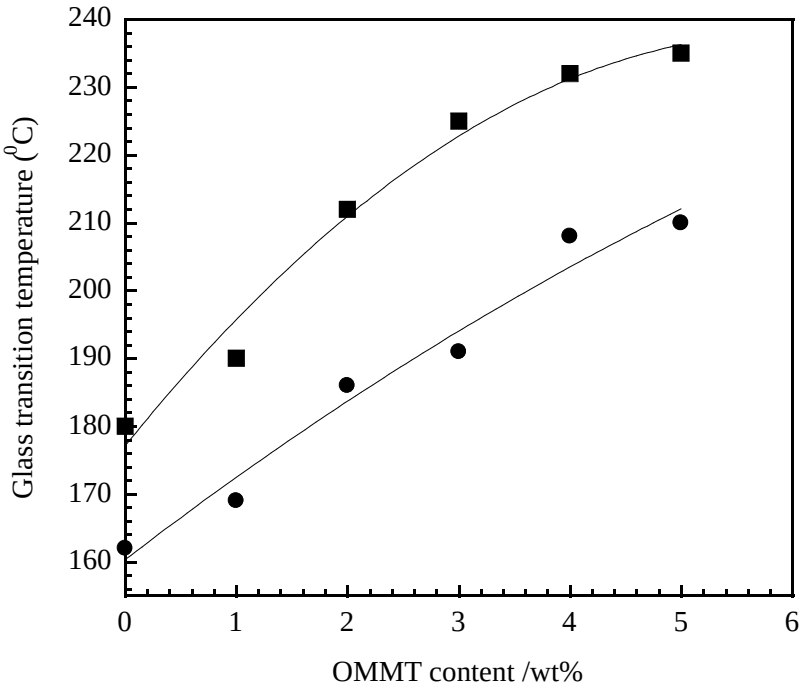

Figure 3.6 Effect of OMMT content on the glass transition temperature of PBZ-PBO/OMMT nanocomposites.

The similar tendency, the storage modulus, the glass transition temperature and thermal stability such as thermal degradation temperature and char yield increase with increasing filler content in all research [68-80].

MMT/polybenzoxazine Nanocomposites based on many modified MMT of different functional group of MMT surface modification, such as dodecyl ammonium chloride [70, Typamine, phenylethylamine, aminoluaric acid, dodecylamine [71]. The acidic onium protons on the MMT surface decrease the onset of the ring opening polymerization which catalyzed the opening of the oxazine ring of the preintercalated benzoxazine within the clay galleries. The similar result was shown for modified-mica polybenzoxazine nanocomposites. The onset and maximum of the exotherm shifted to lower temperature by the inclusion of the ALA-mica as show in Figure 3.7. The ALA-mica content exhibited catalytic effect on the polymerization of benzoxazine [73].

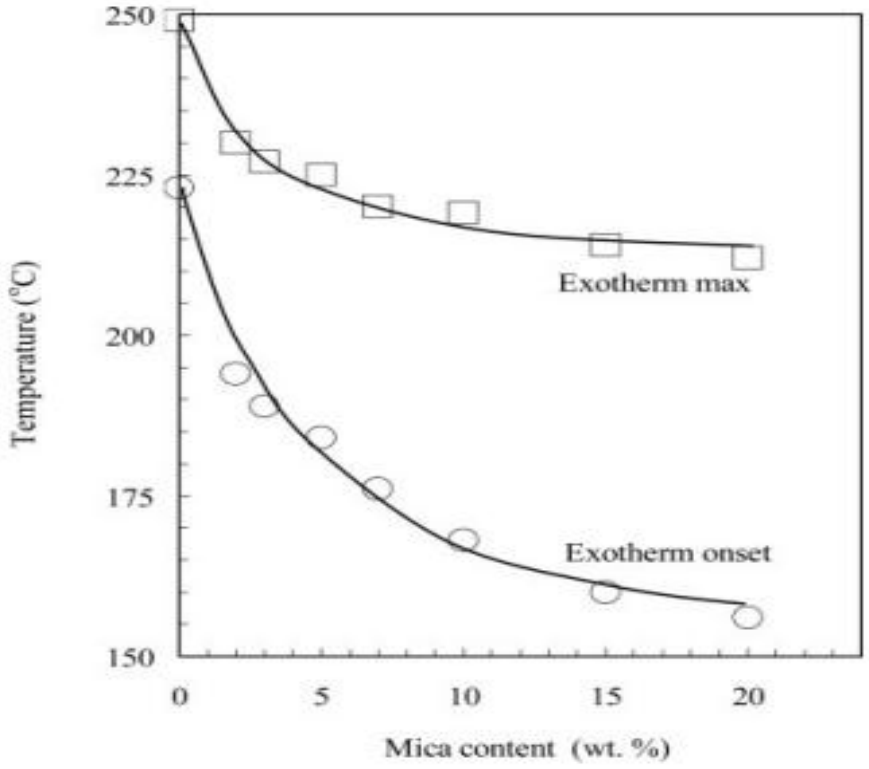

Figure 3.7 Effect of the modified-mica content on the cure of benzoxazine

Polybenzoxazine-POSS have been various reported in many type of benzoxazine monomer. They can be found that the storage modulus, the glass transition temperature and thermal stability such as thermal degradation temperature and char yield increase with increasing POSS content. The enhancement of nanocomposite properties has been studied in the low amount of filler, less than 5% wt [76-79].

In the case of layer nanocomposites system, the properties enhancement can be achieved when a complete exfoliate of clay nanolayers into polybenzoxazine for suitable solvent.

Nowadays there are some researchers investigating polybenzoxazine–nanosilica composites to improve the toughness of resin. At the same time, storage modulus and glass-transition temperature (as shown in Figure 3.8) were enhanced. Moreover, the thermal stability of the SiO_2/polybenzoxazine nanocomposites was enhanced increased with the nano-SiO_2 content [80-81].

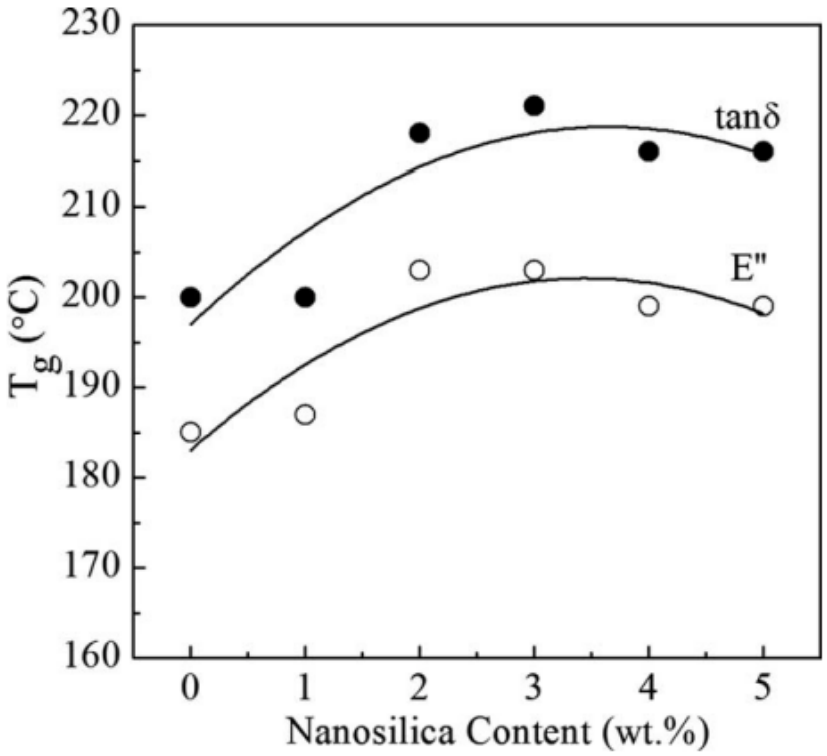

Figure 3.8 The effect of the nano-SiO_2 contents on the T_g of the SiO_2/ polybenzoxazine nanocomposites

In this study, nano-SiO2 were modified with benzoxazine monofunctional silane coupling agent, follow by inclusion in bifunctional benzoxazine and ring-opening polymerization by thermal treatment as present in Figure 3.9.

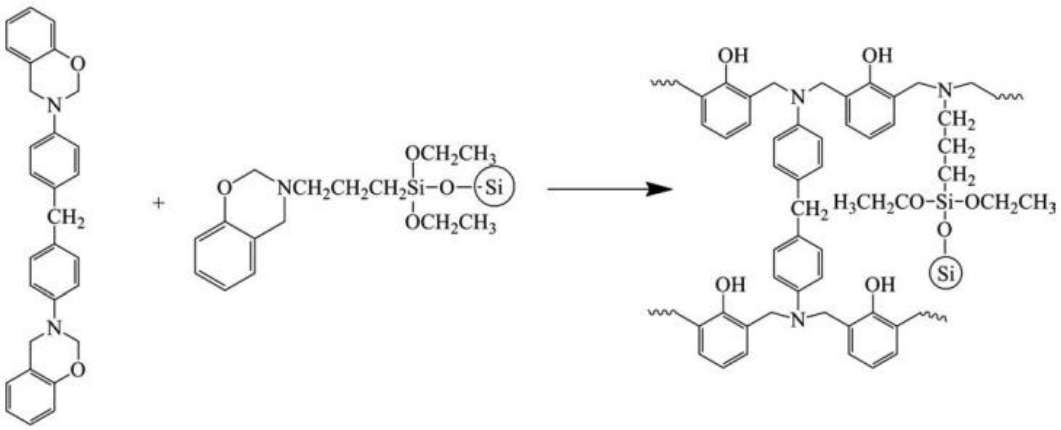

Figure 3.9 Ring-opening polymerization of benzoxazine monomer and modified nano-SiO_2.

In US 7,666,938 B2 [13], the author prepared nanocomposites which composition consist of benzoxazine resin/cationic/initiator/coreactants/toughener/ adhesion promotor (filler) to improve the toughening of benzoxazine resin. 11 samples were prepared and evaluated for physical properties. The most enhance of the glass transition temperature and Flexural modulus were found in sample number 11, which composed B-m type benzoxazine 75% and nano-SiO2 modified with epoxy (XP 0314) 25%.

Ishida H and Rimdusit S. [21] developed highly thermally conductive molding compounds for electronic packaging applications. The authors used large aggregates of flake-like boron nitride crystals and were able to make a composite with a maximum filler content up to 78.5 vol % (88 wt %). The remarkably high value of thermal conductivity of 32.5 W/mK was found at maximum loading of filler. The moduli of the composites expectedly increase with increasing amount of boron nitride. A large increase of ca. 40-45^{o}C in the glass-transition temperatures of the composites were found. And all compositions showed the water uptake at 24 h less than 0.1%.

In addition, the resin was chosen in this investigation to make wood composites with high performance and high processability. Rimdusit S. et al [82] develop a wood composite for high mechanical and thermal stability applications based on a highly-filled polybenzoxazine system. The peak positions of the loss moduli were used to indicate the glass transition temperature (T_g) of the specimens as shown in Figure 3.10, the systematically shifting of the peak maxima with the content of the woodflour to higher temperature signifying the increase in T_g of wood composites with the filler loading. This makes benzoxazine resin highly attractive as a binder or matrix for this woodflour as it helps improve the service temperature of the composites. Indeed, this Tg enhancement of up to 60°C is hardly found in other filled polymeric systems. The excessive presence of the more rigid woodflour filler together with the substantial adhesion between the woodflour and the polybenzoxazine resulted in a restriction of the molecular mobility of the polymer and, thereby, the substantial enhancement in the T_g of the composite materials.

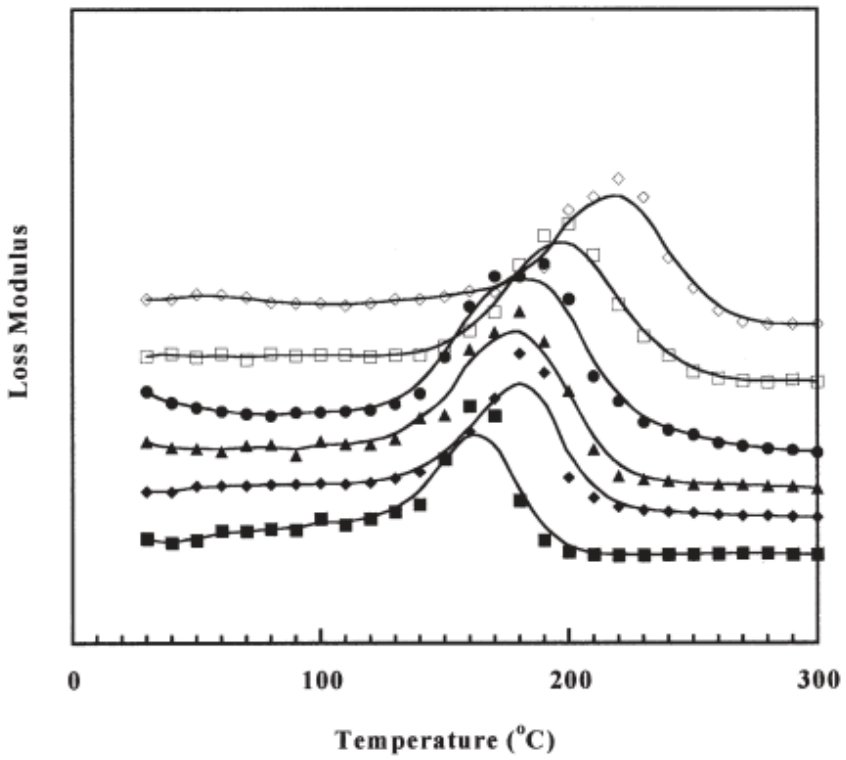

Figure 3.10 Loss modulus of woodflour-filled polybenzoxazine composites as function of temperature at different filler contents: (■) neat resin, (♦) 34.6 vol %, (▲) 44.3 vol %, (●) 54.4 vol %, (▫) 65.0 vol %, (◊)70.5 vol %.

William K. Goertzen and M.R. Kessler [5] studied the effect of different size and volume fraction of nano-SiO_2 on cyanate ester. They mixed the both of component with high shear rate by sonification. The result show the trend of a greater increase in modulus in the rubbery region than for the glassy region for the 40 nm composites, which represents an increase of approximately 75% increase in glassy region and 231% increase in the rubbery at the highest loading (49.2 phr, 20.7 vol%). Analysis of TEM obvious that the smaller nano-SiO_2 particles (12 nm) form much more dominant agglomerates (aggregates entangled together). While the little change in T_g with increasing filler content for both particle sizes. Because the incorporation of the nano-SiO_2 into the polymer will decrease the overall crosslink density of the resin per unit volume, which would decrease T_g. Hydroxyl groups, which are present on the silica surface, have been shown to catalyze the cyclotrimerization of cyanate esters. These catalytic effects will reduce the cross-link density of the polymer in the

interphase region surrounding the particles. And the nano-SiO_2 may add free volume because of disruption in packing of the cyanate ester resin segments, decreasing T_g .

The same research group [83] was found 12-nm silica/BECy suspensions has a faster gel time, indicating that a network has formed and the material's response is dominated by elastic behavior and greater level of thixotropy than the 40-nm silica in BECy monomer, it is possible that some hydrogen bonding is occurring between the nano-SiO_2 aggregates. And they used Kissinger's model, to evaluate curing parameter, the activation energy, E_a, of the reaction of the nano-SiO_2/BECy nanocomposites. Table 3.2 shows the activation energies calculated from the slope of a plot of $\ln(b/T^2_p)$ vs. $1/T_p$. The small changes in activation energy (decrease of less than 9%) are consistent with the small changes in glass transition temperature. However, there is an observable trend showing decreasing activation energy with increasing filler content and surface area. Both of these factors increase the amount of hydroxyl groups available for reaction with the cyanate ester. Nano-SiO_2 does have a slight catalytic effect on the curing kinetics of the BECy resin. It is well documented that active hydrogen additions, such as water and phenol, have a catalytic effect on the polymerization of cyanate esters.

Table 3.2 Activation energies for catalyzed 12- and 40-nm nano-SiO_2/BECy from differential scanning calorimeter.

Sample	Activation energy (kJ/mol)
Pure BECy	76.2
2 phr, 40 nm silica	72.2
5 phr, 40 nm silica	71.8
2 phr, 12 nm silica	72
5 phr, 12 nm silica	69.7

Goertzen and Kessler [13] report the effect that the particle size and volume fraction of nano-SiO_2 have on the thermal expansion behavior. The largest decrease in CTE was for the highest loading of 40-nm nano-SiO_2 (20.7vol%), a composition that reduced the CTE of BECy by 27.0%, from 63.5 to 46.3 ppm/^oC. Also, the 12-nm

nano-SiO_2 nanocomposites had lower CTEs than the 40-nm nanocomposites of the same volume fraction, and this indicated that the increased surface area of the 12-nm nano-SiO_2 was effective in reducing CTE. The lower thermal expansion of nanocomposites can be used in many applications include electronic flip-clip underfills, electronic packaging, metal part replacement, coatings, and structural adhesives.

The reduction of thermal expansion with increasing of nano-SiO_2 content was found by Mahrholz et al [84]. Epoxy–silica nanocomposites are investigated for their suitability as a new type of matrix for fibre-reinforced polymers (FRP) using injection technology (LCM). The silica nanoparticle content varies between 0 and 25wt% for the high performance epoxy resin. Moreover, resin shrinkage and the thermal conductivity increased. At the same time its stiffness, strength and toughness can be increased significantly compared with neat resin. Nanocomposite properties were enhanced because the spherical silica particles dispersed homogeneously in epoxy matrix as well as the absence of any major agglomeration of particles (see Figure 3.11). It is well known that the degree of dispersion of nanoparticles in a polymer matrix is a governing parameter which controls the final properties of the resulting nanocomposites.

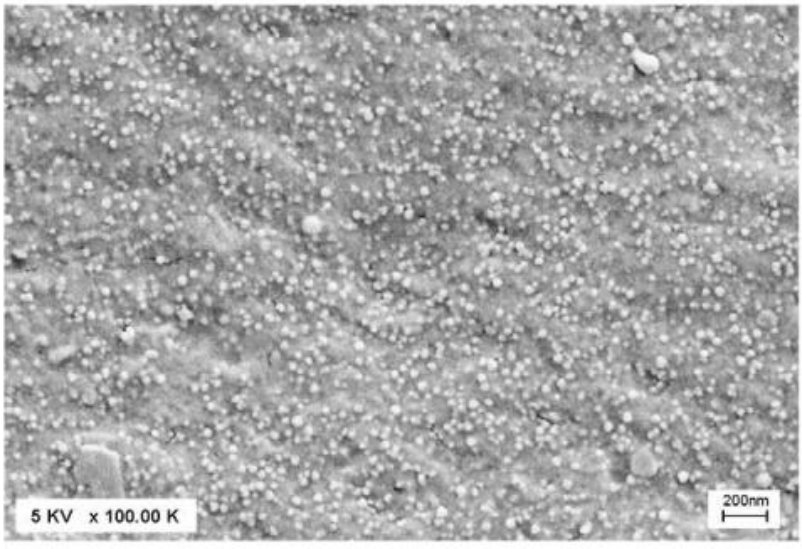

Figure 3.11 SEM image of a nanocomposite based on silica and epoxy resin (25 wt% silica). Surface prepared by cryoscopic fracture.

Mustoa et al [85] prepared polyimide/silica hybrids by a sol–gel process and were evaluated in terms of curing behaviour, morphology and mechanical properties at different temperatures. The spectroscopic examinations showed that the presence of inorganic phase accelerates both the removal of the solvent and the concomitant imidization reaction. Two types of morphology for the silica phase were obtained by tailoring the composition of the precursor solution mixture. The mechanical properties were found to be strongly dependent on the system morphology. The largest increase in rigidity and strength properties were achieved when the two phases were co-continuous. Furthermore, these nanocomposites exhibited better mechanical properties also at high temperatures, thus extending the possible service temperature range of the polyimides 0-28.4%.

The incorporation of inorganic fillers in polymer has been researched to improve the performance of materials. This method synergistically integrates the advantages of the polymers and inorganic fillers, and the properties of the composites can change with the filler components, geometric shape, particle size, dispersion state, surface properties, particle size distribution, and concentration. It has been established that micrometer sized filler (micro-filler) can significantly improve the thermal, electrical, and mechanical properties of a pure polymer matrix. In recent years, with the commercial availability of nanoparticles, the use of a nanometer-sized filler (nano-filler) to modify the polymer has been of increasing interest [83-85]. This is because nano fillers with high surface-to-volume ratios will result in increased interfacial area of the polymer and nano filler and enhanced interaction between them; this can further enhance the properties of the composite.

Bisphenol-A-based polybenzoxazine was subjected to thermal decomposition in a thermogravimetric analyzer by Hemvichian and Ishida [86]. The degradation products are volatile compounds evaporating out of the furnace as gases, are trapped and analyzed further by a gas chromatograph which is coupled with a mass selective detector (GC–MS). From the results, polybenzoxazine began to lose weight at 260^{o}C. Then a three-stage weight loss process was observed, centered approximately at 310, 390, and 470^{o}C, with the one in the middle having the highest maximum rate of weight loss of 0.44%/^{o}C as show in Figure 3.12. The char residue of 30% was found at 800^{o}C. Three overlapped curves mean the evolve gas occurred simultaneously.

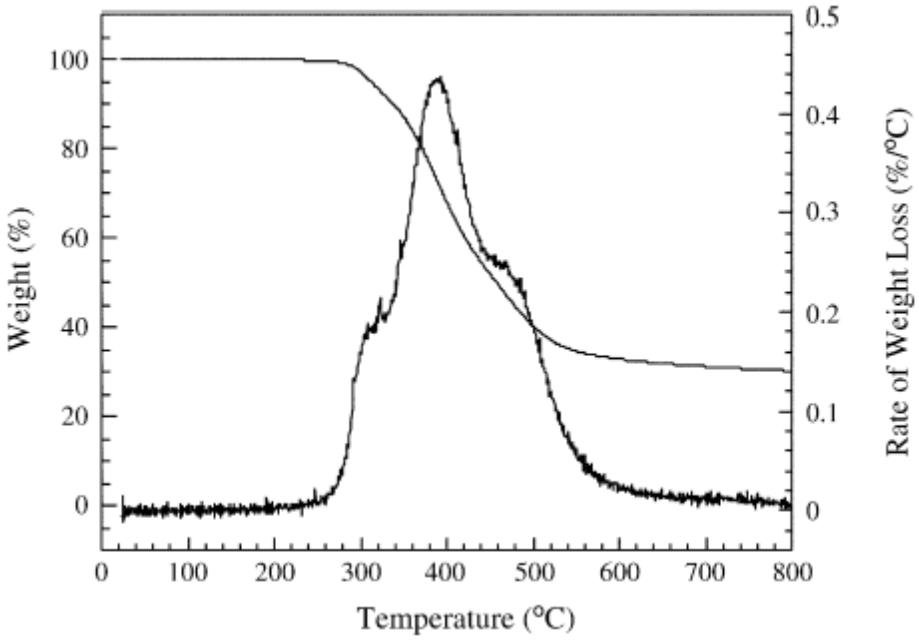

Figure 3.12 TGA thermogram and its derivative from the degradation of BA–a polybenzoxazine in nitrogen

The degradation products from three different aromatic amine-based polybenzoxazines were grouped into eight different types of compounds. These eight families of compounds can be grouped further into two categories. The first category represents the primary decomposition products such as benzene derivatives, amines, phenolic compounds and Mannich base compounds. These compounds are obtained directly from the degradation of the polymer itself. The mechanism involves chain scissions, such as the C–C, C–O and C–N cleavages, of the network structure of the polymer. The proposed network structure of BA–a polybenzoxazine is illustrated in Figure 3.13, in which structures of compounds from the primary degradation products are shown as well. The structure of these degradation products is obviously a part of the network structure of the polymer. The second category contains secondary decomposition products which are 2, 3-benzofuran derivatives, iso-quinoline derivatives, biphenyl compounds and phenanthridine derivatives. Unlike compounds in the first category, these four secondary decomposition products are not present in the polymer network structure. They can be separated further into two groups. The first group, 2, 3-benzofuran derivatives and biphenyl compounds, is derived from the

recombination of radicals formed during the degradation of primary decomposition products like benzene derivatives, amines, and phenolic compounds. The second group, iso-quinoline and phenanthridine derivatives, originates from the degradation of Mannich base. Presence of these four secondary products is very critical for char formation. They are capable of undergoing successive dehydrogenation, cross-linking, and aromatization, all of which will finally lead to formation of highly cross-linked molecules, i.e. the formation of char.

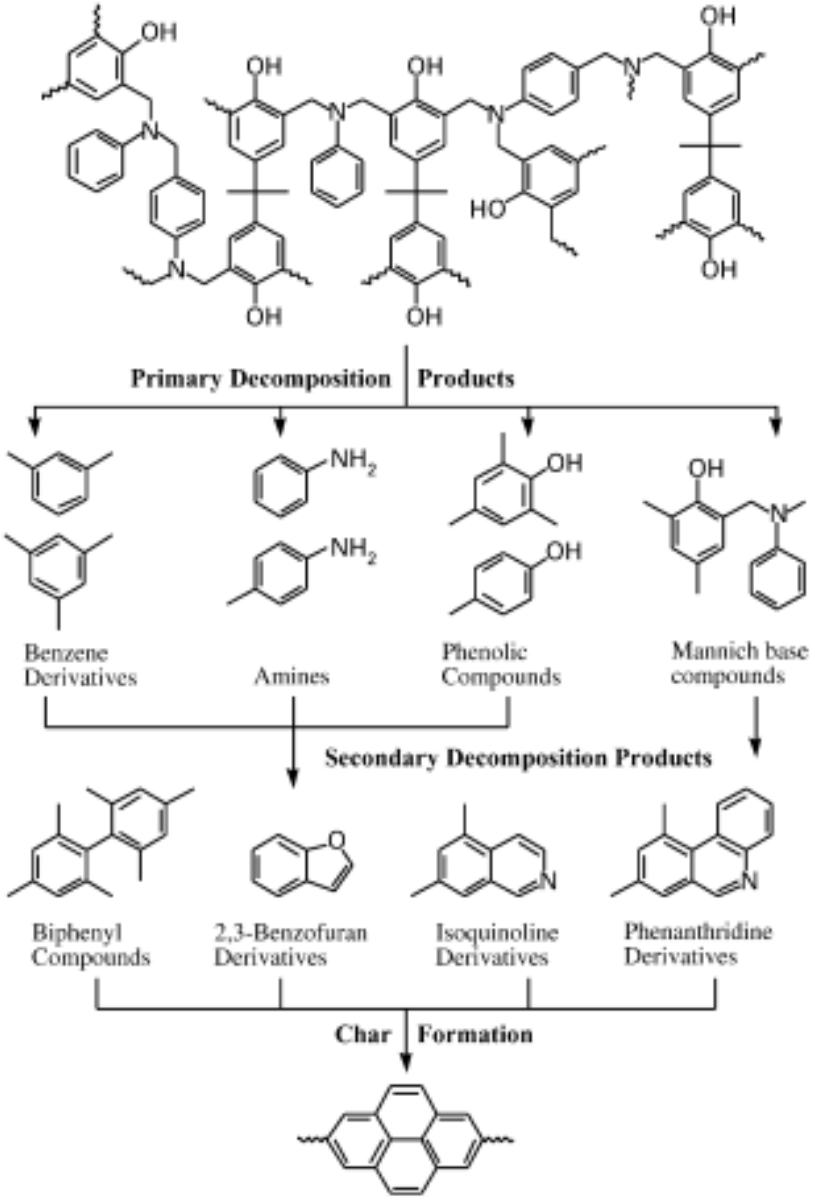

Figure 3.13 The degradation product of BA–a polybenzoxazine.

As compensation for the fire hazards associated with the use of polymeric materials, the use of flame retardants to reduce the combustibility of polymers is a crucial part of developing new polymeric materials. The reduction of smoke and toxic fume production is also very important for preventing the loss of life. In this study, we have been used nano-SiO_2 and precipitated silica to retard the thermal degradation of polybenzoxazine. Because the non-halogenated flame retardants based on silicon has emerged in the recent publications [87].

For the thermal degradation behavior of nano-SiO_2 nanocomposites, Periadurai et al. prepared 5 wt% [88] of nano-SiO_2 was filled in phenolic resin by in-situ method. Nanocomposites possess excellent flame retardant property. The decomposition temperature of SiO_2-phenolic nanocomposite is shifted to higher temperature. The char value at any intermittent temperature is always higher for the nanocomposite than the phenolic resin. In general, increase in char formation reduces the production of combustible gases and decreases the exothermicity during real combustion situations. The limiting oxygen index value of the neat resin is 38 whereas it is 43 for the nanocomposite.

An addition of suitable and inert inorganic filler into the polymers is reported to be a highly effective approach to improve their thermal stability as well as flammability [89-90]. One crucial way to improve flame retardation in polymers is by promoting the formation of stable char since the char layer can act as a thermal insulator and a barrier to oxygen diffusion [41, 91]. An addition of the inherently stable inorganic phase was reported to augment the char formation by making the char more voluminous and mechanically stronger, consequently improving its insulating and barrier properties [91].

The effects of different nanoparticles on various types of polymer thermal stability have been investigated [92-106]. Chrissafis et al. considered the effect of different nano-filler e.g., MMT, MWCNTs and hydrophobic cSiO_2 nanoparticles (dimethylchlorosilane-treated) at a fixed content of 2.5wt% on thermal degradation of HDPE. The authors reported that thermal stability of HDPE was enhanced by the incorporation of different nanoparticles. The degradation kinetics of HDPE and its nanocomposites was found to be the same and is best described by two consecutive mechanisms of nth order autocatalysis. However, the authors reported that the

activation energy of the nanocomposites was higher than that of HDPE i.e. 140 kJ/mol for HDPE vs 230 kJ/mol for HDPE/cSiO_2 of the first reaction mechanism and 260 kJ/mol for HDPE vs 290 kJ/mol for HDPE/cSiO_2 of the second reaction mechanism [104, 106].

CHAPTER IV

EXPERIMENTAL

4.1. Materials

Benzoxazine monomer, bis (3-phenyl-3, 4-dihydro-2H-1,3-benoxzinyl) isopropane (BA-a), was synthesized from 2,2'-bis(4-hydroxyphenyl)-propane (bisphenol-A) with aniline and formaldehyde according to the solventless method described elsewhere [24]. Bisphenol-A (polycarbonate grade) provided by Thai Polycarbonate Co., Ltd. (TPCC) was used as-received. Para-formaldehyde (AR grade) and aniline (AR grade) were purchased from Merck Ltd. Bisphenol A Epoxy resin (EPOTEC YD126) was from Aditaya Birla Chemicals (Thailand) Ltd. (Epoxy Division). The resin is a colorless liquid at room temperature.

Nano-SiO_2 or Nano-SiO2 (Reolosil® QS-20) from Tokuyama Co., Tokyo, Japan, was kindly provided by Cobra International Co., Ltd. Reolosil® QS-20 has the density of 2.203 g/cm^3. It is fluffy, white powder of amorphous structure. An average diameter of primary particles of the nano-SiO_2 is ranging from 5 to 50 nm and a specific surface area is approximately 200 m^2/g.

4.2. Sample Preparations

The benzoxazine (BA-a) resin was well dry-mixed with nano-SiO_2 at a desired weight fraction. The BA-a/nano-SiO_2 mixture was then heated up to 80-100^{o}C and mechanically mixed to ensure nano-SiO_2 particles wet-out by the BA-a resin. The nano-SiO_2/BA-a compound in the form of paste was then compression-molded into various dimensions depending upon the types of experiments. All the specimens were thermally cured at 200^{o}C under a pressure of 0.1 MPa for 3 h. The fully cured specimens were left to cool down at room temperature before their characterizations.

4.3. Sample characterizations

4.3.1. Chemorheology of benzoxazine resins and their mixtures with epoxy

Rheological and gelation behaviors of each resin and resin mixture were investigated using a Rheometer (Haake Rheo Stress 600, Thermo Electron Corp.) equipped with disposable parallel plate geometry. The measuring gap was set at 0.5 mm. The processing window was performed under an oscillatory shear mode at a frequency of 1 rad/s (0.159 Hz). The testing temperature was ramped at a heating rate of 2^{o}C/min to a temperature beyond the gel point of each resin and the dynamic viscosity was recorded. For the gel point determination, frequency sweep in the range of 10-100 rad/s was performed isothermally as a function of time at 170, 180, 190, 200^{o}C for BA-a and 150, 160, 170, 180^{o}C for BA-mt and BA-35x. The gel point is obtained from the point where the loss tangents of different frequencies, i.e. 1.6, 2.8, 5.0, 9.0, and 15.9 Hz, intersect each other**.**

4.3.2. Density measurement

The density of the polymer composites were measured by water displacement method according to ASTM D792-08 (Method A). All specimens were prepared in a rectangular shape of 50 mm×25 mm×2 mm and weighed both in air and in water.

The density was calculated using the following equation:

$$\rho = \frac{A}{A-B}\rho_0 \qquad (4.1)$$

Where ρ, ρ_o is density of the specimen and liquid at the given temperature, respectively (g/cm^3).

A, B is weight of the specimen in air and in liquid, respectively (g).

4.3.3. Fourier transform infrared spectroscopy (FTIR)

Fourier transform infrared spectra of PBA-a, nano-SiO_2, and nano-SiO_2-filled PBA-a at 30% by weight of the filler were carried out on a Spectrum GX FTIR spectrometer from Perkin Elmer instrument with an ATR accessory. All obtained spectra were averaged from 64 scans at a resolution of 2 cm^{-1} within a spectral range of 4000-650 cm^{-1}.

4.3.4. Differential scanning calorimetry measurements

Curing behaviors of BA-a/nano-SiO_2 molding compounds at various nano-SiO_2 contents were investigated by a differential scanning calorimeter (DSC, model 2910) from TA Instruments. Approximately 3-5 mg of the molding compounds was placed in an aluminum pan with lid and characterized at heating rates of 1, 2, 5, and 10^{o}C/min from 30^{o}C to 300^{o}C under nitrogen atmosphere (50ml/min). The heat flow difference between reference blank and the sample pan was recorded.

4.3.5. Hardness measurements

The microhardness of compression-molded specimens was determined using Vickers hardness tester (Future-Tech Corp FM-700, Tokyo, Japan) at a constant load of 500 gf (4.9 N) and dwell time of 15 s. Diagonal length of the indentation was measured through a micrometric eyepiece with objective lens (50× magnification). Average values of six readings were reported as the microhardness of the samples.

4.3.6. Dynamic mechanical analysis

Dynamic mechanical analyzer (DMA, model DMA242) from NETZSCH, was used to investigate thermomechanical properties of the composite specimens. The dimension of each specimen was 50 mm × 10 mm × 2 mm. The test was performed under 3-point bending mode. The strain was applied sinusoidally with a frequency of 1 Hz, and the specimen was heated at a rate of 2^{o}C/min from 30 to 300^{o}C under nitrogen purging.

4.3.7. Morphology of PBA-a /nano-SiO_2 composites

Scanning electron microscopy (SEM) studies were performed using a Hitachi S-4800, field emission scanning electron microscope (FE-SEM) with the accelerating voltage of 3 kV and emission current of 10 mA. The fracture surfaces of the materials were sputter-coated with Pt–Pd under an electric current of 15 mA at 6 Pa for 60 s and then subjected to SEM observation.

4.3.8. Thermogravimetric analysis

Thermogravimetric analysis (TGA) of nano-SiO2-filled polybenzoxazine composites was performed using Rigaku Thermo Plus 2 TG-DTA TG8120. Samples (10-15 mg) were heated from 30 to 800^{o}C at dynamic heating rates of 5, 10, 15 and 20^{o}C/min under argon atmosphere with a flow rate of 80 mL/min.

CHAPTER V

RESULTS AND DISCUSSION

5.1 Selecting Resin Matrix for Nanocomposite Fabrication

5.1.1 Chemorheological Properties

In the composite manufacturing process, resin viscosity plays a major role in controlling the resin flow-out and wetting characteristics. In principle, the variation in viscosity of thermosetting resin depends on the temperature and time. The variation in viscosity of resin due to changes in temperature or time is regarded as the processing window of the resin. In the processing window, sol-gel transition is one critical phenomenon that is affected on the processing condition of the composite fabrication.

Several techniques have been employed as tools to determine the gel point of a material such as static and dynamic light scattering, dissolution and extraction by solvents of the sol fraction, infrared, Raman, and nuclear magnetic resonance spectroscopies, differential scanning calorimetry, dielectric measurement, and rheometry [107-108]. Among these, rheological property measurement is found to be one of the most utilized and sensitive technique for the gel point determination [107, 109]. In this research, chemorheological property development of the benzoxazine-epoxy systems, particularly in the vicinity of a gel point, will be examined. The effect of epoxy on the gelation behaviors of these systems will also be investigated using this rheometry technique. Figure 5.1 shows the plot of dynamic viscosity (Pa.s) as a function of temperature (^{o}C) of the benzoxazine-epoxy systems. All BA-a/Epoxy (YD126) resin mixtures are miscible, giving homogenous and transparent liquid mixture. From the figure, at low temperatures, all resins showed a relatively high viscosity due to the solid state nature of these materials at that temperature. Upon heating, these uncured monomers became softened and viscosity rapidly decreased as the temperature accessed their softening points. Then, the next stage was the lowest viscosity range of the resins as all compositions became liquid. This lowest viscosity range provided a processing window for the compounding process of each material. At the final stage or at higher temperatures, the binary mixtures underwent crosslinking reactions past their gel points resulting in a sharp increase in their

viscosities. As can be seen from the rheograms in Figure 5.1, the complex viscosities of the benzoxazine-epoxy mixtures, compared at the same temperature, tended to decrease with an increase in the amount of the epoxy fraction. The liquefying temperatures of these alloys, determined from an intersection between the horizontal line of the lowest viscosity region and the slope of the first-stage viscosity, also systematically decreased with the increasing phenolic novolac content in the alloys. The results reveal that the BA-a exhibited the highest liquefying temperature of 76^{o}C, while BY91, BY82, BY73 and BY64 are 67, 61, 58 and 48^{o}C, respectively.

The notations B and Y stand for BA-a resin, and Epoxy (YD126) resin, respectively. (The two digits after the notation are the mass ratio of the monomers in the same order.) This is due to the fact that the epoxy resin used is liquid at room temperature while the benzoxazine resin is solid at room temperature. An addition of liquid epoxy into the solid benzoxazine thus lowered the liquefying point of the resulting mixture. On the other hand, the gel point of these binary mixtures tended to increase with an increase in the amount of the epoxy resin in the binary mixtures. The rheograms show that the BA-a resin possessed the lowest gel point of 188^{o}C, while those of BY91, BY82, BY73 and BY64 are 196, 206, 209 and 212^{o}C, respectively.

Furthermore, the temperature range from the liquefying point to the gel point is called processing window which is the range of the lowest viscosity useful for polymer compounding or processing. To see the effect of epoxy on processing window of benzoxazine resins, from the figure we can see that, the processing window of the mixtures was widened by the amount of the epoxy resin. In other words, the processing window of each benzoxazine resin can be partly controlled by adding appropriate amount of epoxy. All resins are low viscosity liquid within the temperature range of 90 to 180^{o}C which renders a sufficiently broad processing window for a compounding process in the manufacture of composites.

The knowledge of factors that control the transition point and the time for gelation to occur will lead to the ability to obtain likable products with appropriate processing conditions and methods. One important feature of thermosetting polymers is their gelation behavior, especially, the kinetics of gelation as well as gel time. Sol-gel transition or liquid-solid transition, known as the gel point, is one critical phenomenon that is significant, especially, for the material processing. In principle,

elastic modulus and viscous modulus present the same power-law variation with respect to the frequency of oscillation at a gel point [107, 119-112]. The corresponding expressions describing the dynamic moduli at the gel point were as follow:

$$\tan\delta = \frac{G''}{G'} = \tan\frac{\pi n}{2} \qquad (5.1)$$

Where G' is storage modulus, G'' is loss modulus and n is the relaxation exponent which is network specific. The above expression suggests frequency independent nature of tan δ at gel point.Gel time of BA-a evaluated isothermally at 150, 160, 170 and 180^{o}C, is shown in Figure 5.2. This figure displays the plot of tan δ at various frequencies, i.e., 1.6, 2.8, 5.0, 9.0, and 15.9 Hz, as a function of time (s). The gel time is obtained from the point where the loss tangent is frequency independent. Experimentally, it is the point where the loss tangents of different frequencies intersect each other [110]. From the figure, the gel times of the mixture expectedly decreased with increasing temperature. Figure 5.3 exhibits the plot of the gel time as a function of gel temperature (^{o}C) or sol-gel diagram of BA-a mixed with epoxy resin at various weight ratio determined as the same method with Figure 5.2. The graph shows an exponential decay behavior of the gel time with increasing gel temperature. This is due to the fact that increasing the processing temperature increases the rate of crosslinking of BA-a/epoxy systems. Consequently, at higher temperature, the systems reach their gel points more quickly and the gel times are shorter [25]. An Arrhenius model is mostly used to predict the gelation behavior of crosslinked network [110]. The gelation of our resin mixtures was found to be well predicted by the Arrhenius equation as follow:

$$t_{gel} = A\exp(\Delta E/T) \qquad (5.2)$$

or

$$\ln(t_{gel}) = \ln A + (\Delta E/T) \qquad (5.3)$$

Where A = constant

ΔE = activation energy with a unit in Kelvin

T = temperature in Kelvin

Consequently, the ΔE or activation energy for gelation can be determined from the slope of the plots of $\ln(t_{gel})$ as a function of 1/T. Meanwhile, an A value can be also determined from the y-axis intercept of the graph. Figure 5.4 illustrates the plot of the $\ln(t_{gel})$ as a function of $1/T*10^3$ (K^{-1}) of BA-a mixed with epoxy resin at various composition determined from Figure 5.3. From the figure, the Arrhenius plot of this gelation shows only single slope or activation energy signifying single thermal event in the gelation process of this binary system. In Figure 5.4, the value of A and ΔE exhibited in Table 5.1. From the figure, the value of A was determined to be 0.74×10^{-7} and ΔE to be 9.987 K or equivalent to 83.0 KJ/mol which consistent with Kasemsiri et al. work [113]. The increasing of kinetic parameters of Arrhenius equation at the gel points were occurred with increasing epoxy resin content. From the Table 5.1, the activation energy values of the gelation of BY91, BY82, and BY73 were approximately the same. This implies the gelation process of these binary mixtures was controlled by the ring opening polymerization of the oxazine ring in both three mixtures thus resulting in the similar ΔE values. This also suggested that the amount of epoxy in the range used do not significantly affect the activation energies of the gelation process of the resin mixtures. While the activation energy and the y-axis intercepts or the A values of BY64 indicated the smallest value. This A value is related to the initial temperature that the mixture can start the gelation process. Therefore, BY64 system tended to require lowest temperature to be able to start the gelation while the other mixtures needed higher starting temperature for the gelation process than BA-a and BY64.

5.1.2 Differential Scanning Calorimetry (DSC) for Curing Process Investigation

The curing reaction of the binary mixtures at various epoxy compositions by differential scanning calorimetry using a heating rate of 10^oC/min at a temperature range of 30-300^oC is depicted in Figure 5.5. From the DSC thermograms, only a single dominant exothermic peak of the curing reaction in each resin composition was observed. From the figure, we can evidently see that the curing reaction of these binary systems can proceed without the need of a catalyst or a curing agent for the polymerization process. The exothermic peak of the neat benzoxazine resin was located at 234^oC which attributed to ring-opening polymerization of ozaxine ring. The

curing peak maximum was observed to shift to a higher temperature when the epoxy fraction in the resin mixtures increased. In Figure 5.5, the positions of the exothermic peaks of BY91, BY82, BY73 and BY64 resin mixtures were found to be 241^{o}C, 244^{o}C, 251 and 254^{o}C, respectively.

Figures 5.6 presents glass transition temperatures (T_g) from DSC of the fully cured BA-a/epoxy alloys after curing at 150^{o}C for 1 hour, 170^{o}C for 1 hour, 190^{o}C for 1 hour and 200^{o}C for 3 hours. In this experiment, the T_g values were taken as the midpoint temperature of the change in specific heat in the transition region. From room temperature up to 300^{o}C, there existed only single T_g in each of these BA-a/epoxy alloys. The T_g of the fully cured BA-a/epoxy alloys were observed to be 161^{o}C in neat PBA-a.

The incorporation of epoxy in the benzoxazine matrix has the effect of increasing the Tg of the material over the pure polybenzoxazine. The highest Tg, 187°C, is demonstrated by the material containing 20% epoxy and is approximately 15 ° higher than the neat benzoxazine. However, at the epoxy composition of 30 and 40wt%, the Tg exhibited lower than that of the pure polybenzoxazine. Ring-opening of the benzoxazine ring at elevated temperatures produces phenolic structures. These phenolic hydroxyl groups can react with epoxy resins at elevated temperatures. Moreover, the ring-opening also produces tertiary amine structure in the backbone of the phenolic resin. These tertiary amine groups can catalyze homopolymerization of epoxy groups. The phenolic groups generated by the oxazine ring opening reaction not only serve to catalyse the copolymerization, but also participate as reactants and therefore are consumed by the reaction, resulting the increasing of the Tg. However, the excess amount of epoxy is approached; unreacted or small molecular weight epoxy molecules may remain and interfere with network formation or act as a plasticizer, thus the decreasing of the Tg was obtained.

5.1.3. Characterization of BY/nano-SiO_2 composites

The BY82 and BY64 alloys were selected as the matrix for the nanocomposite preparation to compare with the neat PBA-a matrix. For all nanocomposites, thermo-mechanical properties were measured and results are presented in Figure 5.7, 5.8, and

5.9 for the PBA-a, BY82, and BY64 based nanocomposite, respectively. The figure demonstrates representative storage modulus and tan δ curves of nanocomposites, as recorded during dynamic mechanical analysis in the temperature range of 30–300^{o}C. As can be seen from the storage modulus (E') curves at room temperatures (35^{o}C), all polymer/SiO_2 nanocomposites have higher E' values than neat matrix. This is likely due to the reinforcing effect of nano-SiO_2 filler on the BY alloys implying substantial interfacial bonding between the matrix and the nanoparticle. Moreover, the storage moduli of the nano-SiO_2-filled BYcomposites increased with the amount of the benzoxazine content in the specimens. This is possibly due to the effect of the more rigid molecular structure of the polybenzoxazine compared with that of the epoxy used.

The peak positions of the tan δ were used to indicate the Tgs of the specimens. The observed increase of the glass transition temperature (Tg) directly reflects the reduction of segmental mobility of polymer chains and the increase in stiffness of the composites as a result of incorporation of SiO2 and evolution of interactions with the respective polymer matrices. As can be seen from Figure 5.7, PBA-a exhibited a glass transition temperature of 185^{o}C. The Tg values for the nanocomposites increased with increasing the silica content. More specifically, the Tg became 193, 199, and finally 201^{o}C for 10, 20, and 30wt % nano-SiO_2 content, respectively. On the other hand, using the BY82 as the matrix resulting in the increasing Tg of 2^{o}C at 30wt% filler content. Moreover, the decreasing of Tg was observed as a function of nanoparticle content in BY64 matrix. There are three major factors that affect the glass transition temperature of these nanocomposites. First, the incorporation of the rigid nano-SiO_2 into the cross-linked network of PBA-a serves to decrease segmental motion, which would serve to increase Tg. Second, the incorporation of the nano-SiO_2 into the polymer matrix will decrease the overall cross-link density of the resin per unit volume, which would decrease Tg. Third; the nano-SiO_2 may add free volume because of disruption in packing of the resin matrix segments, decreasing Tg. A positive effect on Tg was observed, using the PBA-a as the matrix because there is an excess of phenolic hydroxyl groups that can link to the nano-SiO_2 and decrease large scale segmental motion [5].

For nanocomposites, using BY82 and BY64 as the matrix, there is a negative effect on Tg because the excessed phenolic hydroxyl groups of PBA-a were utilized as catalyst for the epoxy ring opening and as reactants for the reaction with hydroxyl group of epoxy. Therefore, the agglomeration of the nano-SiO_2 possibly occurred.

Consequently, the neat benzoxazine is focused as the candidate matrix for nano-SiO_2 composite preparation in this research.

5.2 High Thermal and Mechanical Properties Enhancement Obtained in Highly Filled Polybenzoxazine Nanocomposites with Nano-SiO2

5.2.1 Maximum packing density of highly filled PBA-a/nano-SiO_2 composites

The dependence of the specific density of composites on nano-SiO_2 content is depicted in Figure 5.10. The determination of density is important and highly sensitive measure to check the quality of samples, which can often provide insight into the nature of the particle dispersion within the polymer matrix as well as the presence of voids or air gaps in the specimen. From this figure, the measured nanocomposite density was clearly observed to exhibit a linear relationship following a simple additive rule as given by Eq. (5.4) with relatively high accuracy (straight line)

$$\rho_c = \emptyset_f \rho_f + \emptyset_m \rho_m \quad (5.4)$$

Where ρ_c, ρ_f and ρ_m are the density of the composite, filler and polymeric matrix, respectively, ϕ_f and ϕ_m are the volume fractions of the filler and the matrix. The theoretical densities of the polybenzoxazine nanocomposites were calculated based on the reported density of nano-SiO_2 of 2.203 g/cm^3 [14] and the measured density of polybenzoxazine, BA-a, of 1.19 g/cm^3. This measured density of our polybenzoxazine is also in good agreement with that reported in the literature [20]. In our case, we were able to make a nanocomposite specimen with a packing density as high as 18.8vol% (30wt%). A good homogeneity is achieved with negligible air bubbles in the composite sample as well as with minimal unfilled pores at the polymer/filler interface. The attempt to add nano-SiO_2 at 35wt% resulted in a decrease

in the observed composite packing density to a value lower than the theoretical value likely due to the presence of void or air gap in the nanocomposite.

In low aspect ratio filler, particle size and size distribution are known to play a key role in the obtained packing density of the composite. Normally, relatively large particle size with multimodal particle size distribution will provide a higher packing density than single size small particles. Zhang and coworkers reported property improvements of epoxy filled with high content of nano-SiO_2 up to only 14vol% using nano-SiO_2 particle size of 25 nm. The authors; however, suggested the improvements in flexural modulus, flexural strength, microhardness, and toughness to increase with increasing the amount of the nano-SiO_2 while impact resistance was found to show a maximum value at about 3% by volume of the nano-SiO_2 filler [4]. Goertzen and Kessler reported a relatively high filler loading of nano-SiO2 up to 20.7vol% in cyanate ester resin using 40 nm nano-SiO_2 and only up to 3.4vol% with nano-SiO_2 of 12 nm. Though the nano-SiO_2 in our case has an average particle of only 12 nm, it provides the packing density as high as 18.8vol%. The very low A-stage viscosity of the benzoxazine resin with its good wettability with the filler was again proved to provide a high processability of the highly filled molding compounds. This outstanding characteristic of benzoxazine resin was well documented such as in the development of highly thermally conductive microelectronic packaging as well as in high thermal properties and high mechanical integrity polybenzoxazine wood composites [5].

5.2.2 Spectroscopic properties of the polybenzoxazine nanocomposites

FT-IR spectroscopy was used to verify the molecular structures of nano-SiO_2, PBA-a, and 30wt% nano-SiO_2-filled PBA-a as depicted in Figure 5.11(a), 5.11(b) and 5.11(c), respectively. The spectrum of nano-SiO_2 exhibited the characteristic peaks at about 1107 cm^{-1}, which is due to the asymmetric stretching vibrations of siloxane groups (Si–O–Si), whereas the band at 807 cm^{-1} is attributed to the symmetric stretching of Si–O–Si as observed in Figure 5.11(a). Furthermore, a broad peak with a maximum at 3433 cm^{-1} is attributed to hydroxyl groups (symmetric stretching –OH-) attached to a silicon atom on the nano-SiO_2 surface [25-27]. Figure 5.11(b) shows FT-

IR spectrum of PBA-a with a characteristic peak at 1488 cm^{-1} due to tetra-substituted benzene ring that led to the formation of a phenolic hydroxyl group-based polybenzoxazine (PBA-a) structure. In addition, an indication of ring opening reaction of BA-a upon thermal treatment could also be observed from the appearance of a broad peak about 3300 cm^{-1} which was assigned to the phenolic hydroxyl group formation [114]. The FTIR spectrum of the 30wt% nano-SiO_2 filled polybenzoxazine nanocomposite is presented in Figure 5.11(c). From this figure, though the broad peak centered at around 3320 cm^{-1} due to the hydroxyl group was still observed, its intensity tended to be lowered compared to those of the pure nano- SiO_2 and the unfilled polybenzoxazine implying the consumption of the –OH group in the polymer as well as in the nano- SiO_2 filler. In addition, the new peak at 1075 cm^{-1} assigned to Si-O-C stretching was also clearly observed in Figure 5.11(c). The appearance of this absorption band is a clear evidence of the chemical bonding formed between the polybenzoxazine matrix and the nano- SiO_2 filler. Agag and Takeichi investigated the role of benzoxazine-functional silane coupling agent in the synthesis of benzoxazine resin-SiO_2 hybrids by sol-gel process. The authors used the peak of Si-O-C stretching at 1087cm^{-1} to follow the formation reaction of silica nanoparticles from the starting benzoxazine resin and silanes [114]. As a consequence, the nanocomposites from the polybenzoxazine and the nano- SiO_2 should provide a substantial reinforcing effect as a result of the chemical bonding between the two component s described above.

5.2.3. Curing characteristics of BA-a/nano-SiO_2 molding compounds

The polymerization behaviors of BA-a monomer at different weight fractions of nano-SiO_2 were investigated by non-isothermal DSC as depicted in Figure 5.12. The curing exotherms of these benzoxazine compounds exhibited thermal curability of benzoxazine resin without adding initiator or catalyst. No significant change in the exothermic peak position of the benzoxazine molding compounds was observed indicating that the nano-SiO_2 filler is relatively inert to the benzoxazine curing reaction. Furthermore, the experiments revealed that the exothermic curing enthalpy decreased expectedly with increasing filler content e.g ΔH = 188 J/g at 30wt% nano-SiO_2, 306 J/g for benzoxazine resin. Moreover, curing kinetics of the benzoxazine

resin and its molding compounds was also evaluated using Friedman method [115] based on Eq. (5.5).

$$\ln [Af(\alpha)] = \ln(d\alpha/dt) + E_a/RT = \ln A + n \ln (1 - \alpha) \quad (5.5)$$

The reaction rate, $d\alpha/dt$, at each temperature can be determined from $d\alpha/dt = \varphi/\Delta H$ where φ is the measured heat flow normalized with the sample mass, ΔH is the enthalpy of the curing reaction, while E_a is activation energy, which can be obtained by Kissinger method [55].

Kissinger's model assumes that the maximum reaction rate occurs at the exotherm peak. The E_a, is related to the heating rate, β, and the peak exotherm temperature, T_p , by

$$\ln\left(\frac{\beta}{T_p^2}\right) = \ln\left(\frac{AR}{E_a}\right) - \frac{E_a}{RT_p} \quad (5.6)$$

Where A is a pre-exponential factor. The slope of a plot of $\ln(\beta/T_p^2)$ vs. $1/T_p$ is proportional to the activation energy. The DSC thermograms of the BA-a resin and 30wt% nano-SiO_2 filled BA-a molding compound at different heating rates are shown in Figure 5.13 and 5.14, respectively. With increasing the heating rate, both endothermic peaks due to enthalpic relaxation and exothermic curing peaks were shifted to a higher temperature. From these thermograms, the endotherms due to enthalpic relaxation of the BA-a were observed at about 45-49^oC while that of the nanocomposite showed the values in the range of 42-47^oC. The enthalpic relaxation phemenon of BA-a was also observed by Jubsilp et al. at approximately the same temperature and is attributed to the molecular packing of the benzoxazine monomers [63]. Figure 5.15 reveals a linear relationship between the logarithms of β/T_p^2 with the inverse of the peak temperature of the exothermic curing reaction ($1000/T_p$). The average activation energy values of the BA-a resin and the 10, 20 and 30wt% nano-SiO_2 filled BA-a molding compounds calculated from the slopes of the plots were 79, 81, 84 and 92 kJ/mole, respectively. The obtained activation of the BA-a resin is also consistent with the value of 81 kJ/mole reported by Jubsilp et al. [63]. In the BA-a molding compounds, the activation energy was found to be increased systematically with increasing nano-SiO_2 content. This might be due to the relatively high loading of the nanofiller used which can substantially restrict the mobility or the collision rate of the benzoxazine monomers thus raising the activation energy of the matrix resin.

In the curing kinetic analysis, Friedman suggested that the relationship between ln[Af(α)] against ln(1 − α) should yield a straight line of which the slope corresponds to the order of n of the reaction. On the other hand, Figure 5.16 exhibits Friedman's plot of BA-a and its molding compounds. The plot between ln [Af(α)] and ln (1 − α) showed a maximum of ln(1 − α) approximately around − 0.51 to − 0.22 which is equivalent to α of about 0.2–0.4. This observation implied that curing reaction of our materials is autocatalytic in nature as suggested by Chen et al. [116]. The autocatalytic curing behavior of benzoxazine resin can be explained by the generation of free phenol groups while the benzoxazine ring starts to open. These phenol groups can actually accelerate further ring opening reaction of other monomers and the mechanism was not affected by the presence of the nano-SiO_2 filler used. The slightly acidic nature of the nano-SiO_2 nanoparticles due to the presence of surface silanol groups has been reported to exhibit some reactivity with hydroxyl groups [117]. The reaction of the -OH groups of the benzoxazine resin with the surface silanol of the nano-SiO_2 thus contributes to the observed curing authocatalytic behavior of the benzoxazine/nano-SiO_2 molding compounds.

5.2.4. Microhardness of PBA-a /SiO_2 nanocomposites

One potential application of nano-SiO_2 filled polybenzoxazine is as a surface coating. The use of nano-SiO_2 as filler in coating resin system usually provides a coating material with improved hardness or scratch resistance, greater mechanical and/or thermal properties, as well as maintaining high gloss value. Since slight damage to component surface in the form of relatively small indentation usually has little effect on the specimen's function, micro-hardness test is considered to be a nearly non-destructive test method [118]. Figure 5.17 depicts micro-hardness values of the polybenzoxazine as a function of the nano-SiO_2 content revealing a linear relationship between the hardness values and the amount of the nano-SiO_2. The hardness of the nanocomposites was found to increase from the measured value of 396 MPa for the pure polybenzoxazine to the values of 462, 486, 511, 538 and 589 MPa with the nanosilica contents of 10, 15, 20, 25 and 30wt%, respectively. The large increase in micro-hardness is attributed to a much higher hardness of the nano-SiO_2 (1103-1120 MPa) [119] compared to the neat polybenzoxazine. Moreover, the

relatively small standard deviation in hardness values with strong hardening effect is attributed to the homogeneous dispersion of the nanofiller in the polybenzoxazine matrix and to the strong filler-polymer interactions with decreasing in interparticle distance when the amount of the filler increases. Moreover, our polybenzoxazine nanocomposites showed greater enhancement in hardness than those in epoxy/nano-SiO_2 comparing at the same filler content [4, 120]. That is in the case of epoxy resin, the micro-hardness value was increased from about 177 MPa for the neat epoxy to about 218 MPa for the 25wt% (15vol%) nano-SiO_2 nanocomposite [120]. As a result, polybenzoxazine/ nano-SiO_2 molding compounds show a hardness characteristic suitable for high performance coating material compared to the traditional epoxy coating system.

5.2.5. Dynamic mechanical properties of the polybenzoxazine nanocomposites

Storage modulus is an important material parameter for measuring stiffness and elasticity of polymeric materials. Figure 5.18 shows the dependence of the storage modulus (E′) on temperature of polybenzoxazine/nano-SiO_2 composite systems with the nano-SiO_2 content ranging from 0 to 30wt%. The values of the room temperature modulus as a function of the nano-SiO_2 content were also listed in Table 5.2 and compared with other major nanocomposite materials. From Figure 5.18, the storage modulus of the nanocomposites at its glassy state as well as in the rubbery plateau region was observed to systematically increase with increasing the nano-SiO_2 content. At room temperature, the modulus value was raised from 5.9 GPa for the neat polybenzoxazine to 10.8 GPa for the 30wt% nano-SiO_2 nanocomposite which is about 83% enhancement in the polybenzoxazine stiffness. This value is also substantially higher than that of nano-SiO_2 filled epoxy at its maximum nano-SiO_2 content of 30vol% as reported by Dittanet and Pearson [121]. The authors reported the modulus values of nano-SiO_2 filled epoxy using three different particle sizes at the filler loading of up to 30% by volume. The Young's modulus of the epoxy used was reported to be 3.5 GPa. The modulus values of 5.53 GPa or about 58% enhancement was obtained when the nano-SiO_2 particle size of 23 nm was used comparing with the values of 5.6 GPa and 5.78 GPa when larger particle sizes i.e. 74 nm and 170 nm were filled in epoxy respectively.

Polybenzoxazine is known to form strong bonding with various surface particularly glass surface [122]. Kimura et al. [123] reported that the mechanical properties, flame resistance, and glass transition temperature of polybenzoxazine composite reinforced with glass fiber are superior to the conventional as well as the flame-retardant epoxy reinforced with glass fiber. The authors attribute the property enhancement above to the good resin distribution and interfacial adhesion between the matrix resins and the glass fiber as well as the presence of the large quantity of benzene rigid structure, the high crosslink density, high char yield and nitrogen-rich structures of the benzoxazine fraction. Moreover, Ishida and Low [23] observed that the adhesion properties of glass-cloth-reinforced polybenzoxazine composite were significantly higher than that of the novolac composite when no surface treatment of the glass fiber was applied. In addition, the authors reported that coupling agent or surface modifier was not as effective on polybenzoxazine as it was on novolac due to a better wetting of the glass fiber by the low viscosity benzoxazine resin. This is an advantage in terms of processing.

The observed substantial increase in storage modulus values of the polybenzoxazine/nano-SiO_2 composites can be attributed to the formation of a strong interface between the hydroxyl groups of the nano-SiO_2 and the phenolic hydroxyl groups of the PBA-a as discussed earlier in the spectroscopic analysis of the samples. In addition, the storage modulus in the rubbery plateau region of the 30wt% nano-SiO_2-filled PBA-a composite was found to greatly increase up to 275% over the unfilled PBA-a. The strong reinforcing effect of the nano-SiO_2 on both glassy state and rubbery state of the polybenzoxazine confirms strong bonding to exist between the nano-SiO_2 filler and the polybenzoxazine matrix. Furthermore, the greater enhancement of the storage modulus observed in nano-SiO_2-filled PBA-a than in epoxy and cyanate ester composite systems as compared in Table 1 implies the greater interaction between the nano-SiO_2 and the polybenzoxazine matrix than that in epoxy and cyanate ester resins. These results imply that BA-a resin is a highly effective adhesive for the nano-SiO_2 filler.

5.2.5.1 Modeling studies of modulus of highly filled polybenzoxazine/nano-SiO_2 composites

There are many proposed theoretical models used to predict the properties of particulate filled polymers [3]. In our study, isostress model (or Reuss average), isostrain model (rule of mixtures), Mori-Tanaka, Halpine-Tsai, and Kerner models are evaluated to predict the modulus of the highly filled nano-SiO_2/polybenzoxazine composites. The isostress model assumes that the matrix and filler are stressed equally while the isostrain model assumes that a strain constant in each of the phases. In the Mori-Tanaka method, it is assumed that only the two phases exist (matrix and reinforcement) and are perfectly bonded to each other. The effective Young's modulus for a composite reinforced by spherical particles based on the Mori-Tanaka method could be predicted by the relationship

$$E_c = \frac{9\bar{K}_c\bar{G}_c}{3\bar{K}_c + \bar{G}_c} \tag{5.7}$$

Where E_c, K_c and G_c are the effective Young's modulus, bulk modulus, and shear modulus of nanocomposites, respectively. The values of K_C and G_C can be expressed as follows:

$$\bar{K}_c = \bar{K}_m + \frac{V_f\bar{K}_m(\bar{K}_f - \bar{K}_m)}{\bar{K}_m + \beta_2(1-V_f)(\bar{K}_f - \bar{K}_m)} \tag{5.8}$$

$$\bar{G}_c = \bar{G}_m + \frac{V_f\bar{G}_m(\bar{G}_f - \bar{G}_m)}{\bar{G}_m + \beta_1(1-V_f)(\bar{G}_f - \bar{G}_m)} \tag{5.9}$$

$$\beta_1 = \frac{2(4-5v_m)}{15(1-v_m)} \tag{5.10}$$

$$\beta_2 = 3-5\beta_1 \tag{5.11}$$

Where V_f is volume fraction of nanoparticle and v_m is Poisson's ratio of matrix. This model is based on a low concentration of micrometer-scale or larger inclusions embedded in the matrix. The interactions between the inclusions and the matrix, as well as the inclusion among inclusions are not considered. Another widely used model is the Halpin-Tsai model [3] which can be expressed by the following equation:

$$\frac{E_c}{E_m} = \frac{1+\varsigma\eta\phi}{1-\eta\phi} \tag{5.12}$$

Where E_c and E_m are the moduli for composite material and polymer matrix, respectively. ϕ is the filler sphere volume fraction, and η is expressed by:

$$\eta = \frac{\frac{E_f}{E_m}-1}{\frac{E_f}{E_m}+\varsigma} \tag{5.13}$$

Where E_f is the modulus of filler, and the shape factor (ς) = 2a (where aspect ratio (a) = 1 for a spherical particle). This model takes into consideration the modulus of the composite as a function of filler contents, or specifically, the modulus of filler, E_f, and the modulus of matrix, Em, as well as the aspect ratio by incorporation of a shape factor. These model parameters make the Halpin-Tsai model versatile. Therefore, the Halpin-Tsai model has been found by some to give more accurate predictions for carbon nanotubes, nanoclay and nanosphere silica filled systems [124]. Lastly, another commonly used model for estimating the modulus of composite containing spherical particles is the Kerner equation, generalized by Lewis and Nielsen [3] and given by

$$\frac{E_c}{E_m} = \frac{1+ABV_f}{1-B\varphi V_f} \tag{5.14}$$

Where A is a constant (it is usually referred as k_E - 1, where k_E is the Einstein coefficient), which depends on the geometry of the filler phase and the Poisson's ratio for the matrix (ϑ). B is also a constant that takes into account the relative modulus between the filler and the polymer matrix. Constants A (for spherical particles) and B are given by

$$A = \frac{7-5\vartheta}{8-10\vartheta} \tag{5.15}$$

$$B = \left(\frac{E_f}{E_m}-1\right)/\left(\frac{E_f}{E_m}+A\right) \tag{5.16}$$

The factor φ is the maximum packing fraction of the filler into the matrix. It can be estimated using the following relation:

$$\varphi = 1 + \frac{1 - V_m}{V_m^2} V_f \qquad (5.17)$$

5.2.5.2 Comparison between experimental results and model prediction

All constants for the matrix and fillers used in the model calculations are listed in Table 5.3. Figure 5.19 depicts the comparison of the isostress model (or Reuss average), isostrain model (rule of mixtures), Mori-Tanaka, Halpin-Tsai, and Kerner models to the experimental data for the Young's modulus as a function of volume percentage of fillers. The isostress model (or Reuss average) gives a theoretical lower bound for the composite modulus. The absolute upper bound would be given by an isostrain model, such as the rule of mixtures. The Halpin-Tsai model and Mori-Tanaka model were found to be in good agreement with the experimental data only at low volume fraction up to 5.7 vol% of fillers. The Mori-Tanaka model assumes that only two phases exist (matrix and reinforcement), and that they are perfectly bonded to each other as mentioned previously. This model does not consider the existence of interfacial phase between particle and matrix. Furthermore, both Halpin-Tsai and Mori-Tanaka models do not consider the interaction among fillers which is crucial at high filler loading. Typically, the Mori-Tanaka and Halpin-Tsai approaches have been used to accurately predict the overall properties of composites when the reinforcements are on the micrometer scale or larger [121].

As seen in Figure 5.19, the experimental data is good fitted to the value obtained by Kerner model. In the analysis, we used three different values for the fitting of the maximum packing fraction: ϕ_m = 0.632 (for random close packing without agglomeration), ϕ_m = 0.601 (for random loose packing without agglomeration), and ϕ_m = 0.37 (for random close packing with agglomeration) [3]. The best fit for the modulus of our nanocomposites was obtained when the maximum packing fraction for random loose packing without agglomeration of the nanoparticles, ϕ_m = 0.601, is used with A = 1.357. The values for both parameters (ϕ_m and A) suggest no agglomeration in the system. If the particles are not dispersed but are strong aggregates, the factor A becomes larger as can observe in epoxy/alumina nanocomposites system [125]. At the same ϕ_m = 0.601, the best fit of epoxy/alumina

nanocomposites system is obtained when A has value of at least 3 whereas the coefficient A is larger than our case. Higher values of the constant A are an indication for the agglomerates' existence.

5.2.6. Glass transition temperature (T_g) of highly filled PBA-a/nano-SiO_2 composites

Figure 5.20 presents the variation of tan δ with temperature of the nano-SiO_2-filled PBA-a composite. The peak position of tan δ was used as T_g of our nanocomposites. It can be seen that the T_g of 201°C was observed in 30wt% of the nano-SiO_2-filled PBA-a while that of neat PBA-a was found to be 185°C. In various nano-SiO_2 filled polymeric systems, negligible change in T_g of the matrix polymer was normally observed [5, 15]. In the case of s polystyrene/nano-SiO_2 systems or epoxy/nano-SiO_2 systems, T_g was even found to decrease with the nanofiller loadings [12, 120]. One reason for the improvement of T_g of the polybenzoxazine with an addition of the nano-SiO_2 filler is attributed to an ability of the nano-SiO_2 particles to substantially restrict the motion of the polybenzoxazine chains thus higher temperature is required to provide the requisite thermal energy for the occurrence of a glass transition in the nanocomposites. The huge surface of the nano-SiO_2 as well as the strong interfacial interaction between the nano-SiO_2 and the polybenzoxazine were attributed to such strong restriction of the chains movements in the polybenzoxazine thus the substantial enhancement on its T_g.

Moreover, the width at half height of the tan δ curve of the filled specimens was observed to be greater than those of the neat polybenzoxazine suggesting higher network heterogeneity in the composites. The good reinforcing effect of the nanoparticles resulted in the reduction of free volume in the polymer chain segment as a result of substantial interaction at the interface between the hydrophilic nano-SiO_2 particles and the PBA-a matrix should contribute to the observed enhancement of the material stiffness and the decrease of the damping function seen from the lowering of the tan δ peaks. Damping factor or tan δ can be used to predict the effective interfacial thickness of the interphase between the polymer and particle through a correction parameter, P, based on the following correlation [126]

$$\tan \delta_c = \tan\delta_m (1-P\phi_f) \qquad (5.18)$$

Where $\tan\delta_c$ and $\tan\delta_m$ is the damping of the composite and of the matrix, respectively. P is a significant introduced interaction between the filler and matrix. ΔR or the effective interfacial thickness of the interphase between the polymer and particle is related to P by

$$P = \left(1 + \frac{\Delta R}{R}\right)^3 \quad (5.19)$$

where R is the radius of the particles. The estimation of the effective thickness of our nano-SiO_2 filled polybenzoxazine is tabulated in Table 3. From the table, there is a general decreasing function of ΔR with respect to volume fraction of the nano-SiO_2 filler, indicating that as volume fraction increases, there is a greater amount of overlap in the interphase regions due to increasing nanoparticle agglomeration. This phenomenon usually observed in nanocomposite systems [5]. The ΔR value of our polybenzoxazine nanocomposites was calculated to be 5.9 nm using an average particle size of 12 nm. The value is comparable to the ΔR values of cyanate ester/nano-SiO_2 composites i.e. ΔR = 5.7 nm for nano-SiO_2 particle size of 12 nm and ΔR = 6.4 nm for nano-SiO_2 particle size of 40 nm [5]. In case of epoxy/nano-SiO_2 composite, ΔR value ranges from 2.79 to 10.55 nm was reported based on the nano-SiO_2 particle size of 25 nm [4]. In general, mechanical properties are drastically enhanced with a further reduction of inter-particle distance [4, 6]. This phenomenon can be explained that the nanoparticles are now close enough (in range of their particle diameter size) to be able to construct a three dimensional network of interphase material around them [6].

5.2.7. Microstructure of nano-SiO_2 filled PBA-a

Scanning electron microscope (SEM) was used to visualize the dispersion of the nano-SiO_2 particles in the polybenzoxazine matrix. Figure 5.21 shows the SEM micrograph of fracture surface of pure matrix and 10wt% (5.7 vol%) nano-SiO_2 filled polybenzoxazine. A smooth fracture surface of the pure polybenzoxazine was clearly observed as seen in Fig. 9(a). In the case of the nanocomposite, its fracture surface revealed the silica nanoparticles to be relatively well dispersed in the PBA-a matrix with relatively good interfacial adhesion between the two componenets (see Fig. 9(b)). This appearance was clearly observed because the low viscosity resin generally aids

in filler mixing during the molding compound preparation. No observable void or airgap was detected on the fracture surface of the nanocomposites. This result is also consistent with the density measurement of the nanocomposites discussed in Section 4.1. The significant interfacial adhesion of the nano-SiO_2 and polybenzoxazine also explains the enhancement in dynamic mechanical properties and glass transition temperature of the obtained composites.

5.2.8. Thermal stability of nano-SiO_2 filled PBA-a

Thermal stability determined via degradation temperature at 5% weight loss ($T_{d,5}$) and solid residue at 800^{o}C of neat polybenzoxazine (PBA-a) and nanosilica-filled polybenzoxazine (SiO_2/PBA-a) composites at different nano-SiO_2 contents are exhibted in Figure 5.22. From the figure, we can see that the nanocomposites showed higher $T_{d,5}$ than that of the neat PBA-a and the $T_{d,5}$ of the nanocomposites was found to increase with increasing nano-SiO_2 contents. $T_{d,5}$ of PBA-a was determined to be 320^{o}C while that of 30wt% nano-SiO_2/PBA-a was found to be 360^{o}C. This is due to the shielding effect of nano-SiO_2 filler which can serve as a good thermal cover layer, avoiding the direct thermal decomposition of the polymeric matrix by heat. It is well known that when inorganic filler particles are dispersed in the polymeric matrix, the formed layers are impermeable towards small molecular gases or volatile products that are generated during thermal decomposition and a much longer path around the nanoparticles is needed for their removal from the decomposed matrix [15].

5.3. Thermal Degradation Mechanism of Highly Filled Nano-SiO_2-Polybenzoxazine Nanocomposites

The PBA-a/nano-SiO_2 composites showed significantly higher thermomechanical properties than those of the recently reported nano-SiO_2 filled epoxy or cyanate ester [55, 63]. This property enhancement is likely due to the strong interfacial bonding through –Si-O-C linkages between the nano-SiO_2 and the PBA-a [116].

In general, thermal stability of the polymer composites plays a crucial role in determining their processing and application, because it affects the final properties of the polymer composites such as the upper-limit use temperature and dimensional

stability [127]. The knowledge of the kinetic model driving a process provides a valuable insight regarding the reaction mechanism and it is useful for controlling a process, determining optimum processing temperature or for aging [33]. Consequently, the understanding of the thermal stability and thermal decomposition kinetics of materials makes it possible to develop and extend their applications as various industrial fields.

It is believed that the ability of the nano-SiO_2 to form Si-O-C bonds with polybenzoxazine can significantly alter thermal degradation mechanisms and decomposition behaviors of the polybenzoxazine in a positive manner. The aim of the next part, therefore, is to evaluate the effect of high nano-SiO_2 nanoparticles loading on the thermal decomposition kinetic parameters of the neat PBA-a, e.g., activation energy (E_a), pre-exponential factor (A), and the conversion function f(α) by using three well-known methods, i.e. Kissinger method, Flynn-Wall-Ozawa method, Coats-Redfern method and master plots based on the integral form of the kinetic data method. The strong interfacial bonding above should also be more pronounced and clearly seen in the highly filled system of the nano-SiO_2 in the polybenzoxazine.

5.3.1. Thermogravimetric analysis (TGA) of nano-SiO_2 filled polybenzoxazine

The TGA thermograms of neat PBA-a and PBA-a/nano-SiO_2 composites at different nano-SiO_2 contents from 0-30wt% are presented in Figure 5.23. The high melting point of nano-SiO_2 can serve as a good thermal cover layer, avoiding the direct thermal decomposition of polymer matrix by heat. It is well known that when inorganic filler particles are dispersed in the polymeric matrix, the formed layers are impermeable toward small molecular gases or volatile products that are generated during decomposition and a much longer path around the nanoparticles is needed for their removal from the decomposed matrix [55]. The effect should be more pronounced when nanoparticles with tremendous surface area such as nano-SiO_2 is used as a dispersed phase.

For further kinetic studies of the nanocomposite systems, DTG curves (first derivative of TGA thermogram) are plotted and separated by using Peakfit® program to separate the DTG curves of the matrix and their nanocomposites. After resolving the curves by the computer software, it can be noticed that the DTG curve of the

PBA-a, presented in Figure 5.24, composes of a three-stage weight-loss process. This result is in good agreement with the previous studies [128-131]. This degradation process was observed by FTIR with the middle peak having the highest maximum rate of weight loss which is phenol-substituted compounds and the evolved gas of the final stage are similar with the main stage, while the various amines were detected in first stage [128, 131]. The volatile products emitted during the thermal decomposition processes of aromatic amine-based polybenzoxazines were identified in more details by Hemvichian and Ishida using TGA [86] and GC–MS techniques [132]. The decomposition products were divided into eight categories as follows: benzene derivatives, amines, phenolic compounds, 2,3-benzofuran derivatives, iso-quinoline derivatives, biphenyl compounds, Mannich base compounds, and phenanthridine derivatives [132]. In addition, the overlapped curve in PBA-a indicated that the degradation of the phenolic linkage occurs simultaneously with the degradation of the Mannich base but the onset of each type of degradation is different [131].

The difference in thermal degradation pattern was observed in the polybenzoxazine nanocomposites i.e. the disappearance of thermal degradation at first stage, observed in the neat polybenzoxazine, was observed and the decomposition processes were reduced to two major events in the nanocomposites as clearly seen in Figure 5.25-5.27. Moreover, the maximum decomposition rates were decreased significantly from 3.7 to 3.5, 2.8, and 2.1%/min whereas the peak positions of the maximum decomposition rates were shifted to higher temperature i.e. 395, 398, 400, 406^{o}C with increasing nano-SiO2 contents from 0, 10, 20 and 30 wt% respectively as shown Figure 5.25-5.27.

5.3.1 Thermal degradation kinetics parameters of nano-SiO_2 filled PBA-a system

In order to analyze more thoroughly the effect of the nanoparticles on the degradation mechanism of PBA-a, it is important to determine the kinetic parameters of the thermally degraded composite products. After all the overlapped DTG peaks were resolved, the conversions were calculated from the areas under each peak. Then, the E_a of each decomposition stage was obtained via three previously mentioned methods.

For the nth order reaction type of solid-state reactions, it involves obtaining the temperature values at the peaks (T_p) of the first derivative weight loss curves (DTG). On the other hand, the Kissinger method [55], the approximate relationship, is still widely used in the analysis of structural transformations because of its simplicity and accuracy. For a series of experiments performed at different heating rates, the E_a can be calculated from the slope of the plot of $\ln(\beta/T^2_p)$ versus $1000/T_p$ (E.q. 2.8) as presented in Figure 5.28-5.31 for polybenzoxazine and its nanocomposites. The numerical results were also summarized in Table 5.5. From the table, it is clearly seen that the activation energy showed a substantially greater value when the nanoparticles were added in the polybenzoxazine. The trend was also consistent with the enhancement of the T_d with the amount of the nano-filler.

Kissinger method provides the best accuracy for a single-step process. In the case of complex mechanisms or for transformations involving more than one step, an adequate representation of the commonly encountered multi-step kinetics would normally require more than a single value of the activation energy [56]. Therefore, it is necessary to use an iso-conversional method to back up the validity of the Kissinger estimates.

5.3.2 Isoconversional analysis of nano-SiO_2 filled PBA-a system

Flynn–Wall–Ozawa method (model-free) is an integral iso-conversional method [52, 56], which assumes that the conversion function f(α) does not change with the variation of the heating rate for all values of degree of conversion α. It involves measuring the temperatures corresponding to given values of conversion (α) from experiments at different heating rates (β). Therefore, plotting log(β) against 1/T (E.q. 2.9), the slope of the straight lines thus obtained the values of E_a were calculated. The E_a for different conversion values of 0, 10, 20 and 30wt% nano-SiO_2 filled PBA-a nanocomposites are shown in Figure 5.32, 5.33, 5.34 and 5.35, respectively. At 0, 10, and 20 wt% nano-SiO_2 contents and for all stages of the thermal degradation, the dependence of E_a on α value exhibited a linear increasing tendency as seen in Figure 5.32-5.35 An increase of E_a with increasing α is a relatively common phenomenon and is frequently observed in many polymers [96-97, 55]. On the other hand, the 30wt% nano-SiO_2 filled polybenzoxazine exhibited a relatively constant E_a with

conversion particularly over the 20-80% conversion range. Montero et al reported that E_a of 2.5wt% POSS contained epoxy is approximately constant in the conversion range of 0.3 to 0.8 [102]. Furthermore, our nanocomposite systems showed substantially higher values of E_a than the neat PBA-a as seen in Table 5.5. The phenomenon is attributed to the difficulty to liberate decomposition gases from the matrix containing inorganic particles like nano-SiO_2 as well as an ability to form additional Si-O-C between the nano-SiO_2 and the polybenzoxazine matrix.

In principle, a variation of E_a with conversion in our specimens indicated that the reaction mechanism of their thermal decomposition is a relatively complex reaction mechanism that invalidates the separation of variables involved in the Flynn–Wall–Ozawa analysis [56]. As polymer degradation processes usually involve chain reactions, $f(\alpha)$ in Eq. (1) will represent a series of elemental steps being a function of conversion with each step having its own kinetic parameters.

The kinetic mechanisms can be accomplished by using a simplified version of the Coats–Redfern method. Accordingly, at a specific heating rate, the average activation energy can be estimated for every $g(\alpha)$, as listed in Table 2.6, by plotting ($\ln[g(\alpha)/T^2]$) versus 1/T (E.q2.10). Table 2.6 lists the calculated kinetic parameters for different models at a heating rate of 10^oC/min of the maximum degradation stage. The value of the E_a and mechanism model were selected based on the E_a that was similar to the value obtained by iso-conversional methods and showed linear trend with maximum correlation coefficient greater than 0.98. Table 5.6 lists mechanism models that are sufficiently similar in shape and provide calculated values of the E_a close to the value obtained by the iso-conversional methods. The selected models of our polybenzoxazine and its nanocomposites were then confirmed with the master plots based on the integral form of the kinetics which was found to be most suitable to predict the degradation behaviors of our specimens compared to the differential form or the Criado method [57].

5.3.4 Determination of the kinetic model by means of generalized master plots of nano-SiO_2 filled polybenzoxazine system

From the integral kinetic equation at infinite temperature in integral form, Eq. (2.16), we can obtain the following equation using a reference point at $\alpha = 0.5$.

The p(x) form was proposed by Senum and Yang [50], where x is E_a/RT and $\theta_{0.5}$ is the generalized time at $\alpha = 0.5$. The integral master plot method at infinite temperature can be constructed by comparing the experimental master plot of the reduced-generalized time, $\theta/\theta_{0.5}$, against α with various theoretical master plots of $g(\alpha)/g(0.5)$ against α [58].

Then the experimental master curves were obtained using the determined value of the average E_a from isoconversional method. Comparison of the experimental plots of $\theta/\theta_{0.5}$ against α with the theoretical plots of $g(\alpha)/g(0.5)$ against α was made as shown in Figure 5.36 to Figure 5.39 for 0-30wt% nano-SiO2 filled PBA-a nanocomposites. It is clearly seen from insets of Figure 5.36 to Figure 5.39 that the experimental master curves are in better agreement with the theoretical master curve corresponding to the F1, D3, D3 and D3 mechanisms for the main degradation stage of 0, 10, 20, and 30wt% of nano-SiO2 filled PBA-a nanocomposites, respectively. The corresponding E_a and ln A values for the most probable theoretical kinetic models were determined from Coats-Redfern method and the average values from the heating rates of 5, 10, 15, and 20^oC/min were obtained and listed in Table 5.6.

From the kinetic parameters for all degradation stages in Table 5.7, it is clearly seen that the average E_a and lnA of each degradation stage increases with the addition of the nano-SiO2 nanoparticle. For example, the average E_a and lnA in the main degradation stage are 116 kJ/mol and 13.6 for the neat PBA-a while the 10wt% nano-SiO2 filled PBA-a nanocomposite possesses an average E_a and lnA of 157 kJ/mol and 19.1. Moreover, the relatively high nano-SiO2 content (10-30 wt%) in our nanocomposites was found to provide similar values of the E_a and lnA of the thermal degradation reaction.

Chissafis and coworkers reported the calculated activation energy values of high density polyethylene (HDPE) and silica (5wt%) to be higher than that of neat HDPE suggesting the evidence that SiO_2 causes stabilization in thermal decomposition of HDPE. Bera et al. [102] prepared a series of polystyrene/silica nanocomposites with 2-30wt% of the nanofiller content. It was found that the highest thermal stability of the nanocomposite belongs to the 18% silica content sample. Due

to nanoparticle agglomeration in the sample containing silica above the optimum loading, the thermal stability of the samples is decreasing implying that the systems turn from nanostructure to microstructure composites.

From Table 5.8, it can be observed that the degradation of neat PBA-a at first and second stages were proved to obey the F1 mechanism. In the F1 type of mechanism, the degradation is initiated from random points that act as growth center for the development of the degradation reaction. That means random nucleation with one nucleus on the individual particle [52]. While the diffusion-controlled character (D3) of the thermal degradation processes was took place in the final stage. The similar behaviour was observed in $(C_{29}H_{24}N_{205})_n$ polymeric resin by Perondi and coworkers [133]. The authors reported that the pyrolysis kinetics of the above polymeric resin, formed by the reaction of a polymeric isocyanate and phenolic resin, are controlled by a Fn type chemical reaction at conversions lower than approximately 0.8 whereas at conversions above 0.8, a change in the rate-limiting step, i.e. chemical reaction to diffusion, was also observed [133]. The phenomena observed were attributed to the decrease in mobility of the reacting species possibly from the enhancement crosslink density or viscosity of the polymer at high conversion [134]. The change in degradation mechanism from Avrami-Erofeev model at low conversion to contracting sphere model at higher conversion was also reported in the interpenetrating polymer network of poly(trimethyol propane triacrylate)/poly(hexane diol diacrylate) at weight ratio of 50:50 etc. [135].

For the nano-SiO_2/polybenzoxazine nanocomposites, the mechanism was recognized to be three-dimensional diffusion (D3) reaction for all three degradation stages. The difference in the degradation mechanisms of a polymer matrix and its nanocomposites has been observed in various systems such as in epoxy nanocomposite containing polythiophene nanoparticles [136] and polyurethane–siloxane anionomers [137]. Montero et al. observed that the presence of POSS changed the thermal degradation of an epoxy resin from first order to a mechanism controlled by diffusion [102].

Three-dimensional diffusion mechanism (D3) associated with the diffusion process in three dimensions. When one deal with a solid or with high viscosity melts, the mass transfer processes are rate-determining for the whole process. The

decomposition products must diffuse to the surface to be evaporated through the char formed or through the nanoparticles labyrinth i.e. degradation is a faster process, while it is diffusion of the volatile products to the surface which is rate-controlling process. Therefore, the diffusion mechanism is rate-controlling process at the final decomposition stage of the neat polybenzoxazine with sufficient char formation or for all stages of our highly filled nano-SiO_2/PBA-a composites.

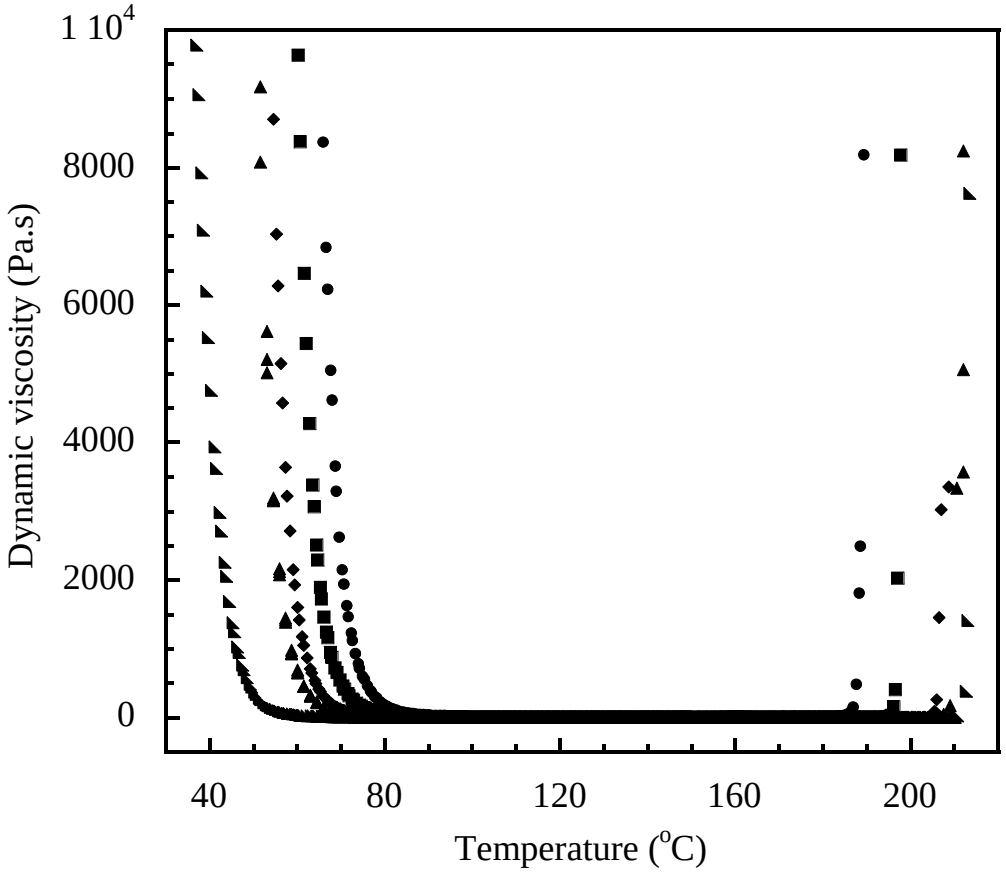

Figure 5.1 Processing window of BA-a/YD126 resin at various compositions: (●) BA-a/YD126 100/0, (■) BA-a/ YD126 90/10, (▲) BA-a/ YD126 80/20, (◣) BA-a/ YD126 70/30 and (◆) BA-a/YD126 60/40.

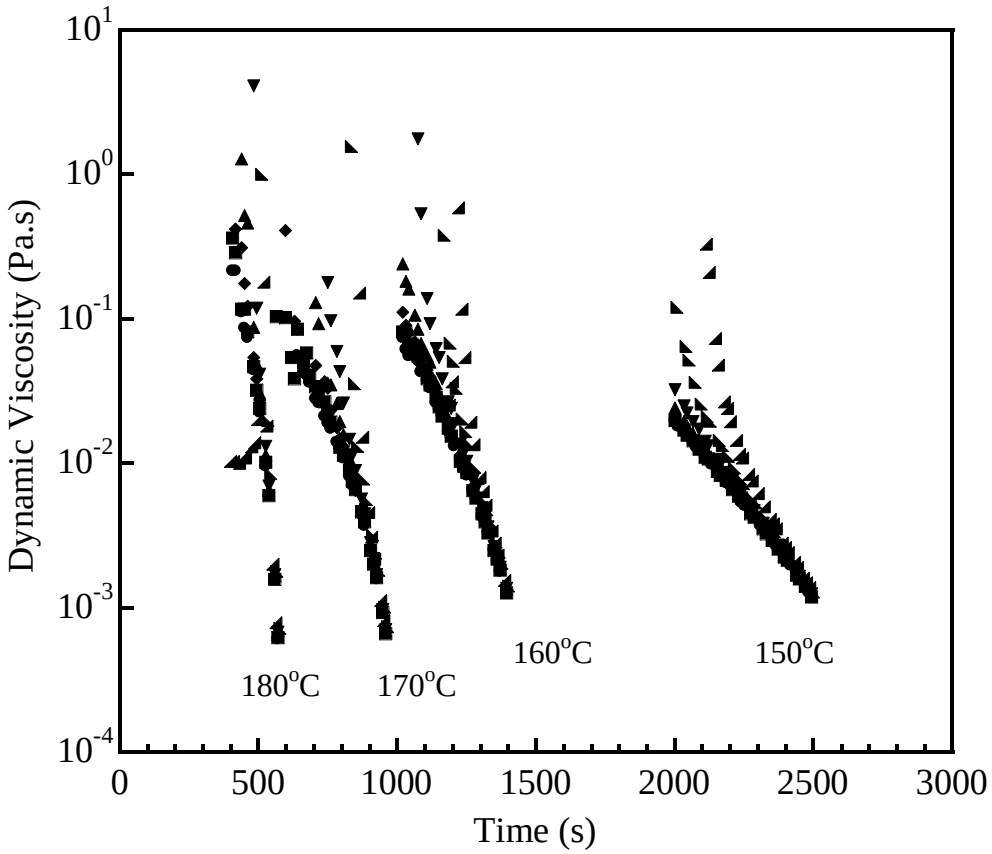

Figure 5.2 Effect of gel temperature on the gel time of BA-a: (●) 1.6Hz, (■) 2.8Hz, (♦) 5.0Hz, (▲) 9.0Hz, and (◣) 15.9Hz.

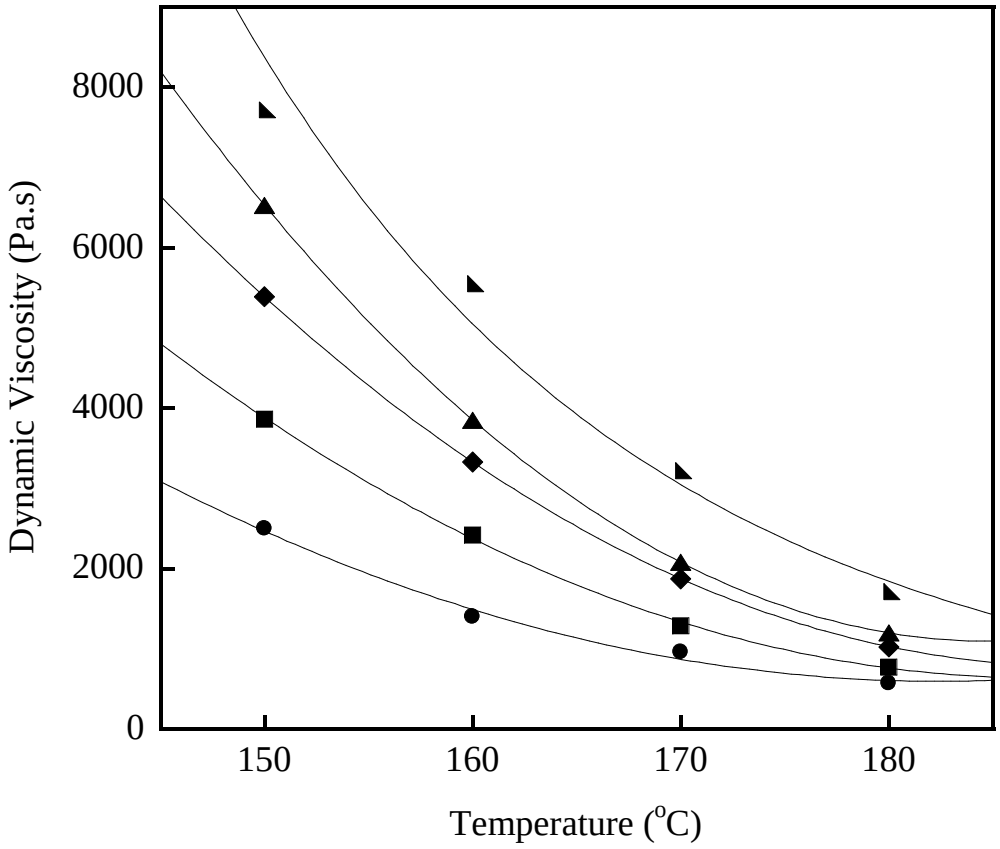

Figure 5.3 Gelation behavior of BA-a mixed with epoxy resin at various composition as a function of gel temperature:(●) BA-a/YD126 100/0, (■) BA-a/ YD126 90/10, (▲) BA-a/ YD126 80/20, (◣) BA-a/ YD126 70/30 and (◆) BA-a/YD126 60/40.

.

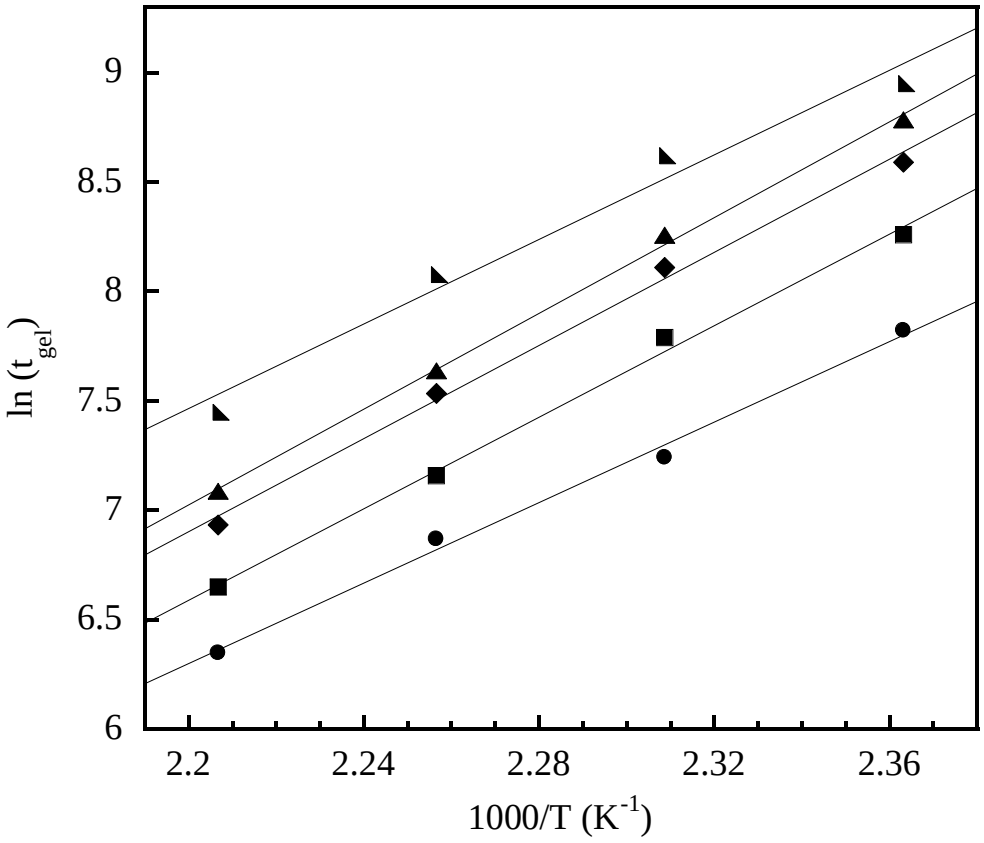

Figure 5.4 The Arrhenius plot of the gelation behavior of BA-a mixed with epoxy resin at various composition:(●) BA-a/YD126 100/0, (■) BA-a/ YD126 90/10, (▲) BA-a/ YD126 80/20, (◣) BA-a/ YD126 70/30 and (◆) BA-a/YD126 60/40.

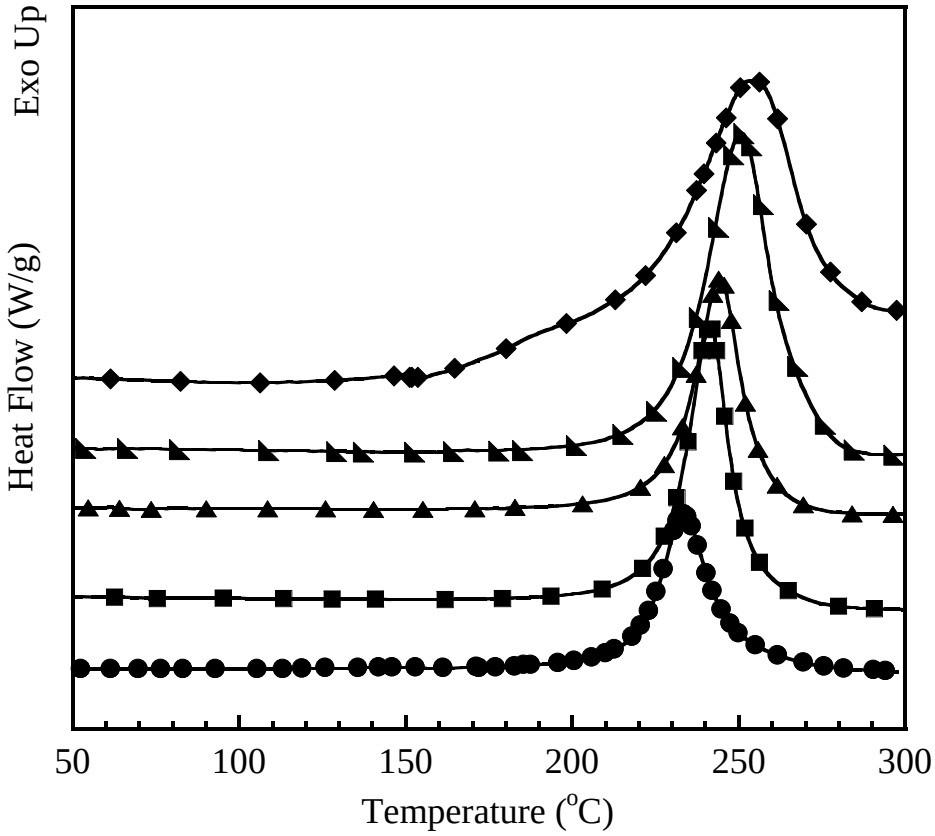

Figure 5.5 DSC thermograms of BA-a/YD126 resin at various compositions: (●) BA-a/YD126 100/0, (■) BA-a/ YD126 90/10, (▲) BA-a/ YD126 80/20, (◣) BA-a/ YD126 70/30 and (◆) BA-a/YD126 60/40.

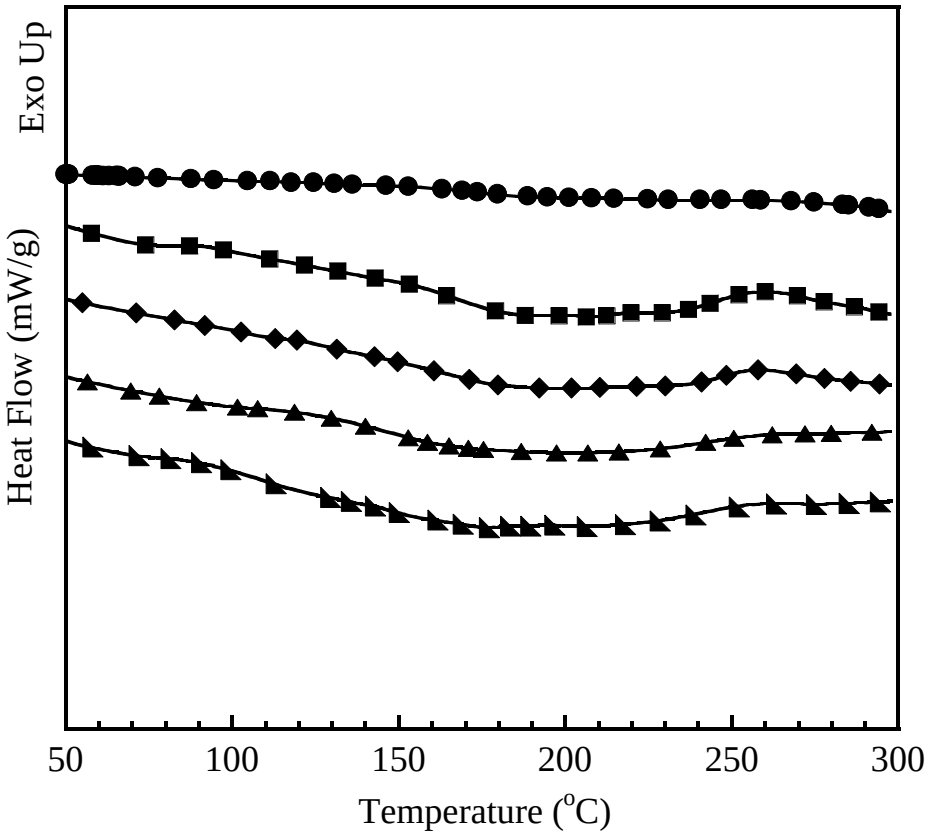

Figure 5.6 DSC thermograms showing glass-transition temperature of BA-a/ YD126 alloys at various compositions : (●) BA-a/YD126 100/0, (■) BA-a/ YD126 90/10, (◆) BA-a/ YD126 80/20, (▲) BA-a/ YD126 70/30 and (▼) BA-a/ YD126 60/40.

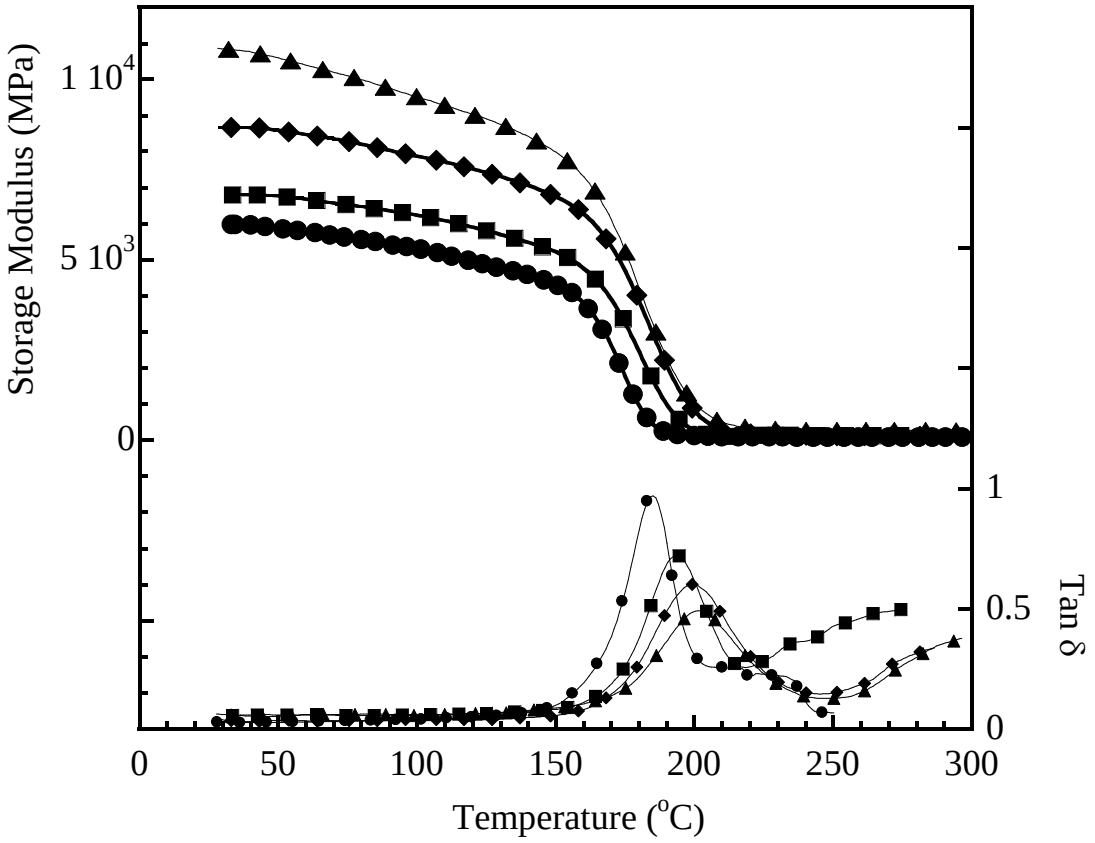

Figure 5.7 Dependence of storage modulus and mechanical damping factor of PBA-a with temperature for samples with different filler contents: (●) 0wt%, (■) 10wt% nano-silica, (♦) 20wt% nano-silica, (▲) 30wt% nano-silica.

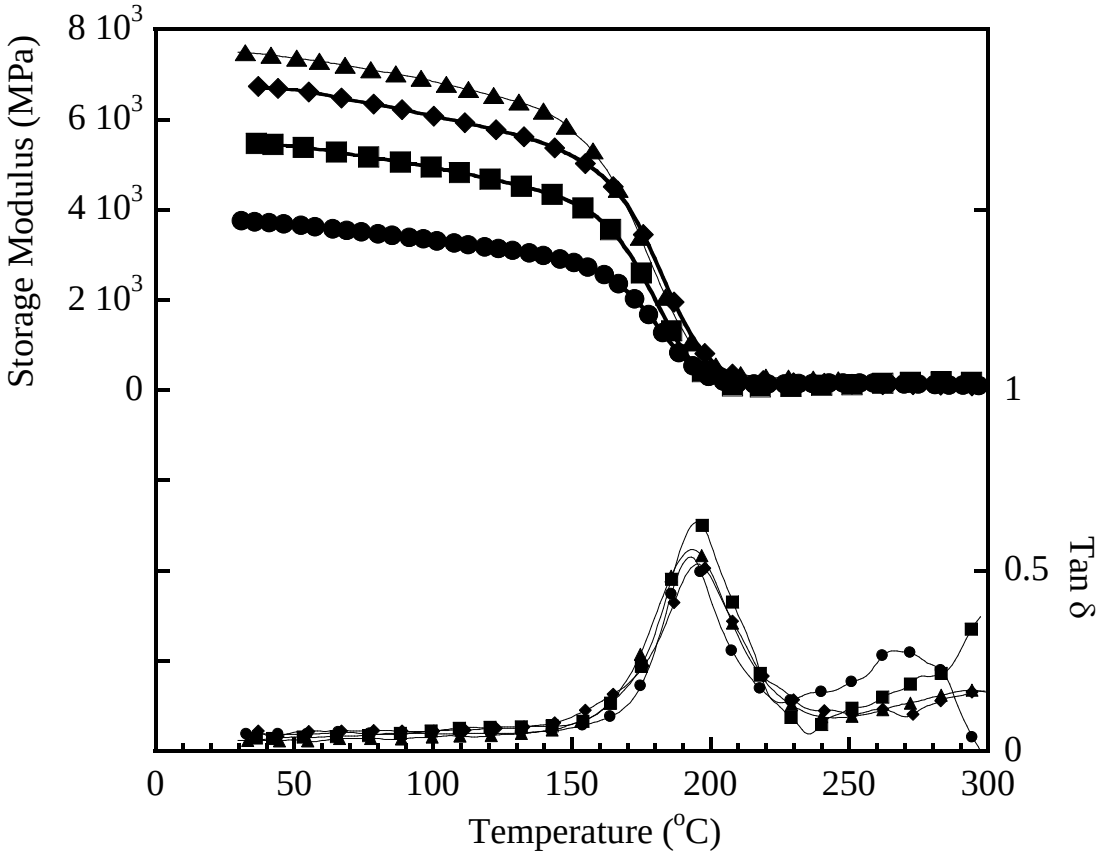

Figure 5.8 Dependence of storage modulus and mechanical damping factor of PBA-a/ YD126 80/20 with temperature for samples with different filler contents: (●) 0wt%, (■) 10wt% nano-silica, (♦) 20wt% nano-silica, (▲) 30wt% nano-silica.

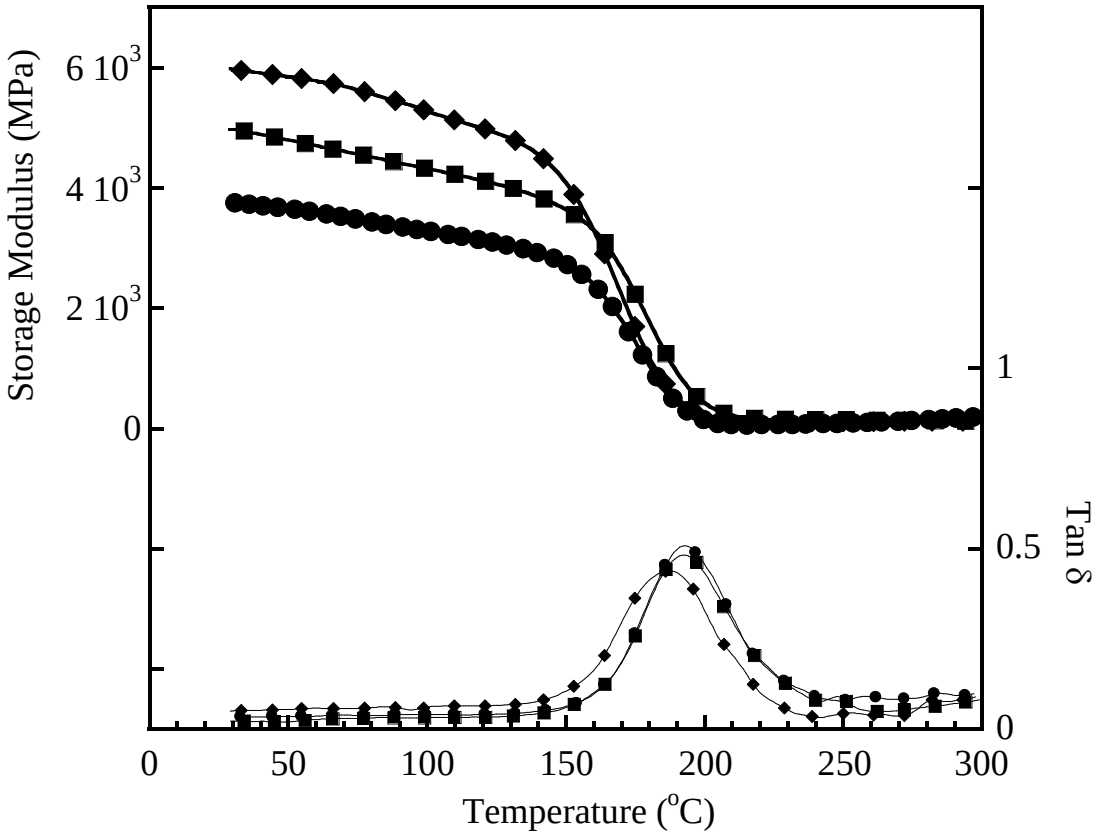

Figure 5.9 Dependence of storage modulus and mechanical damping factor of PBA-a/ YD126 60/40 with temperature for samples with different filler contents: (●) 0wt%, (■) 10wt% nano-silica, (♦) 20wt% nano-silica.

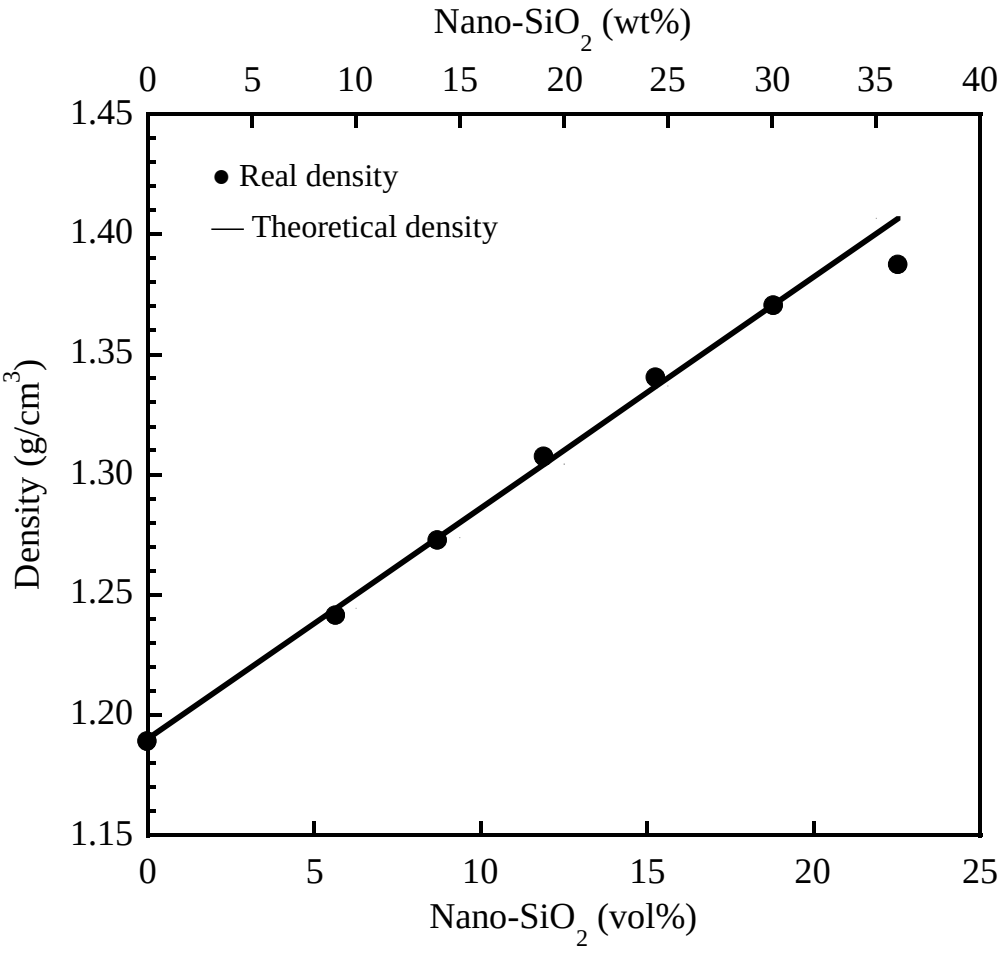

Figure 5.10 Maximum packing density of nano-SiO2-filled polybenzoxazine:

(-) theoretical density, (●) experimental density.

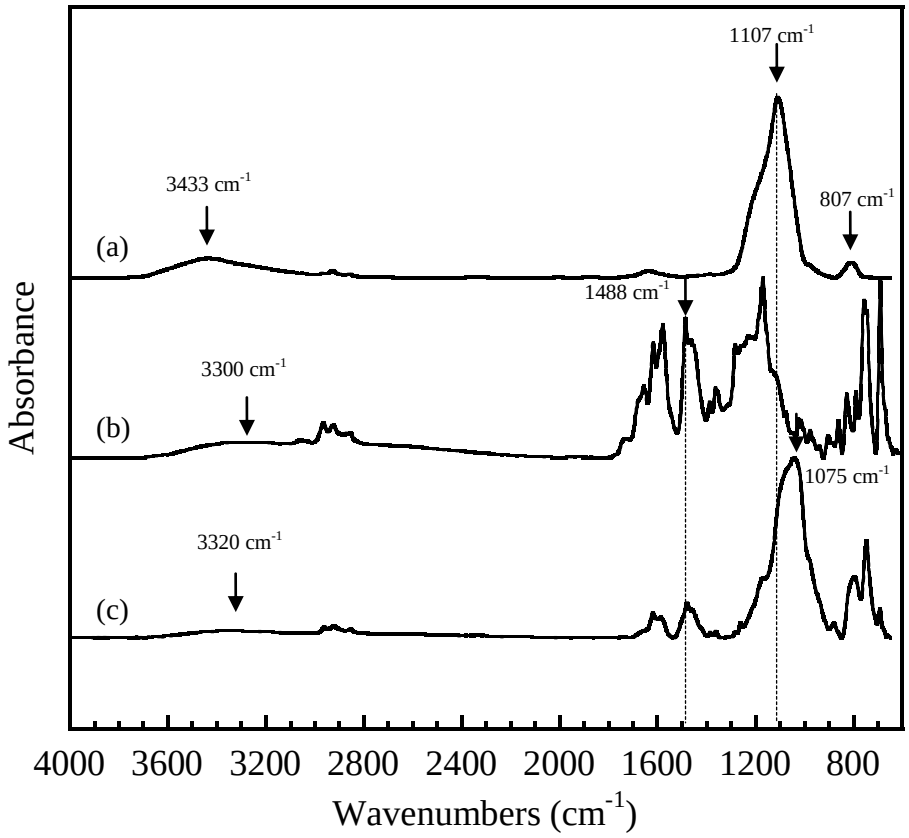

Figure 5.11 FT-IR spectra of (a) nano-silica, (b) PBA-a, and (c) 30wt% nano-SiO_2-filled PBA-a

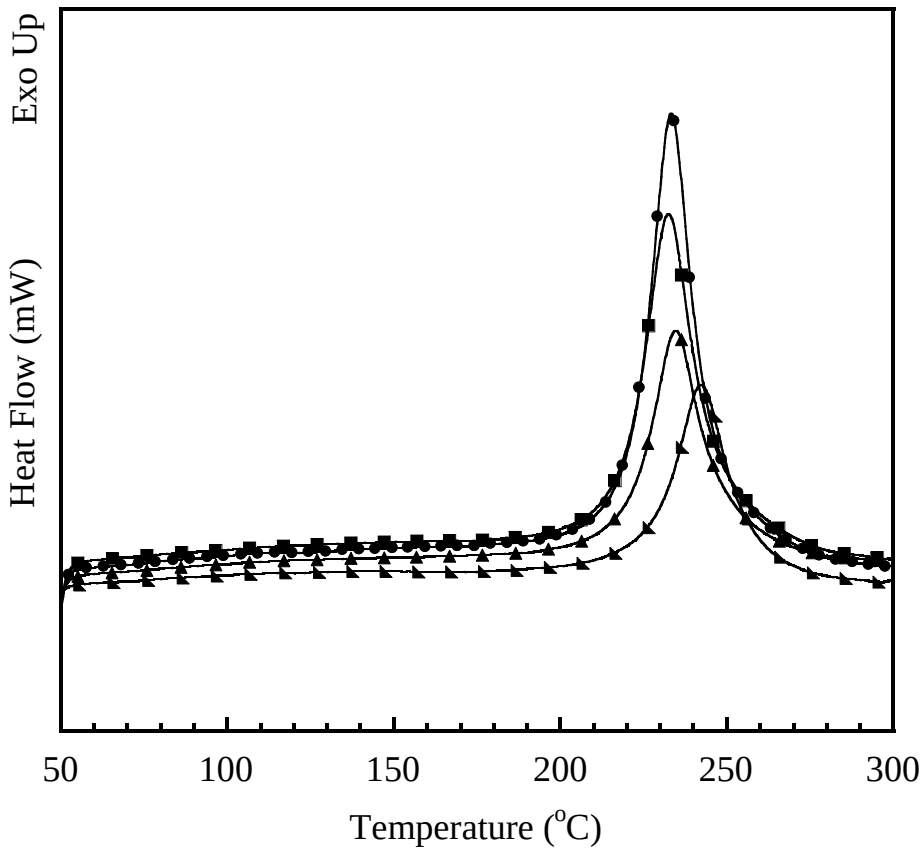

Figure 5.12 DSC thermograms of benzoxazine molding compound at different nano-SiO_2 contents: (●) BA-a, (■) 10wt%, (♦) 15wt%, (▼) 20wt%, (▲) 25wt% and (◣) 30wt% nano-SiO_2-filled BA-a.

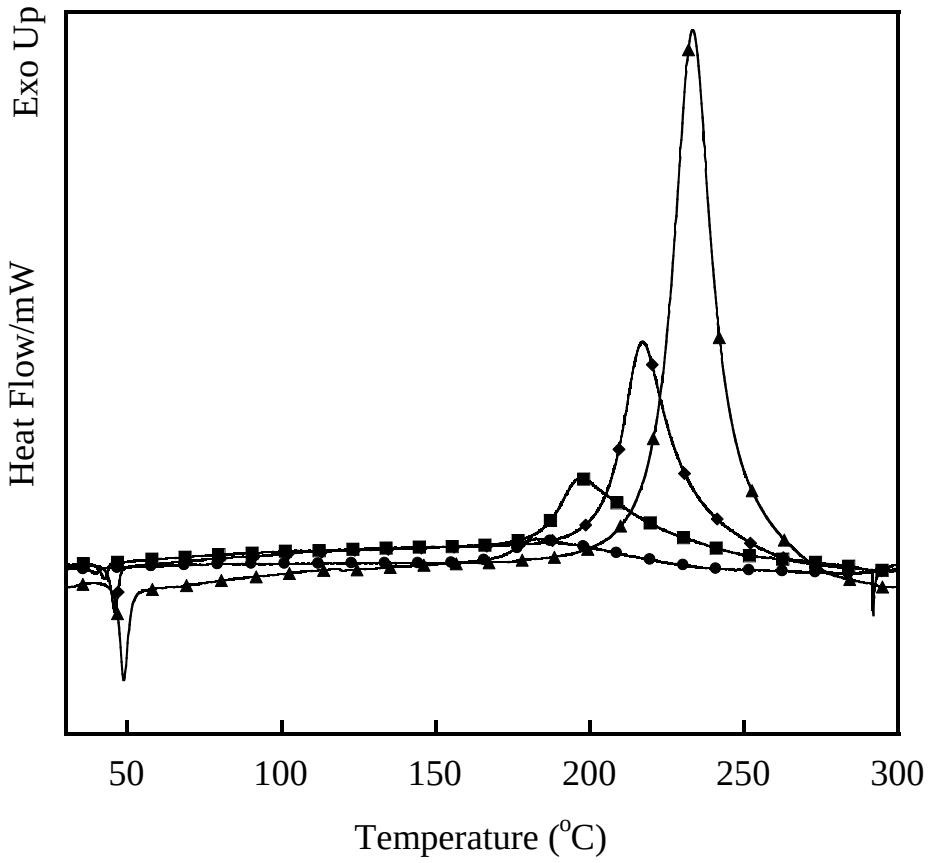

Figure 5.13 DSC thermograms of BA-a at different heating rate: (●) 1 $Kmin^{-1}$, (■) 2 $Kmin^{-1}$, (♦) 5 $Kmin^{-1}$, and (▲) 10 $Kmin^{-1}$.

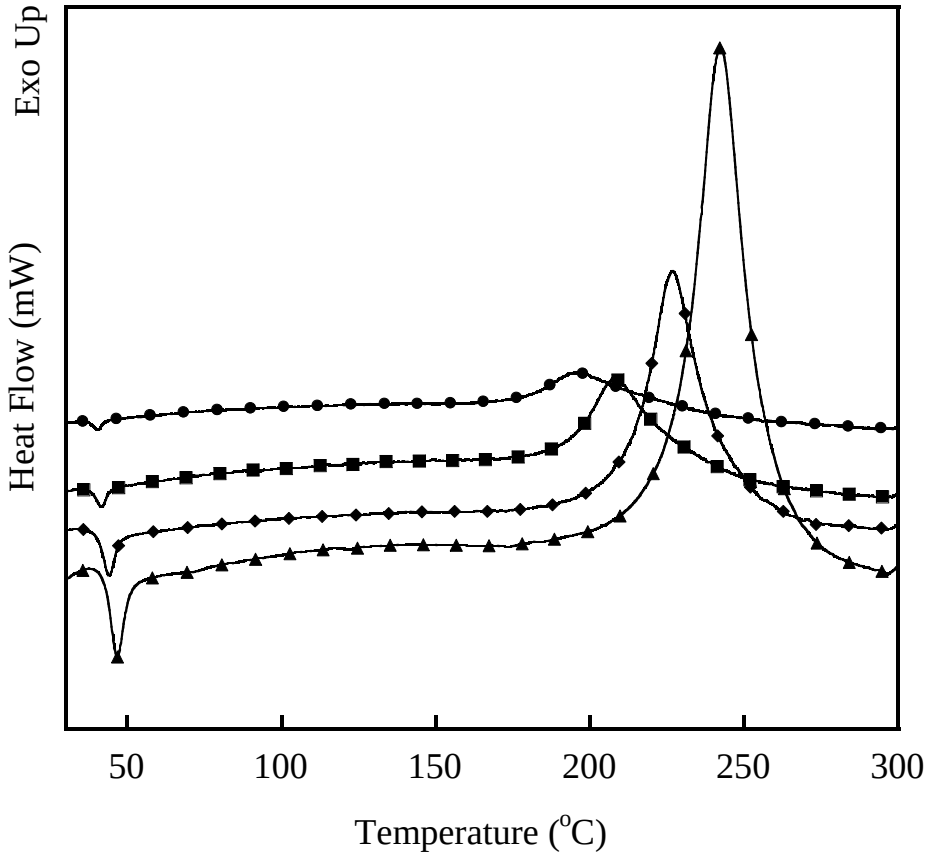

Figure 5.14 DSC thermograms of 30wt% nano-SiO_2-filled BA-a at different heating rate: (●) 1 $Kmin^{-1}$, (■) 2 $Kmin^{-1}$, (♦) 5 $Kmin^{-1}$, and (▲) 10 $Kmin^{-1}$.

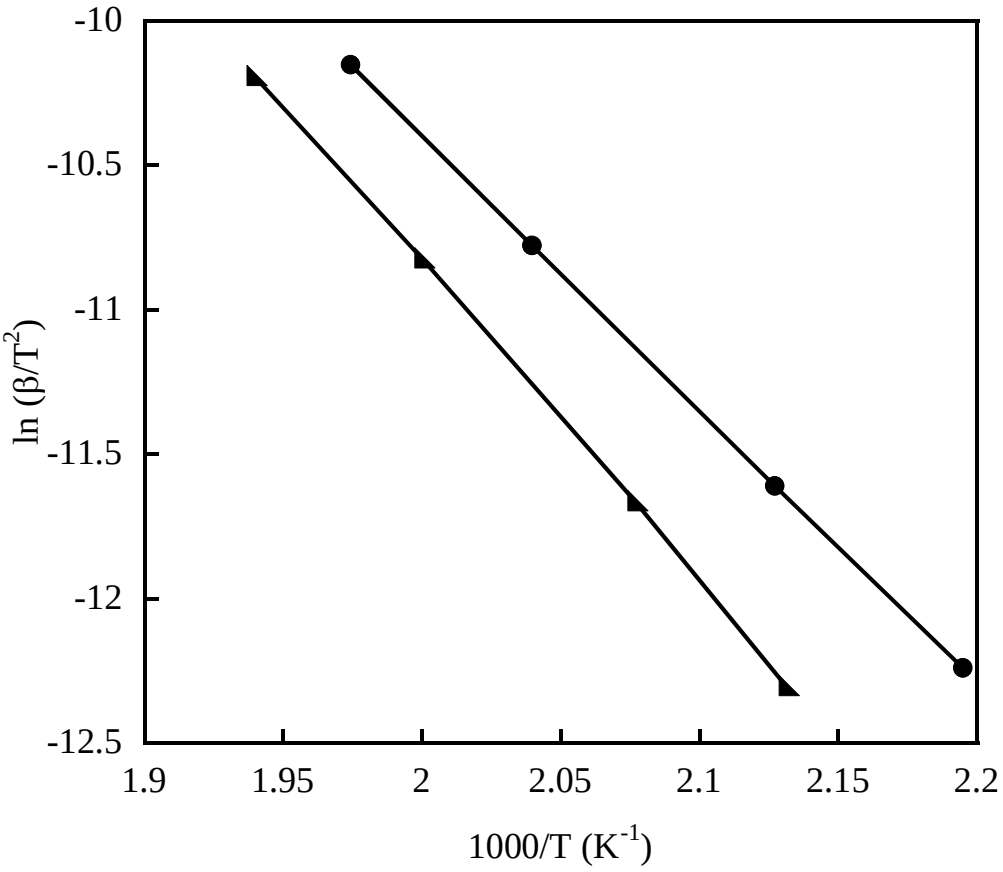

Figure 5.15 Kissinger plot with multi-heating rate of (●) BA-a,

(◣) 30wt% nano-SiO_2-filled BA-a.

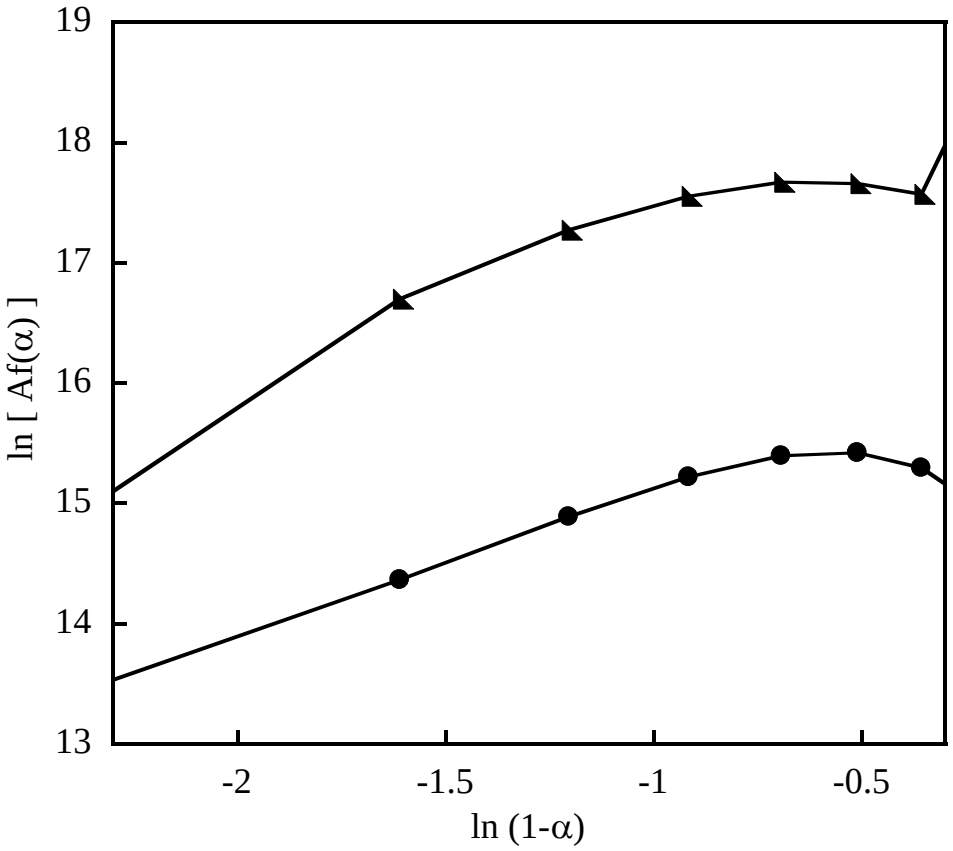

Figure 5.16 Friedman plot with multi-heating rate of (●) BA-a,

(◣) 30wt% nano-SiO_2-filled BA-a.

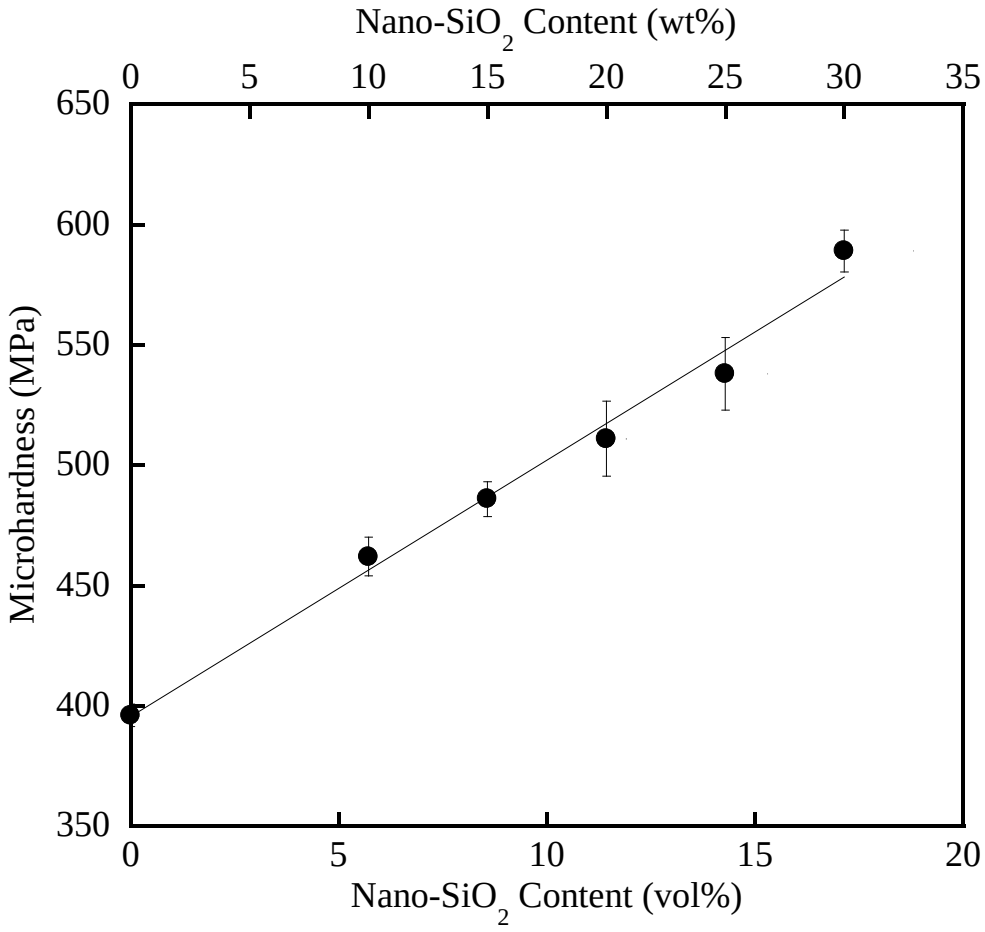

Figure 5.17 Effect of filler volume fraction on the microhardness of PBA-a/SiO_2 nanocompositess.

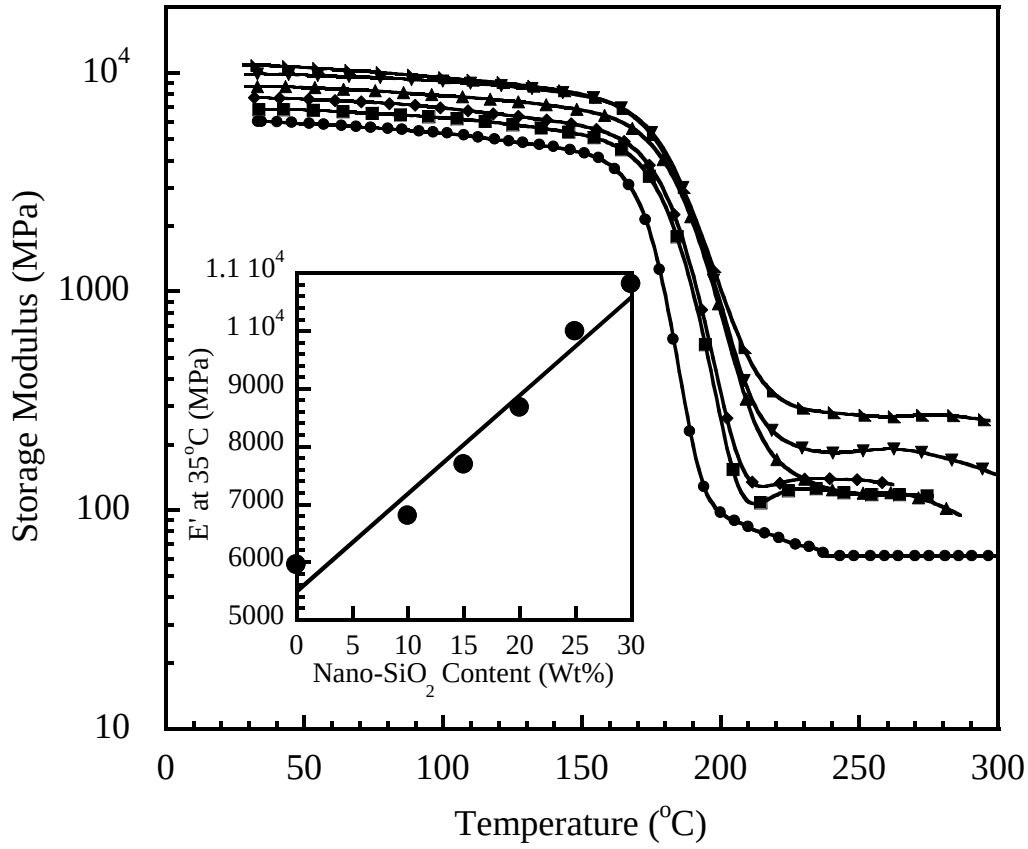

Figure 5.18 Dependence of storage modulus with temperature for samples with different filler contents: (●) PBA-a, (■) 10wt% nano-silica, (♦) 15t% nano-silica, (▲) 20wt% nano-silica, (▼) 25% nano-silica, (◣) 30wt% nano-silica. Inset: storage modulus at glassy state.

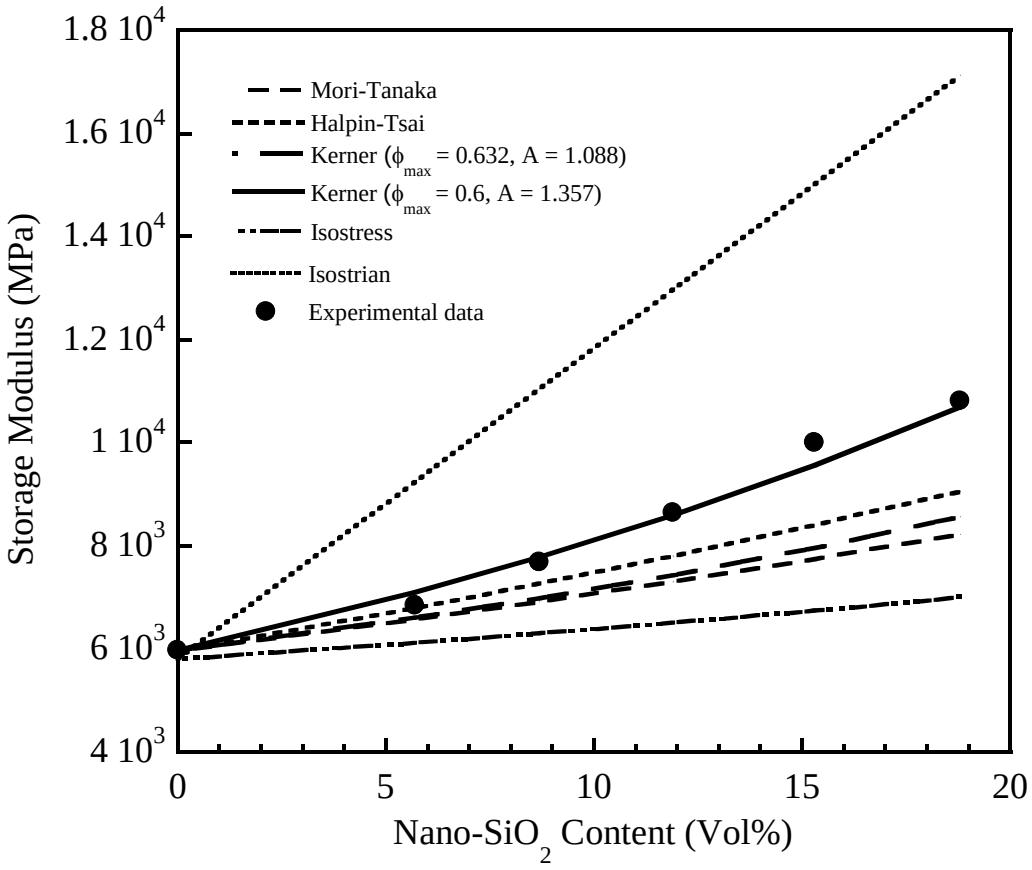

Figure 5.19 Storage modulus at 30°C versus volume content of PBA-a/nano-SiO_2 composite.

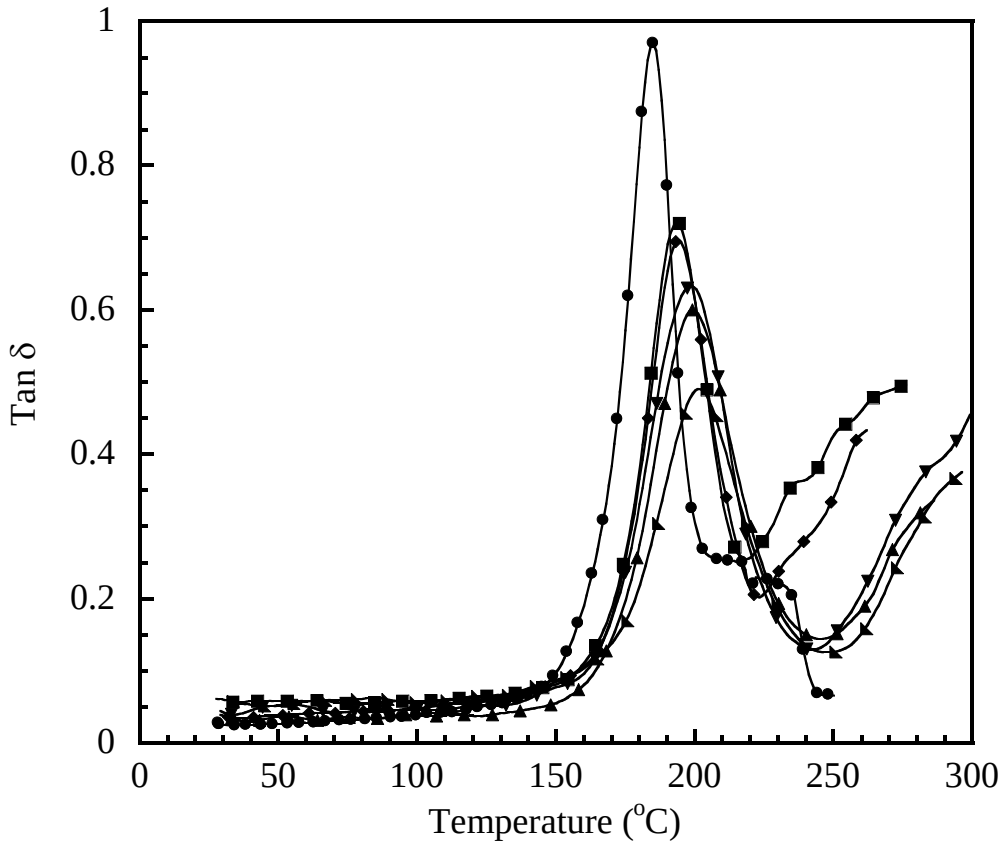

Figure 5.20 Mechanical damping factor of neat PBA-a and different amount of SiO_2-filled PBA-a.

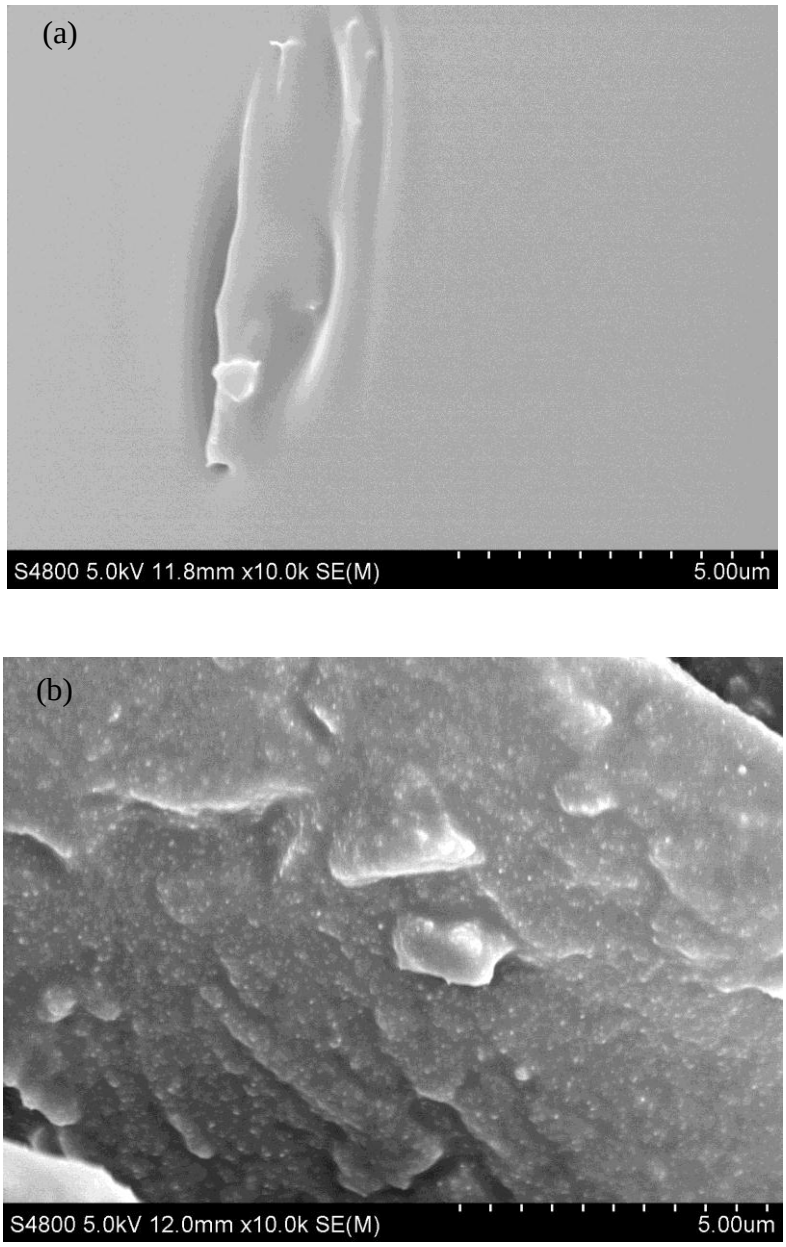

Figure 5.21 Fracture surface of (a) PBA-a (b) 10wt% nano-silica filled PBA-a.

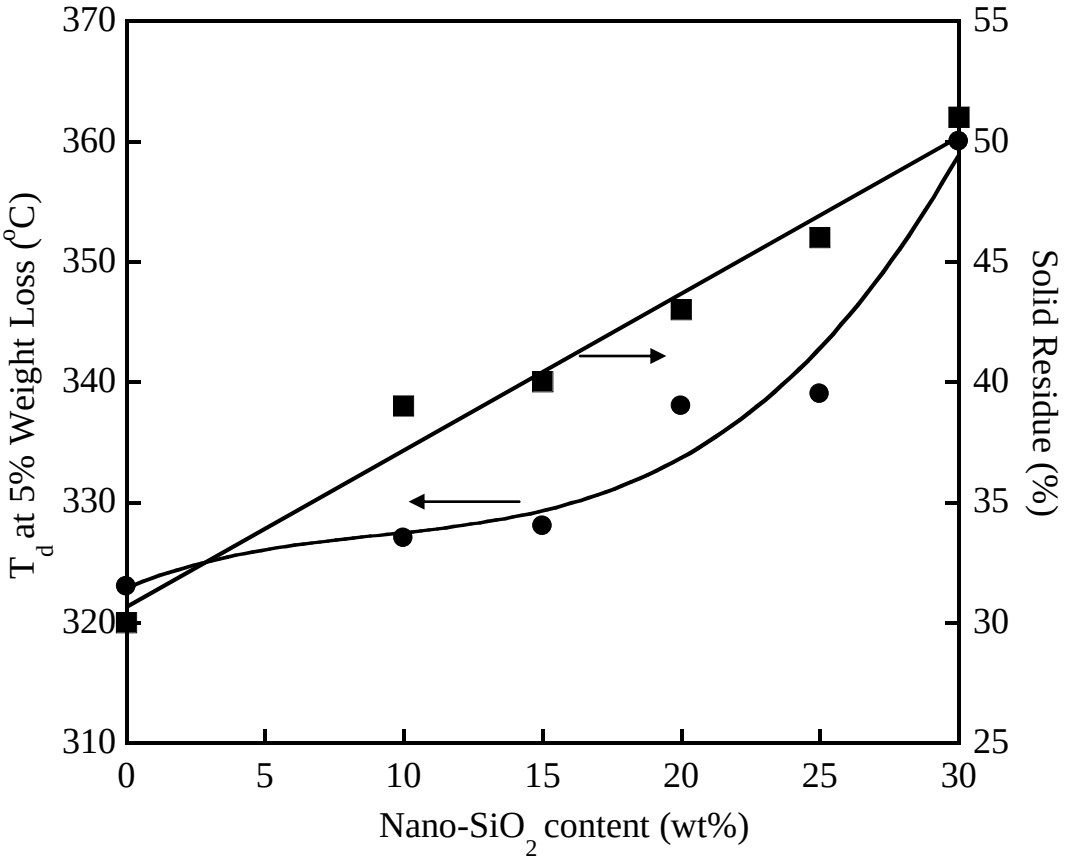

Figure 5.22 (■)Thermal degradation temperature at 5% weight loss and (●) solid residual at 850°C of PBA-a/SiO_2 nanocomposites.

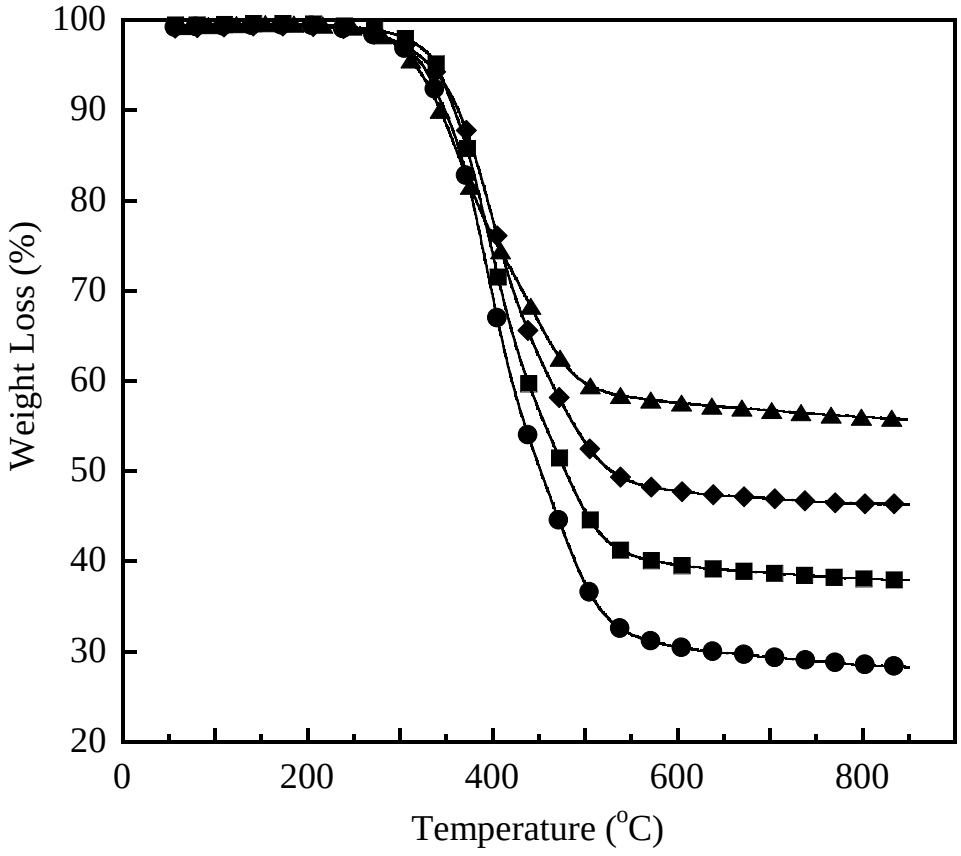

Figure 5.23 Thermogravimetric curves of polybenzoxazine and its nanocomposites at various nano-SiO2 contents: (●) PBA-a, (■) 10 wt%, (◆) 20 wt%, (▲) 30 wt% of nano-SiO_2 filled PBA-a composites.

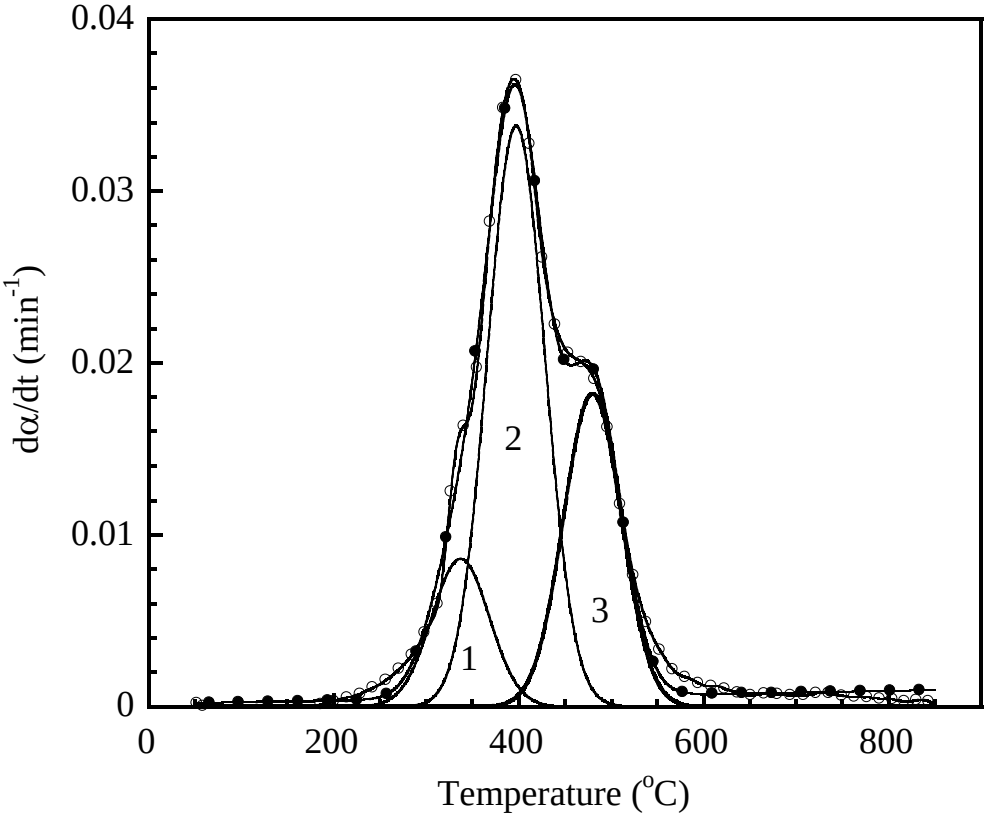

Figure 5.24 DTG curve and individual contributions of PBA-a, $R^2 = 0.9962$ (●) experimental data, (○) simulated curve at 10°C/min, (—) deconvolution of each stage.

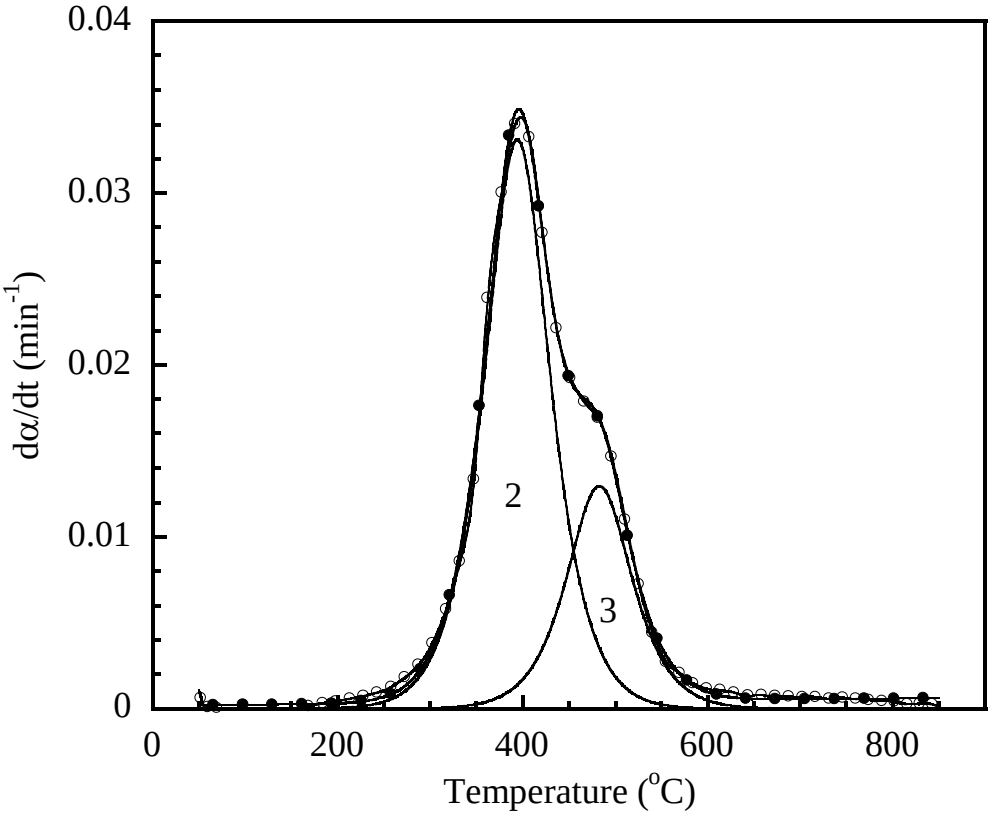

Figure 5.25 DTG curve and individual contributions of 10wt% nano-SiO2-filled PBA-a nanocomposites, $R^2 = 0.9982$ (●) experimental data, (○) simulated curve at 10°C/min, (—) deconvolution of each stage.

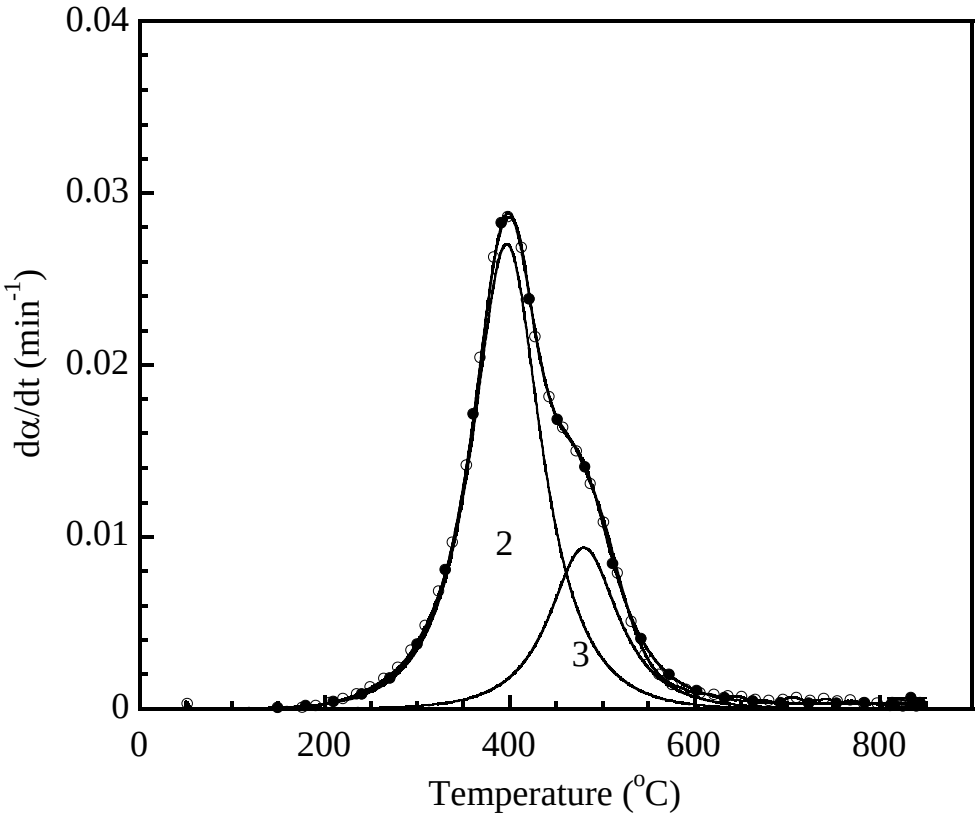

Figure 5.26 DTG curve and individual contributions of 20wt% nano-SiO2-filled PBA-a nanocomposites, $R^2 = 0.9993$ (●) experimental data, (○) simulated curve at 10°C/min, (—) deconvolution of each stage.

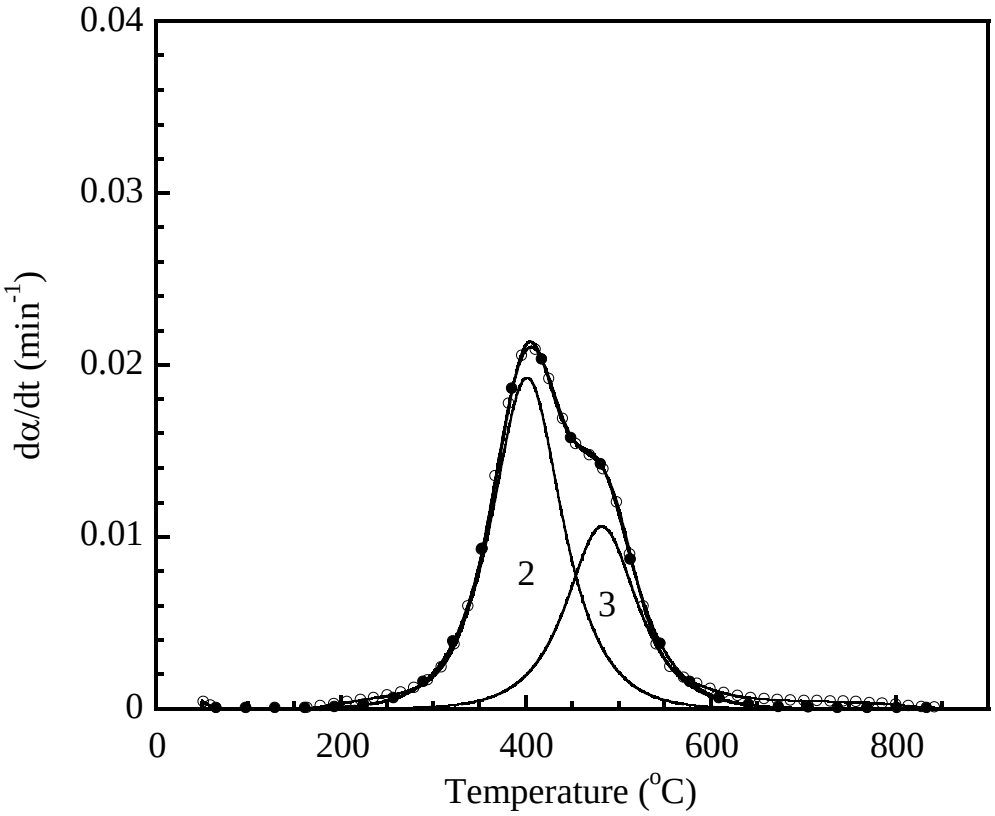

Figure 5.27 DTG curve and individual contributions of 30wt% nano-SiO2-filled PBA-a nanocomposites, $R^2 = 0.9978$ (●) experimental data, (○) simulated curve at 10°C/min, (—) deconvolution of each stage.

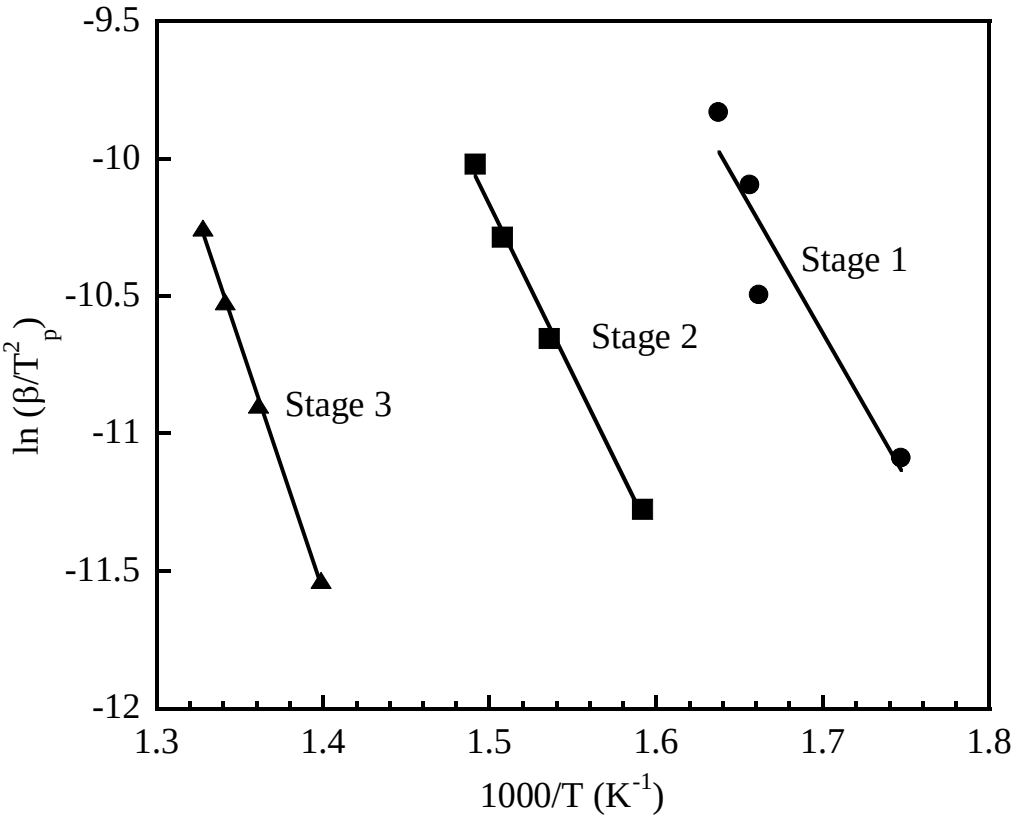

Figure 5.28 Plots of ln β/T^2_p versus $1000/T_p$ at different heating rates according to Kissinger method for the PBA-a.

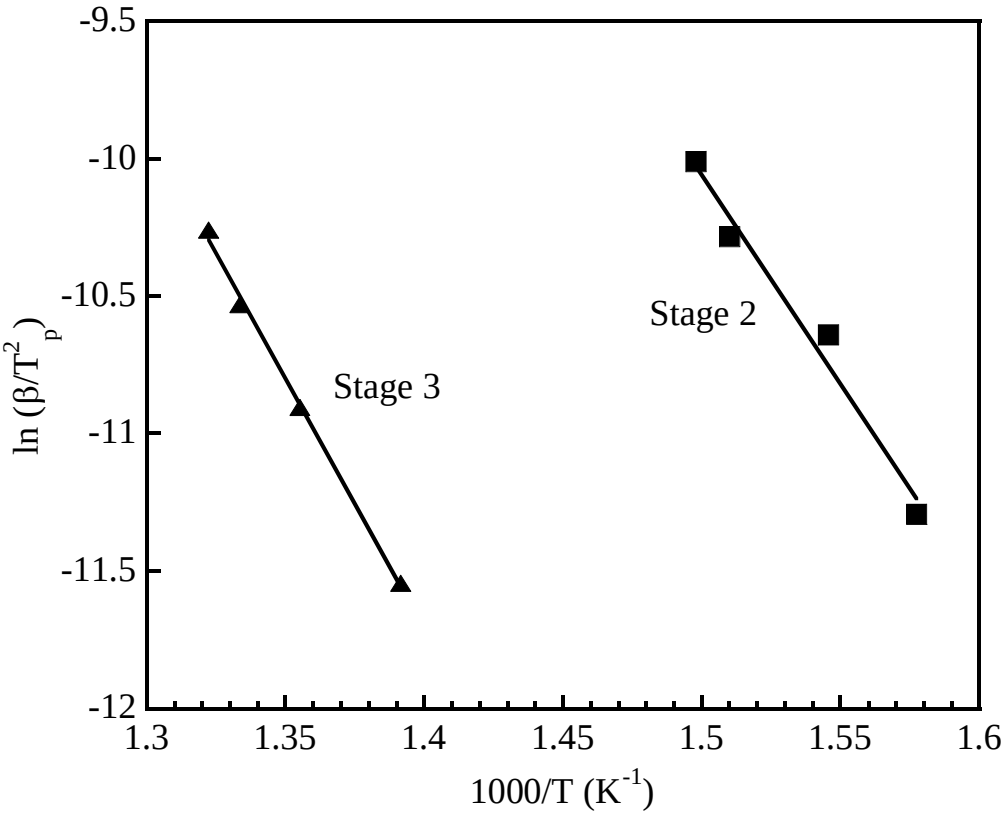

Figure 5.29 Plots of ln β/T^2_p versus $1000/T_p$ at different heating rates according to Kissinger method for the 10wt% nano-SiO2-filled PBA-a nanocomposites.

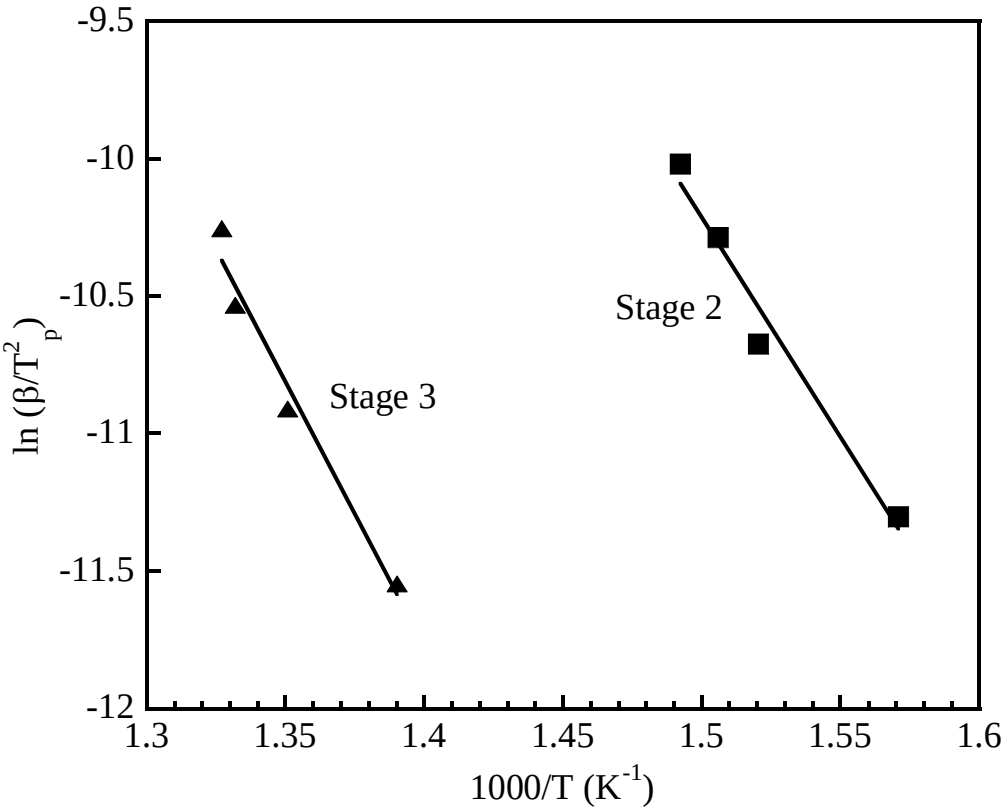

Figure 5.30 Plots of ln β/T^2_p versus $1000/T_p$ at different heating rates according to Kissinger method for the 20wt% nano-SiO2-filled PBA-a nanocomposites.

.

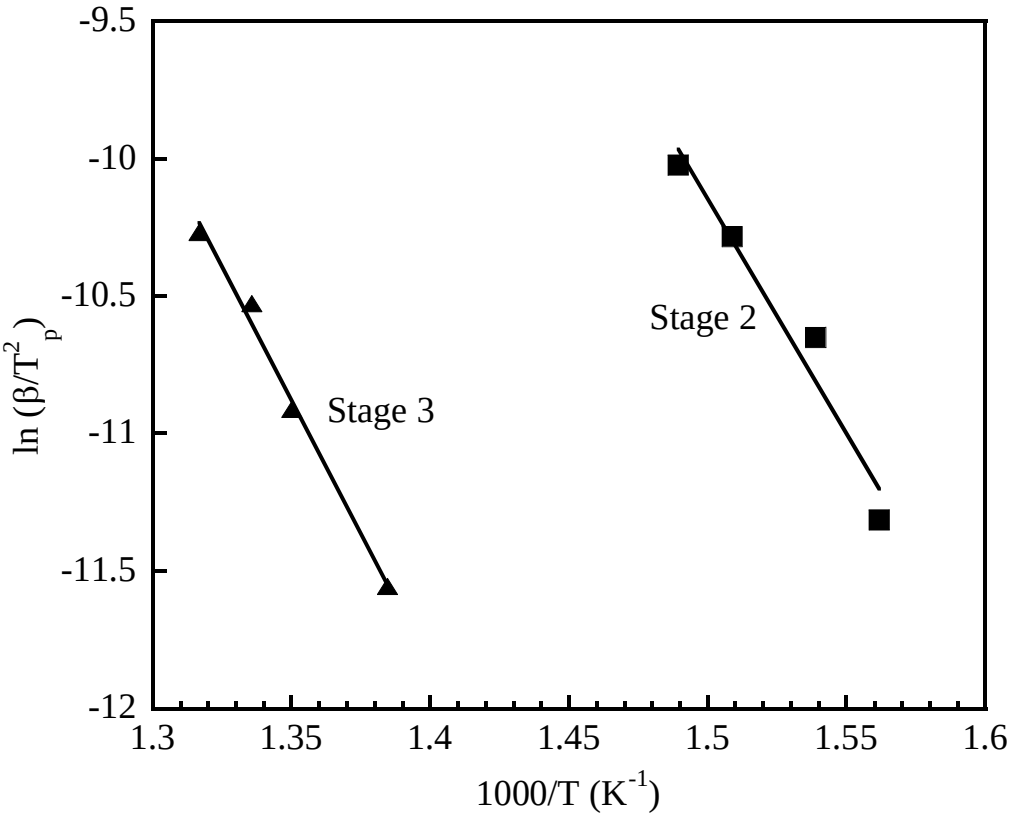

Figure 5.31 Plots of ln β/T^2_p versus $1000/T_p$ at different heating rates according to Kissinger method for the 30wt% nano-SiO2-filled PBA-a nanocomposites.

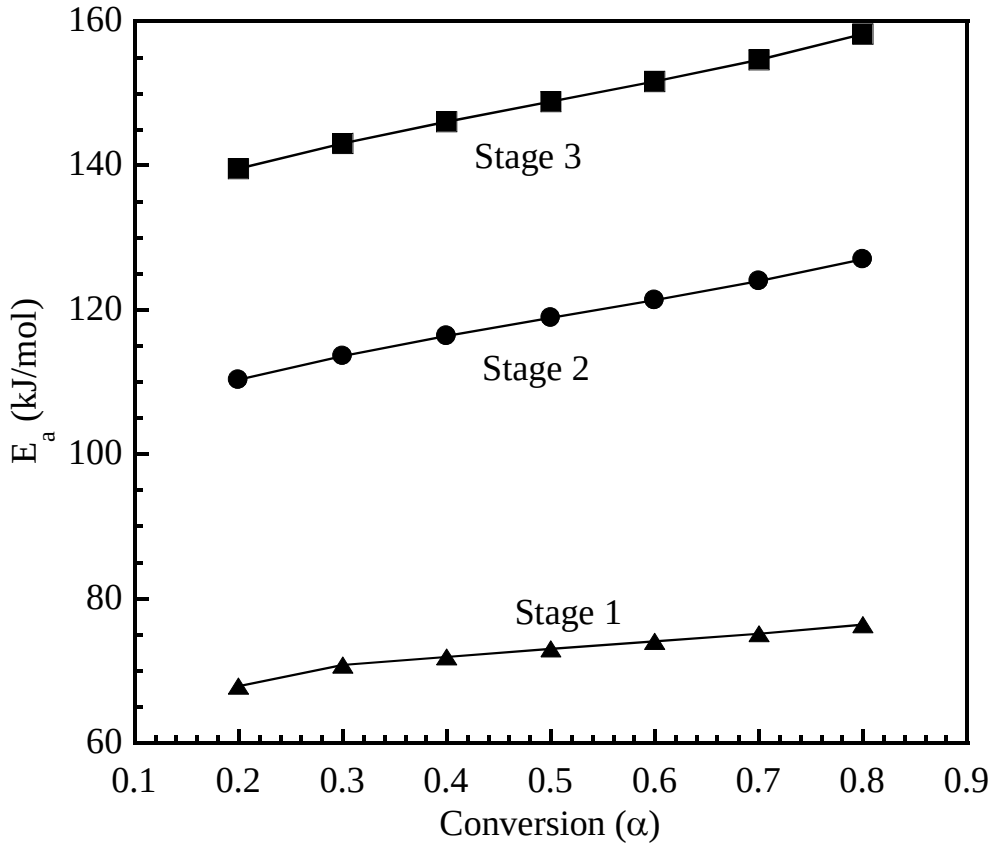

Figure 5.32 Dependence of activation energy (E_a) on degree of the conversion (α) of the weight loss for the main degradation process as determined by Flynn–Wall–Ozawa's method of PBA-a.

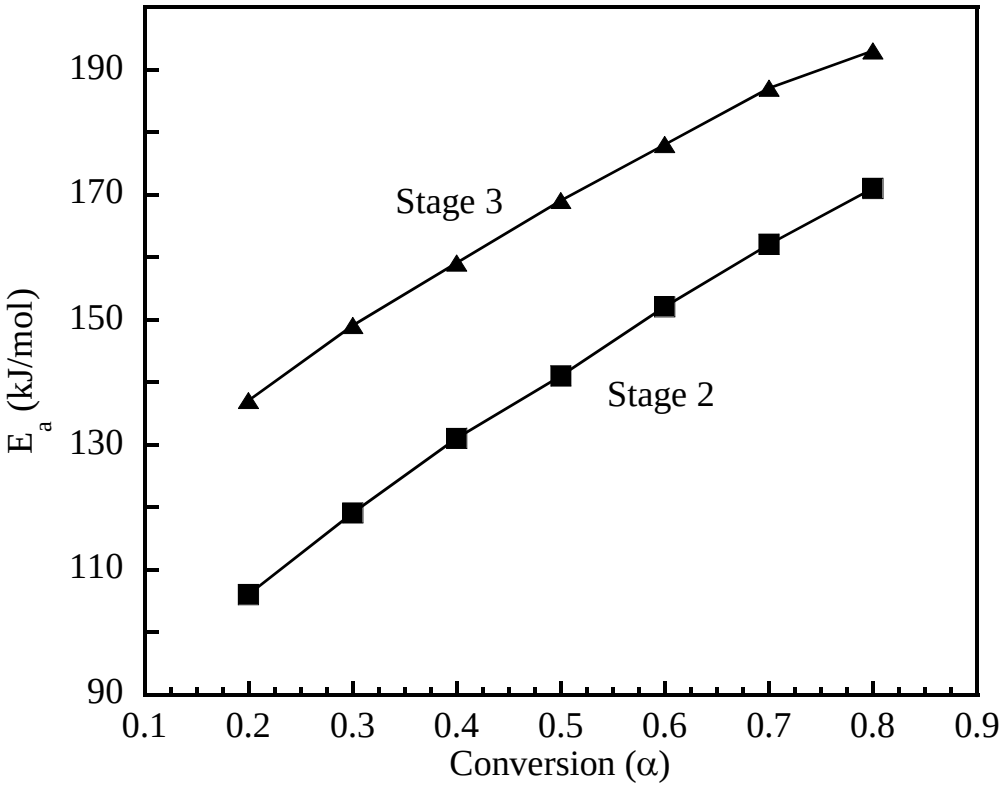

Figure 5.33 Dependence of activation energy (E_a) on degree of the conversion (α) of the weight loss for the main degradation process as determined by Flynn–Wall–Ozawa's method of 10wt% nano-SiO2-filled PBA-a.

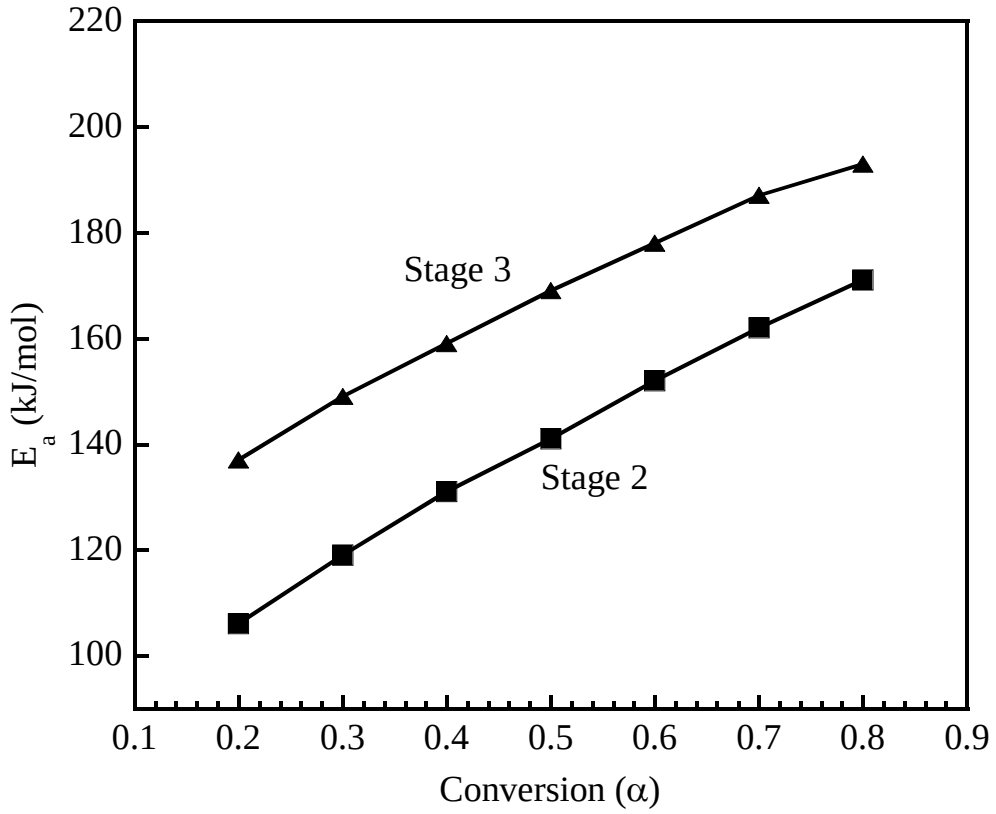

Figure 5.34 Dependence of activation energy (E_a) on degree of the conversion (α) of the weight loss for the main degradation process as determined by Flynn–Wall–Ozawa's method of 20wt% nano-SiO2-filled PBA-a.

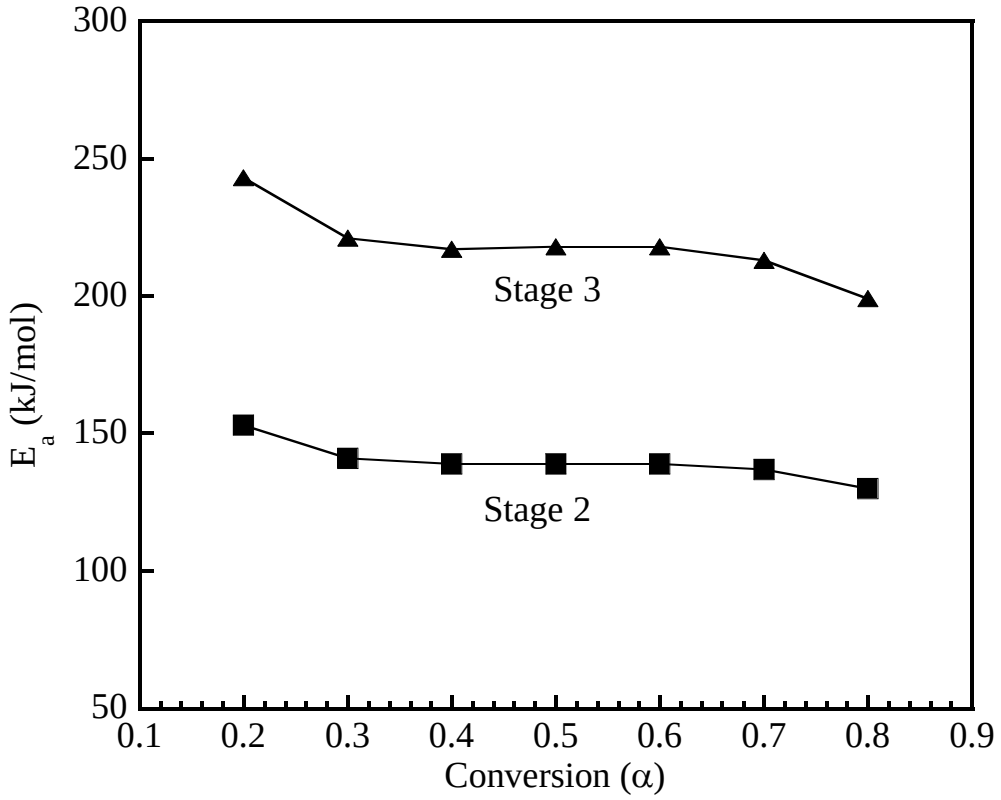

Figure 5.35 Dependence of activation energy (E_a) on degree of the conversion (α) of the weight loss for the main degradation process as determined by Flynn–Wall–Ozawa's method of 30wt% nano-SiO2-filled PBA-a nanocomposites.

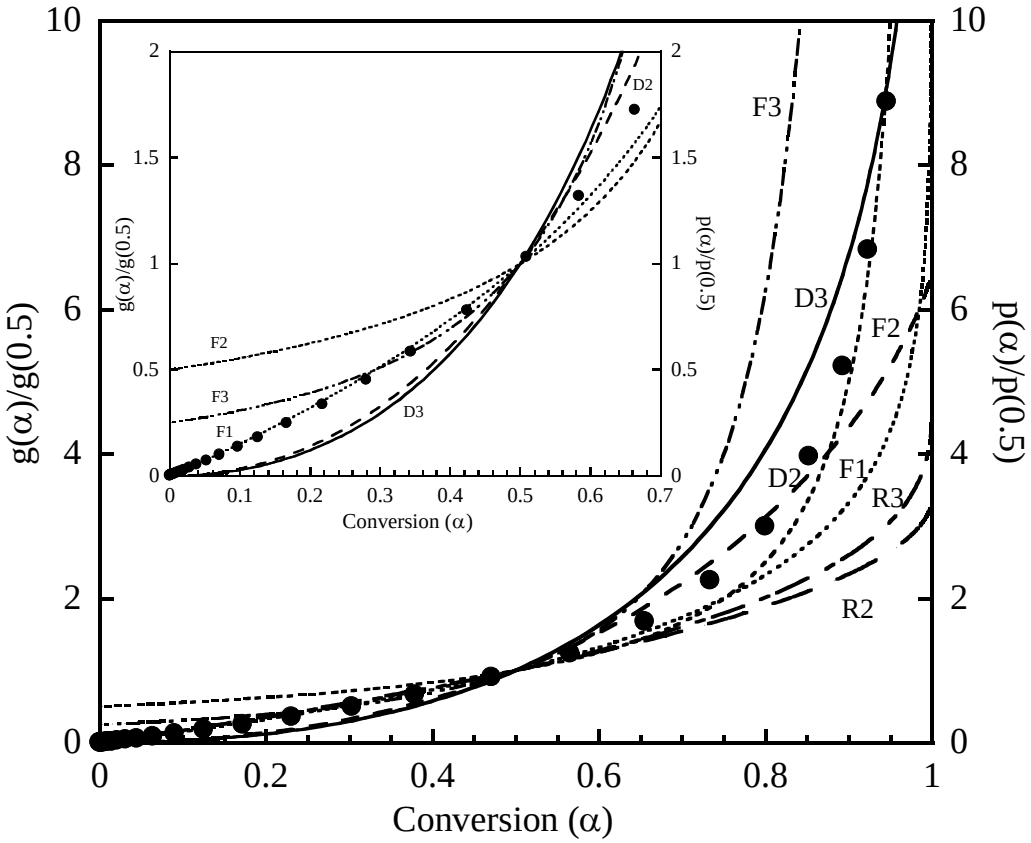

Figure 5.36 Integral master plot as a function of α at different mechanism models of the main degradation stage of PBA-a: (—) theoretical model and (●) experimental data. Inset: Integral master plot as a function of α = 0-0.7.

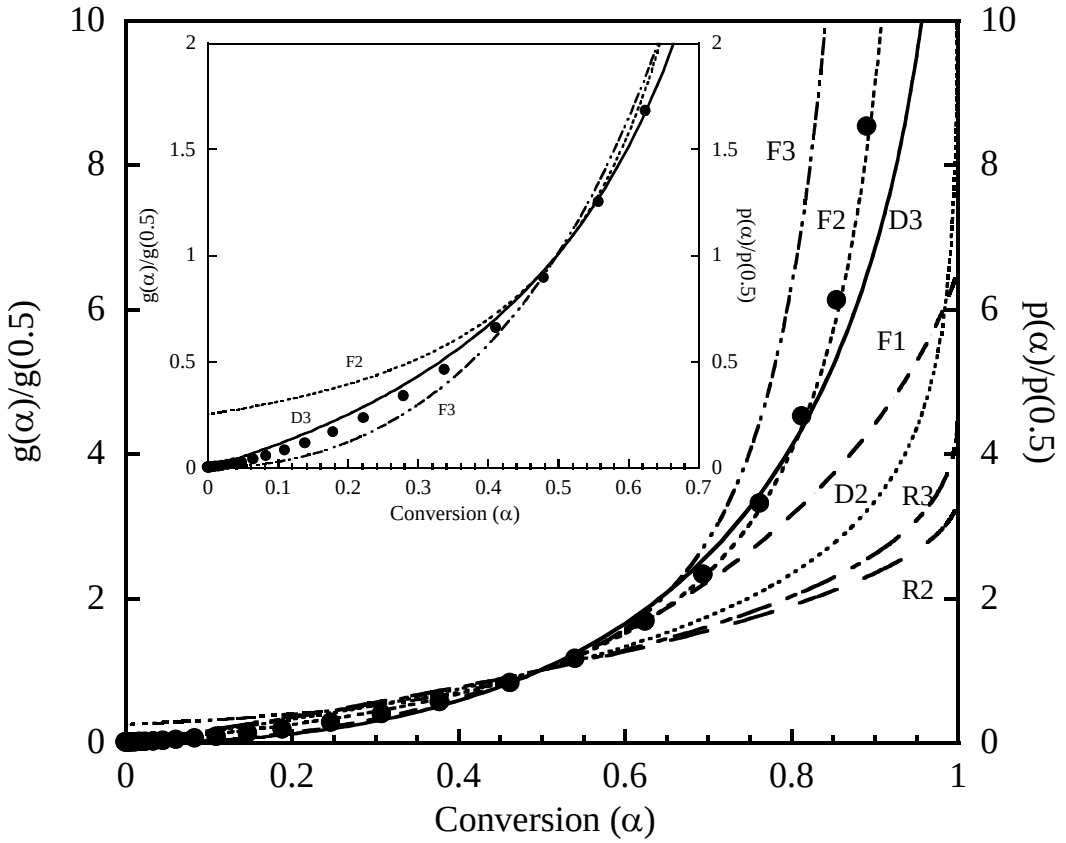

Figure 5.37 Integral master plot as a function of α at different mechanism models of main degradation stage of 10wt% nano-SiO2-filled PBA-a nanocomposites: (—) theoretical model and (●) experimental data. Inset: Integral master plot as a function of α =0-0.7.

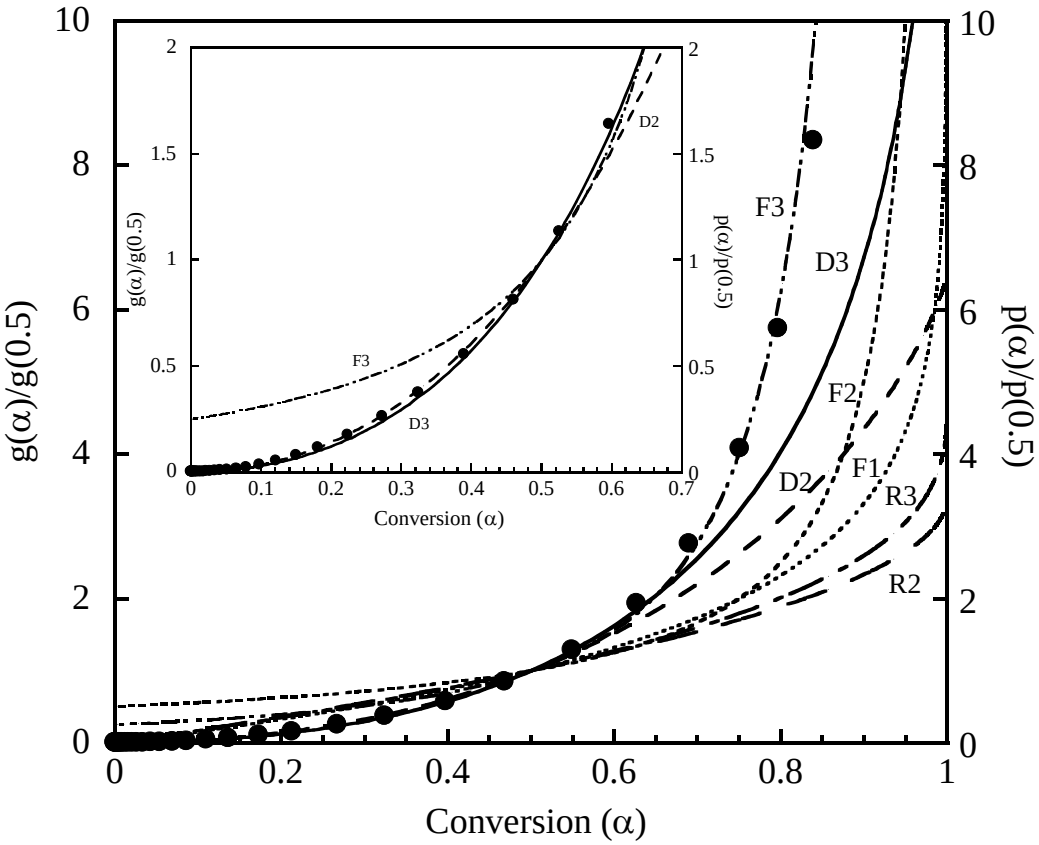

Figure 5.38 Integral master plot as a function of α at different mechanism models of the main degradation stage of 20wt% nano-SiO2-filled PBA-a nanocomposites: (—) theoretical model and (●) experimental data. Inset: Integral master plot as a function of α =0-0.7.

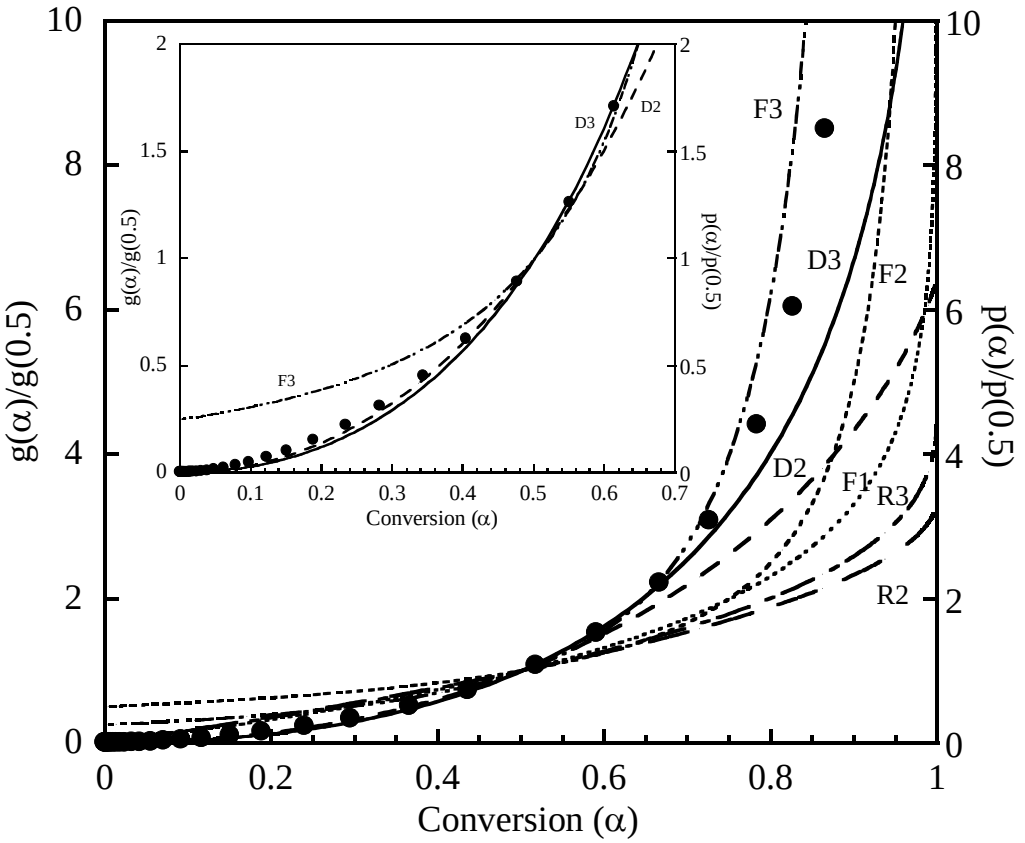

Figure 5.39 Integral master plot as a function of α at different mechanism models of the main degradation stage of 30wt% nano-SiO2-filled PBA-a nanocomposites: (—) theoretical model and (●) experimental data. Inset: Integral master plot as a function of α =0-0.7.

Table 5.1: The kinetic parameter of Arrhenius equation at the gel points of benzoxazine resins mixed with epoxy resin at various epoxy content.

Matrix	**ΔE**	**A (min^{-1})**
Neat BA-a	9.9872	$0.74\ 10^{-7}$
90/10 BA-a/YD126	10.469	$1.38\ 10^{-7}$
80/20 BA-a/YD126	10.647	$1.50\ 10^{-7}$
70/30 BA-a/YD126	10.947	$2.56\ 10^{-7}$
60/40 BA-a/YD126	9.6729	$0.10\ 10^{-7}$

Table 5.2: Mechanical property comparison of polymer matrix/nano-SiO_2 composite with particle size of 5-50 nm.

Matrix	Nano-SiO_2 content (% by volume)	Young's modulus		Reference
		Absolute value (GPa)	Enhancement (%)	
BA-a	0	5.9	0	
	5.7	6.8	15.2	
	8.7	7.7	30.5	
	11.9	8.6	45.8	
	15.3	9.9	67.8	
	18.8	10.8	83.0	
Maximum content of nano-SiO_2				
Epoxy	14	4.18	37	[4]
Epoxy	15.3	4.5	30	[15]
Cyanate ester	15.3	4.25	57	[5]
	20.7	4.75	75	
Epoxy	30	5.53	58	[34]

Table 5.3: Material parameters used in composite CTE and moduls predictions.

Parameters	Symbol	Value	Reference
Bulk modulus of PBA-a, GPa	K_m	4.12	[20]
Bulk modulus of nano-SiO_2, GPa	K_f	35.35	[41]
Shear modulus of PBA-a, GPa	G_m	1-3	[20]
Shear modulus of nano-SiO_2, GPa	G_f	29.91	[41]
Young's modulus of PBA-a, GPa	E_m	5.955	[20]
Young's modulus of nano-SiO_2, GPa	E_f	70	[41]
Poisson's ratio of PBA-a	v_m	0.29	[20]
Poisson's ratio of nano-SiO_2	v_f	0.17	[41]

Table 5.4: Thermo-mechanical parameters of PBA-a and its nanocomposites.

φ_f	Tg (^oC)	$Tan\delta_{max}$ (height)	ΔR (nm)
0.00(0.0)	185	0.9690	-
0.057(0.10)	193	0.7212	7.79
0.087(0.15)	194	0.6965	5.74
0.119(0.20)	199	0.5999	5.68
0.153(0.25)	199	0.4906	5.73
0.188(0.30)	201	0.4808	4.67
Average ΔR (nm) for 12 nm			5.92

Table 5.5: Activation energies obtained by using Kissinger method and Flynn-Wall-Ozawa method for polybenzoxazine and theirs nanocomposites.

Nano-SiO2 content (wt%)	**E_a (kJ/mol)**					
	Kissinger method			Flynn-Wall-Ozawa method		
	Stage 1	Stage 2	Stage 3	Stage 1	Stage 2	Stage 3
0	96	111	126	72	119	149
10		133	155		148	169
20		145	180		140	167
30		153	190		140	218

Table 5.6: Values of E_a and A by using Coats-Redfern method for maximum stage process at a heating rate of 10^oC/min for PBA-a and theirs nanocomposites.

Type	E_a (kJ/mol)	ln A (min^{-1})	R^2	Type	E_a (kJ/mol)	ln A (min^{-1})	R^2
PBA-a				10 wt% nano-SiO_2-filled PBA-a			
P2	32	-3.75	0.9219	P2	14	-7.76	0.8785
P3	18	-6.85	0.8892	P3	8	-9.42	0.7974
P4	11	-8.62	0.8341	P4	8	-9.42	0.7974
F1	112	12.12	0.9917	F1	95	8.96	0.9927
F2	76	6.41	0.9056	F2	63	3.98	0.8990
F3	162	24.02	0.9162	F3	137	19.35	0.9121
A2	50	0.24	0.9894	A2	42	-1.43	0.9902
A3	30	-3.98	0.9863	A3	24	-5.17	0.9865
A4	20	-6.24	0.9818	A4	16	-7.21	0.9807
D2	182	23.84	0.9669	D2	156	19.06	0.9696
D3	207	27.40	0.9827	D3	159	17.83	0.9844
R2	92	7.36	0.9729	R2	78	4.72	0.9748
R3	98	8.23	0.9805	R3	83	5.43	0.9821
Type	**E_a (kJ/mol)**	**ln A (min^{-1})**	**R^2**	**Type**	**E_a (kJ/mol)**	**ln A (min^{-1})**	**R^2**
20 wt% nano-SiO_2-filled PBA-a				30 wt% nano-SiO_2-filled PBA-a			
P2	10	-8.70	0.8518	P2	10	-8.95	0.8582
P3	5	-10.32	0.7086	P3	5	-10.57	0.6829
P4	5	-10.32	0.7086	P4	5	-10.57	0.6829
F1	78	5.97	0.9935	F1	76	5.22	0.9919
F2	51	1.82	0.8896	F2	50	1.25	0.8878
F3	113	15.21	0.9062	F3	110	14.16	0.9053
A2	38	-2.52	0.9899	A2	33	-3.45	0.9883
A3	19	-6.33	0.9859	A3	18	-6.64	0.9823
A4	12	13.46	0.9774	A4	11	-8.45	0.9713
D2	129	14.45	0.9713	D2	127	13.33	0.9720
D3	157	17.9	0.9858	D3	154	18.47	0.9852
R2	64	2.18	0.9758	R2	62	1.55	0.9756
R3	68	2.75	0.9831	R3	67	2.08	0.9823

Table 5.7: Degradation mechanism by using Coat-Redfern method of all degradation stages.

Type of samples	Stage 1	Stage 2	Stage 3
PBA-a	F1, F2, R2, R3	F1, R2, R3	F1, F3, D2, D3
10 wt% nano-SiO_2-filled PBA-a		F1, F3, D2, D3, R2, R3	F1, F2, F3, D2, D3
20 wt% nano-SiO_2-filled PBA-a		F3, D2, D3	F2, F3, D2, D3
30 wt% nano-SiO_2-filled PBA-a		F3, D2, D3	D2, D3

Table 5.8: Degradation parameter by using Coat-Redfern method Integral Master curves of all degradation stages.

Type of samples	Stage 1			Stage 2			Stage 3		
	*E_a	*ln A	model	*E_a	*ln A	model	*E_a	*ln A	model
PBA-a	95	11.55	F1	116	13.6	F1	147	16.47	D3
10 wt% nano-SiO_2-filled PBA-a				157	19.1	D3	208	23.9	D3
20 wt% nano-SiO_2-filled PBA-a				157	18.7	D3	203	22.5	D3
30 wt% nano-SiO_2-filled PBA-a				153	18.2	D3	205	22.5	D3

*average value from experimental result by heating rate of 5, 10, 15 and 20^{o}C/min.

CHAPTER VI

CONCLUSIONS

Epoxy act as diluent for benzoxazine resin. A synergistic behavior with the maximum glass transition temperature value was found at the benzoxazine-epoxy composition of 80:20 mass ratio. A novel highly filled polymer nanocomposites of nano-SiO_2 reinforced polybenzoxazine was prepared by melt mixing method. The adhesion between the nano-SiO_2 and PBA-a was observed to be strong with relatively uniform distribution of the nanofiller. The FTIR result suggested the formation of Si-O-C bonds between the polybenzoxazine and the nano-SiO_2 filler. Storage modulus and micro-hardness of the nanocomposites showed a substantial enhancement of 83% and 49 % from those of the polybenzoxazine matrix, respectively with an addition of 30% by weight of the nano-SiO_2. The glass transition temperature measured from the peak of the loss tangent was substantially increased with the addition of the nano-SiO_2. These property enhancements were likely due to the strong interfacial bonding observed in the nanocomposites. Finally, degradation temperature of the polybenzoxazine/nano-SiO_2 composites was found to increase with the nano-SiO_2 content. The molding compound is attractive as a coating material for high temperature, high mechanical property as well as high scratch resistant applications.

An introduction of nano-SiO_2 into polybenzoxazine was found to lead to a change of thermal degradation mechanism and decomposition behaviours from that of the pure matrix. Thermal stability in term of degradation temperature at 5% weight loss of PBA-a was substantially enhanced with increasing nano-SiO_2 content. The results are likely from the relatively high loading up to 30wt% of the nano-SiO_2 used and the ability to form stable Si-O-C bond of the benzoxazine resin with the silica nanoparticles. The reduction from three to two thermal decomposition stages, with the disappearance of the lowest thermal decomposition stage of the neat PBA-a, were observed in DTG results when the nano-SiO_2 was added in the polymer. From the kinetic analysis, activation energy of the nano-SiO2 filled PBA-a nanocomposites was observed to be higher than that of the PBA-a. The principal degradation mechanism of the PBA-a was determined to be a random nucleation type with one nucleus on the

individual particle (F1 model) while that of the PBA-a nanocomposites was best described by diffusion- controlled reaction (D3 model).

REFERENCES

[1] Jajam, K. C.; and Tippur, H. V. Quasi-static and dynamic fracture behavior of particulate polymer composites: A study of nano- vs. micro-size filler and loading-rate effects. Composite Part B. 43(2012): 3467-3481.

[2] Kemaloglu, S.; Ozkoc, G.; and Aytac, A. Properties of thermally conductive micro and nano size boron nitride reinforced silicon rubber composites. Thermochim Acta. 499(2010): 40–47.

[3] Nielsen, L. E.; and Landel, R. F. Mechanical properties of polymers and composites. 2nd edition. New York: Marcel Dekker, 1994.

[4] Zhang, H.; Zhang, Z.; Friedrich, K.; and Eger, C. Property improvements of in situ epoxy nanocomposites with reduced interparticle distance at high nanosilica content. Acta Mater. 54(2006): 1833–1842.

[5] Goertzen, W. K.; and Kessler, M. R. Dynamic mechanical analysis of nano-SiO_2/cyanate ester nanocomposites. Composites: Part A. 39(2008): 761-768.

[6] Preghenella, M.; Pegoretti, A.; and Migliaresi, C. Thermo-mechanical characterization of nano-SiO2-epoxy nanocomposites. Polymer. 46(2005): 12065–12072.

[7] Lin, Y.; Song, M.; Stone, C. A.; and Shaw, S. J. A comprehensive study on the curing kinetics and network formation of cyanate ester resin/clay nanocomposites. Thermochim Acta. 552(2013): 77-86.

[8] Chen, Q.; Xu, R.; and Yu, D. Multiwalled carbon nanotube/polybenzoxazine nanocomposites: Preparation, characterization and properties. Polymer. 47(2006): 7711-7719.

[9] Chrissafis, K.; Paraskevopoulos, K. M.; Stavrev, S. Y.; Docoslis, A.; Vassiliou, A.; and Bikiaris, D. N. Characterization and thermal degradation mechanism of isotactic polypropylene/carbon black nanocomposites. Thermochim Acta. 465(2007): 6-17.

[10] Fu, S. Y.; Feng, X. Q.; Lauke, B.; and Mai, Y. W. Effects of particle size, particle/matrix interface adhesion and particle loading on mechanical properties of particulate–polymer. Composites: Part B. 39(2008):

933–961.

[11] Vassiliou, A. A.; Bikiaris, D.; Mabrouk, K. E.; and Kontopoulou, M. Effect of evolved interactions in poly(butylene succinate)/nano-SiO2 biodegradable *'in situ'* prepared nanocomposites on molecular weight, material properties, and biodegradability. J. Appl Polym Sci. 119(2010): 2010–2024.

[12] Vaziri, H. S.; Omaraei, I. A.; Abadyan, M.; Mortezaei. M.; and Yousefi, N. Thermophysical and rheological behavior of polystyrene/silica nanocomposites: Investigation of nanoparticle content. Mater. Des. 32(2011): 4537–4542.

[13] Goertzen, W. K.; and Kessler, M. R. Thermal expansion of nano-SiO_2/cyanate ester nanocomposites. J Appl Polym Sci. 109(2008): 647–653.

[14] Chrissafis, K.; Paraskevopoulos, K. M.; Papageorgiou, G. Z.; and Bikiaris, D. N. Thermal and dynamic mechanical behavior of bionanocomposites: nano-SiO_2 nanoparticles dispersed in poly(vinyl pyrrolidone), chitosan, and poly(vinyl alcohol). J. Appl. Polym. Sci. 110(2008): 1739-1749.

[15] Periadurai, T.; Vijayakumar, C.T.; and Balasubramanian, M. J. Thermal decomposition and flame retardant behaviour of SiO_2-phenolic nanocomposite. Anal Appl Pyrol. 89(2010): 244-249.

[16] Mahrholz, T.; Stangle, J.; and Sinapius, M. Quantitation of the reinforcement effect of silica nanoparticles in epoxy resins used in liquid composite moulding processes. Composites Part A. 40(2009): 235-243.

[17] Composite materials for aerospace. http://www.gurit.com/files/documents/aerospace-brochurev10312pdf.pdf.

[18] New RTM system based on benzoxazine chemistry for high performance composite applications. http://www.huntsman.com/advanced_materials_2004.pdf.

[19] Rimdusit, S.; Tiptipakorn, S.; Jubsilp, C.; and Takeichi, T. Polybenzoxazine alloys and blends: Some unique properties and applications. React. Funct. Polym. 73(2012): 369-380.

[20] Ishida, H.; and Agag, T. Handbook of Benzoxazine Resin. Oxford: Elsevier Press, 2012.

[21] Ishida, H.; and Rimdusit, S. Very high thermal conductivity obtained by boron nitride-filled polybenzoxazine. Thermochim Acta. 320(1998): 177-186.

[22] Jubsilp, C.; Takeichi, T.; Hiziroglu, S.; and Rimdusit, S. High performance wood composites based on benzoxazine-epoxy alloys. Bioresour Technol. 99(2008): 8880–8886.

[23] Ishida, H.; and Low, H. Y. Synthesis of benzoxazine functional silane and adhesion properties of glass-fiber-reinforced polybenzoxazine composites. J Appl Polym Sci. 69(1998): 2559–2567.

[24] Ishida, H. Process for preparation of benzoxazine compounds in solventless systems. US Patent 5,543,516 (1996).

[25] Jubsilp, C.; Takeichi, T.; and Rimdusit, S. Effect of novel benzoxazine reactive diluent on processability and thermomechanical characteristics of bifunctional polybenzoxazine. J. Appl Polym Sci. 104(2007): 2928–2938.

[26] Rao, B. S.; Reddy, K. R.; Pathak, S. K.; and Pasala, A. R. Benzoxazine epoxy copolymers: effect of molecular weight and crosslinking on thermal and viscoelastic properties. Polym Int. 54(2005): 1371–1376.

[27] Ishida, H.; and Allen D. J. Mechanical characterization of copolymers based on benzoxazine and epoxy. Polymer. 37(1996): 4487-4495.

[28] Rimdusit, S.; and Ishida, H. Synergism and Multiple Mechanical Relaxations Observed in Ternary Systems Based on Benzoxazine, Epoxy, and Phenolic Resins. J Polym Sci B: Polym Phys. 38(2000): 1687–1698.

[29] Radhakrishnan, T. S. New method for evaluation of kinetic parameters and mechanism of degradation from pyrolysis-GC studies: Thermal degradation of polydimethylsiloxane. J Appl Polym Sci. 73(1999): 441-450.

[30] Sánchez-Jiménez, P. E.; Pérez-Maqueda, L. A.; Perejón, A.; and Criado, J. M.

Generalized master plots as a straightforward approach for determining the kinetic model: the case of cellulose pyrolysis. Thermochim Acta. 552(2013): 54–59.

[31] William, D.; and Callister, Jr. Materials science and engineering: an introduction. 7thedition. Wiley & Sons: New York, 2007.

[32] Zou, H.; Wu, S.; and Shen, J. Polymer/Silica Nanocomposites: Preparation, Characterization, Properties, and Applications. Chem. Rev. 108(2008): 3893–3957.

[33] Harry, S. K. Handbook of fillers for plastics. Van Nostrand Reinhold: U.S.A, 1987.

[34] Barthel, H.; Heinemann, M.; Stintz, M.; and Wessely, B. Particle sizes of nano-SiO_2. Part. Part. Syst. Charact. 16(1999): 169-176.

[35] Barthel, H.; Achenbach, F.; and Maginot, H. Proc. Int. Symp. on Mineral and Organic Functional Fillers in Polymers (MOFFIS 93), Universite de Namur, Belgium, 301 (1993).

[36] Ulrich, G. D. Chem. Eng. New. 62(1984): 22-29.

[37] Barthel, H.; Roesch, L.; and Weis, J. In: Auner, N.; and Weis, J. eds. Organosilicon Chemistry II. From Molecules to Materials, VCH: Weinheim. 1996. p. 761.

[38] Barthel, H. Basic characteristics of aerosil, technical bulletin Pigments. Colloids Surf, A. 101(1995): 217-223.

[39] Kim, H. C.; and Dubois, G. D. Encyclopedia of Nanoscience and Nanotechnology. Taylor & Francis: New York, 2005.

[40] Jana, S. C.; and Jain, S. Dispersion of nanofillers in high performance polymers using reactive solvents as processing aids. Polymer. 42(2001): 6897-6905.

[41] Takeichi, T.; Zeidam, R.; and Agag, T. Polybenzoxazine/clay hybrid nanocomposites: influence of preparation method on the curing behavior and properties of polybenzoxazine. Polymer. 43(2002): 45-53.

[42] Nair, C. P. R. Advances in Addition-Cure Phenolic Resins. Prog. Polym. Sci. 29(2004): 401-498.

[43] Ning, X.; and Ishida, H. Phenolic materials via ring-opening polymerization

of benzoxazine: effect of molecular structure on mechanical and dynamic peoperties. J. Polym. Sci., Polym. Phys. Ed. 32(1994): 921-927.

[44] Lee, S. M. International encyclopedia of composites. 2nd edition. VCH Publishers: New York, 1990.

[45] Liu, Z.; Erhan, S. Z.; and Xu, J. Preparation characterization and mechanical properties of epoxidized soybean oil/clay nanocomposites. Polymer. 46 (2005): 10119-10127.

[46] Stephenson, M. Technical information from the manufacturer. Miller Stephenson.

[47] Kroschwitz, J. I. High performance polymers and composites. 2nd edition. New York: John Wiley& Sons, 1991.

[48] Merfeld, G. D.; Yeager, G. W.; Chao, H. S.; and Singh, N. Phase behavior and morphology of poly(phenylene ether)/epoxy blends. Polymer 44 (2003): 4981-4992.

[49] Datasheet from Thai Organic Chemical CO., LTD. (Epoxy Divition).

[50] Kroschwitz, J. I. High performance polymers and composites. 2ndedition. John Wiley& Sons: New York, 1991.

[51] Khawam, A.; and Flanagan, D. R. Basics and applications of solid-state kinetics: A pharmaceutical perspective. J. Pharm. Sci. 95(2006): 472–498.

[52] Khawam, A.; and Flanagan, D. R. Solid-state kinetic models: basics and mathematical fundamentals. J Phys Chem B. 110(2006): 17315-17328.

[53] Vyazovkin, S.; Burnham, A. K.; Criado, J. M.; Maqueda, L. A. P.; Popescu, C.; and Sbirrazzuoli, N. ICTAC kinetics committee recommendations for performing kinetic computations on thermal analysis data. Thermochim Acta. 520(2011): 1–19.

[54] Doyle, C. D. Kinetic analysis of thermogravimetric data. J Appl Sci. 5(2003) 285–292.

[55] Kissinger, H. E. Reaction kinetics in differential thermal analysis. Anal Chem. 29(1957): 1702-1705.

[56] Ozawa, T. Kinetic analysis of derivative curves in thermal analysis. J. Therm.

Anal. 2(1970): 301-324.

[57] Coats, A. W.; and Redfern, J. P. Kinetic parameters from thermogravimetric data. Nature. 201(1964): 68-69.

[58] Koga, N.; and Criado, J. Kinetic analyses of solid-state reactions with a particle-size distribution. J. Am. Ceram. Soc. 81(1998): 2901-2909.

[59] Kasemsiri, P. Development of light weight ballistic armor from fibers-reinfored with benzoxazine alloys. Doctoral's degree. Department of Chemical Engineering, Faculty of Engineering, Chulalongkorn University, 2012.

[60] Takeichi, T.; Kano, T.; and Agag, T. Synthesis and thermal cure of high molecular weight polybenzoxazine precursors and the properties of the thermosets. Polymer. 46(2005): 12172-12180.

[61] Kimura, H.; Matsumoto, A.; Hasegawa, K.; Ohtsuka, K.; and Fukuda, A. Epoxy resin cured by bisphenol A based benzoxazine. J Appl Polym Sci. 68(1998): 1903-1910.

[62] Rimdusit, S.; Kunopast, P.; and Dueramae, I. Thermomechanical properties of arylamine-based benzoxazine resins alloyed with epoxy resin. Polym. Eng. Sci. 51(2011): 1797–1807.

[63] Jubsilp, C.; Damrongsakkul, S.; Takeichi, T.; and Rimdusit, S. Curing kinetics of arylamine-based polyfunctional benzoxazine resins by dynamic differential scanning calorimetry. Thermochim Acta. 447(2006): 131-140.

[64] Ishida, H.; and Rodriguez, Y. Curing kinetics of a new benzoxazine-based phenolic resin by differential scanning calorimetry. Polymer. 36(1995): 3151-3158.

[65] Ishida, H.; and Rodriguez, Y. Catalyzing the curing reaction of a new benzoxazine-based phenolic resin. J. Appl. Polym. Sci. 58(1995): 1751-1760.

[66] Ragosta, G.; Abbate, M.; Musto, P.; Scarinzi, G.; and Mascia, L. Epoxy-silica particulate nanocomposites Chemical interactions, reinforcement and fracture toughness. Polymer. 46(2005):10506-10516.

[67] William, K. G.; Sheng, X.; Akinc, M.; and Kessler, M. R. Rheology and

curing kinetics of fumed silica/cyanate ester nanocomposites. Polym. Eng. Sci. 48(2008): 875–883.

[68] Fredrich, K.; Fakirov, S.; Zhang, Z. Polymer Composites from Nano-to Macroscale. Springer Science: New York, 2005.

[69] Usuki, A.; Hasegawa, N.; and Kato, M. Advances in polymer science. Adv. Polym. Sci. 179(2005): 135-195.

[70] Agag, T.; and Takeichi, T. Polybenzoxazine-montmorillonite hybrid nanocomposites: synthesis and characterization. Polymer. 41(2000): 7083-7090.

[71] Agag, T.; and Takeichi, T. Prepararion and cure behavior of organoclay-modified allyl functional benzoxazine resin and the properties of their nanocomposites. Polym.Compos. 29(2008): 750–757

[72] Chen, Q.; Xu, R.; and Yu, D. Multiwalled carbon nanotube/polybenzoxazine nanocomposites: Preparation, characterization and properties. Polymer. 47(2006): 7711–7719.

[73] Agag, T.; Taepaisitphongse, V.; and Takeichi, T. Reinforcement of polybenzoxazine matrix with organically modified mica. Polym. Compos. 28(2007): 680-689.

[74] Takeichi, T.; and Guo, Y. Synthesis and characterization of poly(urethane-benzoxazine)/clay hybrid nanocomposites. J Appl Polym Sci. 90(2003): 4075-4083.

[75] Chozhan, C. K.; Alagar, M.; and Gnanasundaram, P. Synthesis and characterization of 1,1-bis(3-methy-4-hydroxy phenyl)-cyclohexane polybenzoxazine-organoclay hybrid nanocomposites. Acta Mater. 57(2009): 782-794.

[76] Zhang, J.; Xu, R.; and Yu, D. A novel polybenzoxazinyl functionalized polyhedral oligomeric silsesquioxane and its nanocomposite with polybenzoxazine. Eur Polym J. Macromol Nanotechnol. 43(2007): 743-752.

[77] Huang, K.W.; and Kuo, S.W. High-performance polybenzoxazine nanocomposites containing multifunctional POSS cores presenting vinyl-terminated benzoxazine groups. Macromol. Chem. Phys. 211

(2010): 2301-2311.

[78] Liu, Y.; Zhang, W.; Chen, Y.; and Zheng, S. Polybenzoxazine containing polysilsesquioxane: Preparation and thermal properties. J. Appl Polym Sci. 99(2006): 927-936.

[79] Lee, Y.J.; Kuo, S.W.; Feng, H.C.; and Chang, F.C. Synthesis and characterization of polybenzoxazine networks nanocomposites containing multifunctional polyhedral oligomeric silsesquioxane (POSS). Polymer. 47(2006): 4378-4386.

[80] Yan, C.; Fan, X.; Li, J.; and Shen, S. Z. Study of surface functionalized nano-SiO_2/polybenzoxazine composites. J Appl Polym Sci. 120(2011): 1525–1532.

[81] Li, W. H.; Lehmann, S. L.; and Wong, R.S. Nanoparticle silica filled benzoxazine composites. US 7,666,938 B2. 2011.

[82] Rimdusit, S.; Tanthapanichakoon, W.; and Jubsilp, C. High performance wood composites from highly filled polybenzoxazine. J Appl Polym Sci. 99(2006): 1240-1253.

[83] William, K. G.; Sheng, X.; Akinc, M.; and Kessler, M.R. Rheology and curing kinetics of nano-SiO2/cyanate ester nanocomposites. Polym. Eng. Sci. 48(2008): 875-883.

[84] Mahrholz, T.; Stängle, J.; and Sinapius, M. Quantitation of the reinforcement effect of silica nanparticles in epoxy resins used in liquid composite moulding processes. Composites Part A. 40(2009): 235-243.

[85] Mustoa, P.; Ragostaa, G.; Scarinzi, G.; and Mascia, L. Polyimide-silica nanocomposites Spectroscopic, morphological and nechanical investigations. Polymer. 45(2004): 1697-1706.

[86] Hemvichian, K.; Ishida, H. Thermal decomposition processes on aromatic amine-base polybenzoxazine investigated by TGA and GC-MS. Polymer. 43(2002): 4391-4402.

[87] Gilman, J.W.; Kashiwagi, T.; Nyden, M.; and Harris, R. H. Jr. Fire Retardants, 2001.

[88] Periadurai, T.; and Vijayakumar, C. T.; and Balasubramanian, M. Thermal

decomposition and flame retardant behavior of SiO_2-phenolic nanocomposite. J. Analy and Appl Pyr. 89(2010): 244-249.

[89] Javier, T.; and Lattimer, B.Y. Modelling thermal degradation of composite materials. Fire Mater. 31(2007): 147-171.

[90] William, D.; and Callister, Jr. Materials science and engineering: an introduction. 7th edition. Wiley & Sons: New York, 2007.

[91] Moczo, J.; Pukanszky, B. Polymer micro and nanocomposites: Structure, interactions, properties. J Ind and Eng Chem. 14(2008): 535-563.

[92] Agag, T.; Tsuchiya, H.; and Takeichi, T. Novel organic–inorganic hybrids prepared from polybenzoxazine and titania using sol–gel process. Polymer. 45(2004): 7903–7910.

[93] Yei, D. R.; Fu, H. K.; Chen, W. Y.; and Chang, F. C. Synthesis of a novel benzoxazine monomer-intercalated montmorillonite and the curing kinetics of polybenzoxazine /clay hybrid nanocomposites. J Polym Sci. Part B: Polym Phys. 44(2006): 347–358.

[94] Kambour, R. P.; Ligon, W.V.; and Russell, R. R. Enhancement of the limiting oxygen index of an aromatic polycarbonate by the incorporation of silicone blocks. J Polym Sci Polym Lett. 16(1978): 327-333.

[95] Liu, Y. L.; Wei, W. L.; Hsu, K. Y.; and Ho, W. H. Thermal stability of epoxy-silica hybrid materials by thermogravimetric analysis. Thermochim Acta. 412(2004): 139–147.

[96] Carrasco, F.; and Pages, P. Thermal degradation and stability of epoxy nanocomposites: Influence of montmorillonite content and cure temperature. Polym Degrad Stab. 93(2008): 1000-1007.

[97] Laachachi, A.; Ferriol, M.; Cochez, M.; Lopez Cuesta, J. M.; and Ruch, D. A. comparison of the role of boehmite (AlOOH) and alumina (Al_2O_3) in the thermal stability and flammability of poly(methyl methacrylate). Polym Degrad Stab. 94(2009): 1373–1378.

[98] De Fenzo, A.; Formicola, C.; Antonucci, V.; Zarrelli, M.; amd Giordano, M. Effects of zinc-based flame retardants on the degradation behavior of an aerospace epoxy matrix. Polym Degrad Stab. 94(2009): 1354–1363.

[99] Quan, H.; Zhang, B.; Zhao, Q.; Yuen, R. K. K.; and Li, R. K. Y. Facile preparation and thermal degradation studies of graphite nanoplatelets (GNPs) filled thermoplastic polyurethane (TPU) nanocomposites. Composites: Part A. 40(2009): 1506–1513.

[100] Macan, J.; Brnardic, I.; Orlic, S.; Ivankovic, H.; and Ivankovic, M. Thermal degradation of epoxy-silica organic-inorganic hybrid materials. Polym Degrad Stab. 91(2006): 122-127.

[101] Montero, B.; Ramırez, C.; Rico, M.; Barral, L.; Dıez, J.; and Lopez, J. Effect of an epoxy octasilsesquioxane on the thermodegradation of an epoxy/amine system. Polym Int. 59(2010): 112–118.

[102] Beraa, O.; Pilic, B.; Pavlicevic, J.; Jovicic, M.; Hollo, B.; Szecsenyi, K. M.; and Spirkova, M. Preparation and thermal properties of polystyrene/silica nanocomposites. Thermochim Acta. 515(2011): 1–5.

[103] Vassiliou, A. A.; Chrissafis, K.; and Bikiaris, D. N. In situ prepared PBSu/SiO_2 nanocomposites: Study of thermal degradation mechanism. Thermochim Acta. 495(2009): 120–128.

[104] Chrissafis, K.; Paraskevopoulos, K. M.; Tsiaoussis, I.; and Bikiaris, D. Comparative study of the effect of different nanoparticles on the mechanical properties, permeability, and thermal degradation mechanism of HDPE. J. Appl. Polym. Sci. 114(2009): 1606–1618.

[105] Tarrıo-Saavedra, J.; Lopez-Beceiro, J.; Naya, S.; and Artiaga, R. Effect of silica content on thermal stability of nano-SiO2/epoxy composites. Polym Degrad Stab. 93(2008): 2133–2137.

[106] Chrissafis, K.; Paraskevopoulos, K. M.; Pavlidou, E.; and Bikiaris, D. Thermal degradation mechanism of HDPE nanocomposites containing fumed silica nanoparticles. Thermochim Acta. 485(2009): 65–71.

[107] Winter, H. H.; and Mours, M. Rheology of polymers near liquid-solid transitions. Adv. Polym. Sci. 134(1997): 165–234.

[108] Clark, A. H.; and Ross-Murphy S. B. Structural and mechanical properties of biopolymer gels. Adv. Polym. Sci. 83(1987): 57–192.

[109] Kavanagh, G. M.; and Ross-Murphy S. B. Rheological characterisation of polymer gels. Prog. Polym. Sci. 23(1998): 533–562.

[110] Rimdusit, S.; and Ishida, H. Gelation study of high processability and high reliability ternary systems based on benzoxazine, epoxy, and phenolic resins for an application as electronic packaging materials. Rheol. Acta. 41 (2002): 1–9.

[111] Ishida, H.; and Allen D. J. Gelation behavior of near-zero shrinkage Polybenzoxazines. J. Appl. Polym. Sci. 79 (2001): 406–417.

[112] Kwak, G. H.; Park, S. J.; and Lee, J. R. Viscoelastic behavior of anhydride cured epoxy system initiated by thermal latent catalyst. J. Appl. Polym. Sci. 81(2001): 646–653.

[113] Kasemsiri, P.; Hiziroglu, S.; and Rimdusit, S. Effect of cashew nut shell liquid on gelation, cure kinetics, and thermomechanical properties of bezoxazine resin. Thermochim Acta. 520(2011) 2011: 84-92.

[114] Agag, T.; and Takeichi, T. Synthesis and characterization of benzoxazine resin-SiO_2 hybrids by sol-gel process The role of benzoxazine-functional silane coupling agent. Polymer. 52(2011): 2757-2763.

[115] Sbirrazzuoli, N.; and Vyazovkin, S. Learning about epoxy cure mechanisms from isoconversional analysis of DSC data. Thermochim Acta. 388(2002)*:* 289–298.

[116] Chen, L. W.; Fu, S. C.; and Cho, C. S. Kinetics of aryl phosphinate anhydride curing of epoxy resins using differential scanning calorimetry. Polym. Int. 46 (1998): 325–330.

[117] Vassiliou, A. A.; Bikiaris, D.; Mabrouk, K. E.; Kontopoulou, M. Effect of evolved interactions in poly(butylene succinate)/nano-SiO2 biodegradable *'in situ'* prepared nanocomposites on molecular weight, material properties, and biodegradability. J. Appl Polym Sci. 119(2010): 2010–2024.

[118] Grellmann, W.; and Seidler, S. Polymer testing. Hanser: Ohio, 2007.

[119] Harry, S. K. Handbook of Fillers for Plastics. Van Nostrand Reinhold: USA, 1987.

[120] Zhang, H.; Tang, L. C.; Zhang, Z.; Friedrich, K.; and Sprenger, S. Fracture behaviours of in situ silica nanoparticle-filled epoxy at different temperatures. Polymer. 49(2008): 3816–3825.

[121] Dittanet, P.; and Pearson, R. A. Effect of silica nanoparticle size on toughening mechanisms of filled epoxy. Polymer. 53(2012): 1890–1905.

[122] Yan, C.; Fan, X.; Li, J.; and Shen, S. Z. Study of surface-functionalized nano-SiO_2/ polybenzoxazine composites. J Appl Polym Sci. 120(2011): 1525–1532.

[123] Kimura, H.; Matsumoto, A.; and Ohtsuka, K. Glass fiber-reinforced composite based on benzoxazine resin. J Appl Polym Sci. 114(2009): 1256–1263.

[124] Johnsen, B. B.; Kinloch, A. J.; Mohammed, R. D.; Taylor, A. C.; and Sprenger, S. Toughening mechanisms of nanoparticle-modified epoxy polymers. Polymer. 48(2007): 530-541.

[125] Vassileva, E.; and Friedrich, K. Epoxy/Alumina Nanoparticle Composites. I. Dynamic Mechanical Behavior. J. Appl. Polym. Sci. 89(2003): 3774–3785.

[126] Goyanes, S. N.; Konig, P. G.; and Marconi, J. D. Dynamic mechanical analysis of particulate-filled epoxy resin. J. Appl. Polym. Sci. 88(2003): 883–892.

[127] Grellmann, W.; and Seidler, S. Polymer testing. Ohio: Hanser, 2007.

[128] Low, H. Y.; and Ishida, H. Structural effects of phenols on the thermal and thermo- oxidative degradation of polybenzoxazines. Polymer. 40(1999): 4365-4376.

[129] Tiptipakorn, S.; Damrongsakkul, S.; Ando, S.; Hemvichian, K.; and Rimdusit, S. Thermal degradation behaviors of polybenzoxazine and silicon-containing polyimide blends. Polym Degrad Stab. 92(2007): 1265-1278.

[130] Lorjai, P.; Wongkasemjit, S.; Chaisuwan, T.; and Jamieson, A. M. Significant enhancement of thermal stability in the non-oxidative thermal degradation of bisphenol-A/aniline based polybenzoxazine aerogel. Polym Degrad Stab. 96(2011): 708-718.

[131] Low, H. Y.; and Ishida, H. Mechanistic Study on the thermal decomposition

of polybenzoxazines: effects of aliphatic amines. J Polym Sci, Part B: Polym Phys. 36(1998): 1935–1946.

[132] Hemvichian, H.; Kim, H. D.; and Ishida, H. Identification of volatile products and determination of thermal degradation mechanisms of polybenzoxazine model oligomers by GC-MS. Polym Degrad Stab. 87(2005): 213-224.

[133] Perondi, D.; Broetto, C. C.; Dettmer, A.; Wenzel, B. M.; and Godinho, M. Thermal decomposition of polymeric resin [$(C_{29}H_{24}N_{205})_n$]: Kinetic parameters and mechanisms. Polym Degrad Stab. 97(2012): 2110-2117.

[134] Jankovi, B. Kinetic analysis of the nonisothermal decomposition of potassium metabisulfite using the model-fitting and isoconversional (model-free) methods. Chem Eng J. 139(2008): 128–135.

[135] Goswami, A.; Srivastava, G.; Umarji, A. M.; and Madras, G. Thermal degradation kinetics of poly(trimethylol propane triacrylate)/poly(hexane diol diacrylate) interpenetrating polymer network. Thermochim Acta. 547(2012): 53–61.

[136] Zabihi, O.; Khodabandeh, A.; and Mostafavi, S. M. Preparation, optimization and thermal characterization of a novel conductive thermoset nanocomposite containing polythiophene nanoparticles using dynamic thermal analysis. Polym. Degrad. Stab. 97 (2012): 3-13.

[137] Krol, P.; Pielichowska, K.; and Byczynski, L. Thermal degradation kinetics of polyurethane–siloxane anionomers. Thermochim Acta. 507–508(2010): 91–98.

APPENDIX

APPENDIX A

LIST OF PUBLICATIONS

1. Dueramae, I.; Jubsilp, C.; Takeichi, T.; and Rimdusit, S. High thermal and mechanical properties enhancement bbtained in highly filled polybenzoxazine nanocomposites with nano-SiO2. (In revised manuscript number: JCOMB-D-13-00035R1)
2. Rimdusit, S.; Ramsiri, B.; Jubsilp, C.; and Dueramae, I. Characterizations of polybenzoxazine modified with isomeric biphenyltetracarboxylic dianhydrides. eXPRESS Polym Let. 6 (2012): 773–782.
3. Rimdusit, S.; Kunopast, P.; and Dueramae, I. Thermomechanical properties of arylamine-based benzoxazine resins alloyed with epoxy resin. Polym. Eng. Sci. 51(2011): 1797–1807.
4. Rimdusit, S.; Punson, K.; Dueramae, I.; Somwangthanaroj, Anongnat.; and Tiptipakorn, Sunan. Rheological and thermomechanical characterizations of nano-SiO2-filled polybenzoxazine nanocomposites. Engineering J. 15(2011): 27-38.
5. Dueramae, I.; Jubsilp, C.; Takeichi, T.; and Rimdusit, S. "Thermal Degradation Kinetics of Highly Filled Silica-Polybenzoxazine Nanocomposites," Proceeding of 25th MAMIP2012 Asian International Conference on Materials, Minerals and Polymer, March. 23- 24, 2012, Vistana Hotel, Penang, p. 50 (Oral presentation).
6. Dueramae, I.; Jubsilp, C.; Takeichi, T.; and Rimdusit, S. "Thermomechanical properties of nano-SiO_2 from highly filled polybenzoxazine," Abstract of 5th Asian conference on Nanoscience and Nanotechnology 2010, Nov. 1-3, 2010, Tokyo, Japan, PB031 (Poster presentration).

VITAE

Isala Dueramae was born on January 27th, 1983 in Yala, Thailand. She finished high school from Prince of Songkla University, Pattani Campus, Demonstration School in 2002, and received the bachelor's degree of Chemical Engineering from Faculty of Engineering, Prince of Songkla University, Hatyai Campus in 2006. In 2008, she received the Degree of Master of Engineering in Chemical Engineering at the Department of Chemical Engineering, Kasetsart University, Bang Khen Campus. After the M.Eng graduation, she was a lecturer at the Faculty of Science and Technology, Phranakhon Si Ayutthaya Rajabhat University. In 2009, she pursued her graduate study for a Doctoral Degree in Chemical Engineering at Chulalongkorn University.